

**DEVELOPMENT OF A SOLAR PARABOLIC TROUGH RECEIVER
USING FLAME SPRAY TECHNIQUE**




**A Thesis Submitted to the Graduate School of Naresuan University
in Partial Fulfillment of the Requirements
for the Doctor of Philosophy Degree in Renewable Energy**

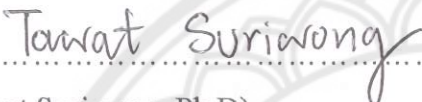
March 2016


Copyright 2016 by Naresuan University

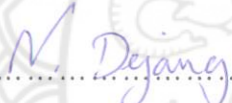
Thesis entitled “Development of a solar parabolic trough receiver using flame spray”
by Mr.Chanon Bunmephiphit
has been approved by the Graduate School as partial fulfillment of the requirements
for the Doctor of Philosophy Degree in Renewable Energy of Naresuan University


Oral Defense Committee


..... Chair
(Associate Professor Santi Wangnipparnto, Ph.D)


..... Advisor
(Tawat Suriwong, Ph.D)


..... Co - Advisor
(Assistant Professor Somchai Jiajitsawat, D.Eng.)


..... Co - Advisor
(Nuchjira Dejang, Ph.D)


..... Internal Examiner
(Sukruedee Sukchai, Ph.D)

Approved



.....
(Panu Putthawong, Ph.D.)

Associate Dean for Administration and Planning
for Dean of the Graduate School

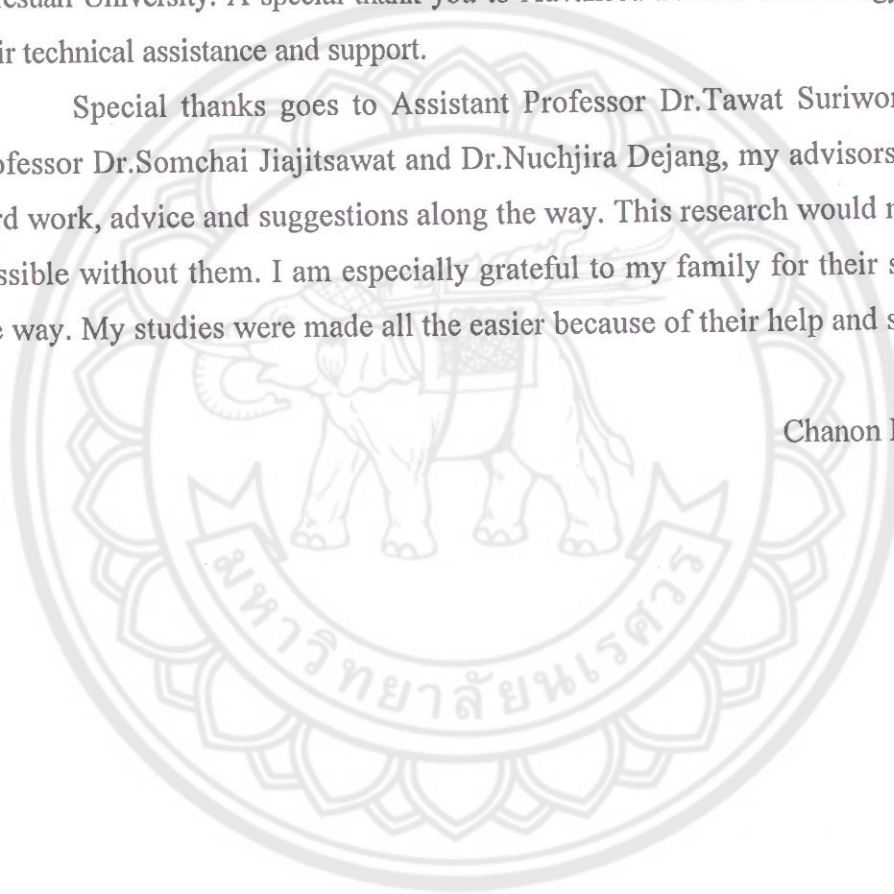
- 8 MAR 2016

ACKNOWLEDGEMENT

This research project would not have been possible without the efforts and assistance of many people. The author offers grateful thanks to the University of Phayao, for offering me a scholarship to complete my studies. I also need to thank the School of renewable energy technology, Faculty of Science, Department of Physics at Naresuan University. A special thank you to Advanced Surface Technology Co., Ltd for their technical assistance and support.

Special thanks goes to Assistant Professor Dr.Tawat Suriwong, Assistant Professor Dr.Somchai Jiajitsawat and Dr.Nuchjira Dejang, my advisors, for all their hard work, advice and suggestions along the way. This research would not have been possible without them. I am especially grateful to my family for their support along the way. My studies were made all the easier because of their help and support

Chanon Bunmephiphit



Title DEVELOPMENT OF A SOLAR PARABOLIC TROUGH RECEIVER USING FLAME SPRAY

Author Chanon Bunmephiphit

Advisor Assistant Professor Tawat Suriwong, Ph.D.

Co - Advisor Assistant Professor D. Eng Somchai Jiajitsawat, Ph.D.
Nuchjira Dejang, Ph.D.

Academic Paper Thesis Ph.D. in Renewable Energy, Naresuan University, 2015

Keywords Flame spray technique, Ni-Al composite, Nickel aluminides, parabolic trough collector, solar absorber, Heat collecting element (HCE)

ABSTRACT

In this study, a Ni-Al solar absorber was successfully prepared by the flame spray technique with Ni-5 wt.% Al particles as a starting material. The particles were melted and sprayed onto the outer surface of a stainless steel 316L tube in order to form a Ni-Al composite coating. The phase, morphology and reflectance (R) spectrum of the Ni-Al solar absorber were characterized by X-ray Diffraction (XRD), a Scanning electron microscope (SEM) equipped with an Energy Dispersive Spectrometer (EDS) analyzer and an Ultraviolet-visible-near infrared spectrophotometer at the wavelength 300-2500 nm. The results revealed that the surface of the Ni-Al solar absorber length and its cross-section was overlapped layer by layer. Flame spray coating technique coated Ni-Al particles difference thickness on stainless steel substrate as 195 μm , 215 μm and 299 μm . The surface coating was composed of Nickel (Ni) and aluminum (Al) phases. In addition, NiO and Al₂O₃ phases were also found on the surface. The chemical composition of the Ni-Al solar absorber was Ni 72.94 wt.%, Al 11.76 wt.% and O 15.29 wt.%. The solar absorptance (α) of the three Ni-Al coating thicknesses are tested with the following results: thickness 195 μm 0.75, thickness 215 μm 0.74 and thickness 299 μm 0.74 respectively.

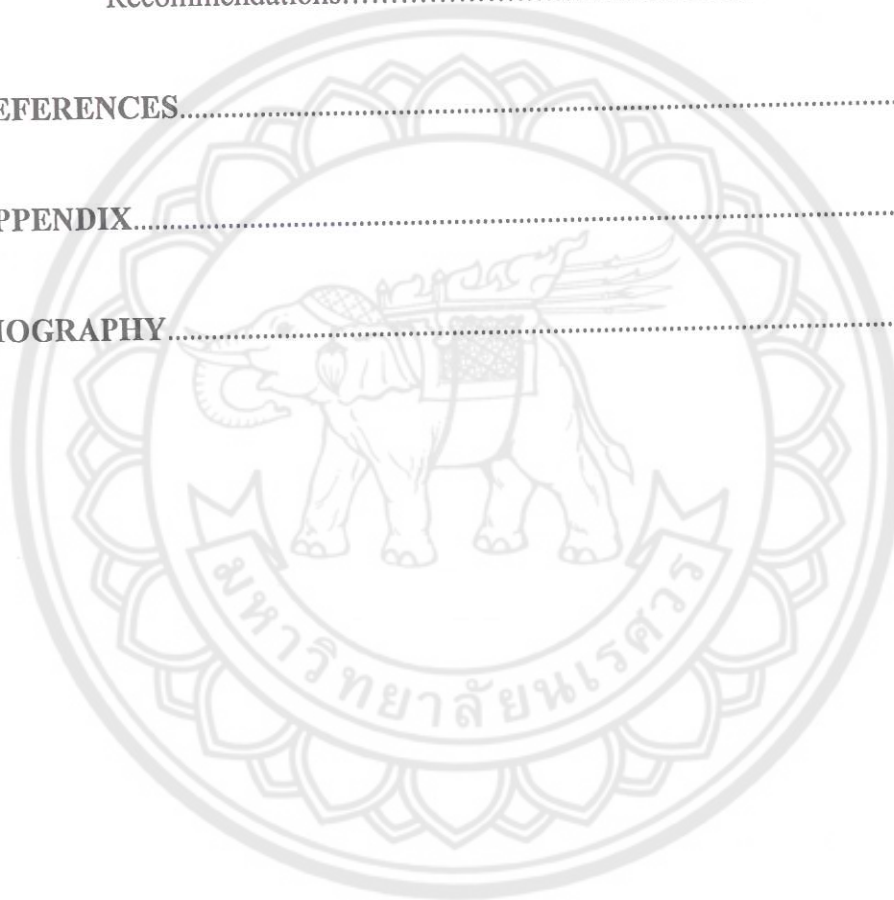
The receiver tube was designed typically suitable for a solar absorber of the Parabolic Trough Collector (PTC). Stainless steel 316L with 1 m length, 0.033 m outer diameter and 2.7 mm thickness was used as absorber tube and coated with Ni-Al solar absorber. In order to minimize heat loss to surrounding, the absorber tube was assembled with a glass tube for maintaining the vacuum inside the receiver tube. The heat loss analysis for receiver tube with various Ni-Al thicknesses was measured. The experimental results with three different coating thicknesses have clearly shown that the heat loss in the absorber cannot be totally eliminated by the vacuum tube and also found increased as the absorber area increased. The heat loss was found to be the maximum with the 299 μm thickness Ni-Al coating due to the largest area compared with other lower thickness coatings. Thermal emittance (ϵ) was evaluated for the heat loss results. At 100°C, the ϵ increased with the thickness of Ni-Al solar absorber and reached its highest to 0.28 for 299 μm thickness. Thermal performance of PTC by using absorber tube coated with difference thickness of Ni-Al solar absorber as receiver tube was determined. It is observed that the thickness of Ni-Al solar absorber was effective on the increasing of thermal performance of PTC. The highest thickness of the sample (299 μm) exhibited the highest ability to convert the solar radiation into thermal energy more than both two thicknesses.

LIST OF CONTENTS

Chapter	Page
I INTRODUCTION.....	1
Background.....	1
Objectives of study.....	3
Keyword.....	3
Limitation of the study.....	3
Expectation of the study.....	3
II THEORIES AND RELATED LITERATURE.....	4
Solar selective materials and Coating technique.....	5
Solar collector.....	19
Parabolic trough collector designs.....	25
Collector thermal analysis.....	28
Application of solar collector.....	35
III RESEARCH METHODOLOGY.....	37
Experimental procedures.....	37
Equipment.....	38
Preparation.....	40
Surface and thermal analysis.....	52
IV RESULTS AND DISSCUSION.....	58
Surface coating with flame spray technique.....	58
Surface analysis.....	59
Thermal analysis.....	70

LIST OF CONTENTS (CONT.)

Chapter	Page
V CONCLUSION AND RECOMMENDATION.....	86
Conclusion.....	86
Recommendations.....	87
REFERENCES.....	88
APPENDIX.....	96
BIOGRAPHY.....	120

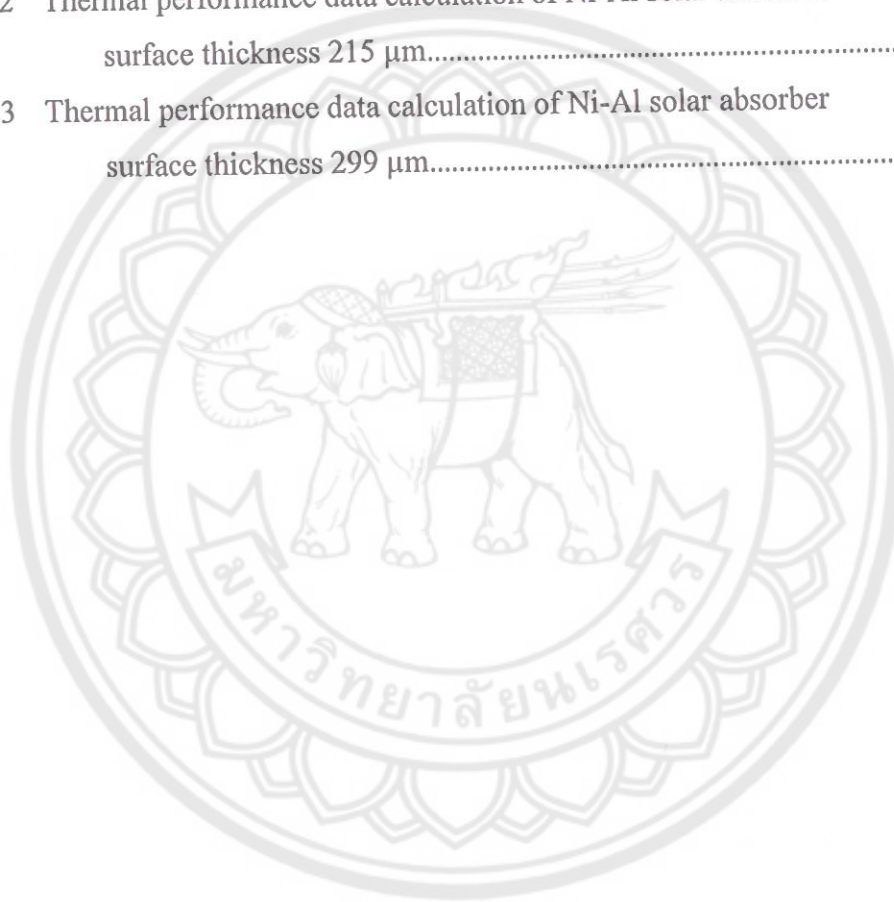


LIST OF TABLES

Table	Page
1 Solar selective materials and coating techniques review.....	9
2 Thermal spray process comparisons.....	15
3 Two types of solar collector.....	20
4 Heat process using in industrials.....	35
5 Specification of Ni-5wt.%Al powder.....	41
6 Chemical composition, Mechanical and Physical properties of stainless steel 316L pipe.....	43
7 Condition parameter of flame spraying process.....	44
8 Structure and dimensions of parabolic trough receiver and parabolic trough testing stand.....	46
9 PTC hot water generation system specification.....	56
10 The thickness from flame spray coating.....	63
11 Solar absorptance and reflectance with difference thickness.....	69
12 Solar absorptance of Ni-Al compare with another materials and coating technique.....	69
13 The result of thermal performance and Ni-Al solar selective thickness...	83
14 Comparison of collector efficiency equation.....	84
15 Heat loss testing of Ni-Al coated thickness 195 μm	101
16 Heat loss testing of Ni-Al coated thickness 215 μm	102
17 Heat loss testing of Ni-Al coated thickness 299 μm	103
18 Solar absorptance data calculation of Ni-Al solar absorber surface thickness 195 μm	104
19 Solar absorptance data calculation of Ni-Al solar absorber surface thickness 215 μm	106
20 Solar absorptance data calculation of Ni-Al solar absorber surface thickness 299 μm	108

LIST OF TABLES (CONT.)

Table	Page
21 Thermal performance data calculation of Ni-Al solar absorber surface thickness 195 μm	110
22 Thermal performance data calculation of Ni-Al solar absorber surface thickness 215 μm	111
23 Thermal performance data calculation of Ni-Al solar absorber surface thickness 299 μm	113



LIST OF FIGURES

Figures	Page
1	Spectral performance of an ideal selective solar absorber..... 6
2	ASTM G173-03 Air Mass 1.5 reference spectra derived from SMARTS v. 2.9.2..... 7
3	Thermal spray process..... 14
4	Schematic of flame spraying of a powder..... 16
5	Schematic of a section of a plasma torch..... 17
6	Schematic of an arc-spraying installation..... 18
7	Schematic of an HVOF torch..... 18
8	Schematic of the vacuum plasma spraying process..... 19
9	Cross-section of flat plate solar collector..... 20
10	Diagram of an evacuated tube collector..... 21
11	Diagram of compound parabolic collector..... 22
12	Fresnel collector, (a) Fresnel lens collector (FLC), (b) Liner Fresnel-type parabolic trough collector..... 22
13	Parabolic dish collector..... 23
14	Schematic of central receiver system..... 24
15	Parabolic trough collector (PTC)..... 25
16	Cross-section of a parabolic trough collector with circular receiver..... 26
17	(a) One-dimensional steady-state energy balance and (b) thermal resistance model..... 30
18	Experimental procedures..... 37
19	Rigaku miniflex II X-ray diffractometer..... 38
20	JEOL JSM-5910 LV scanning electron microscope..... 39
21	UV-3101PC Ultraviolet-Visible-Near Infrared Spectrophotometer..... 40
22	Nickel-5% Aluminum thermal spray powders..... 41

LIST OF FIGURES (CONT.)

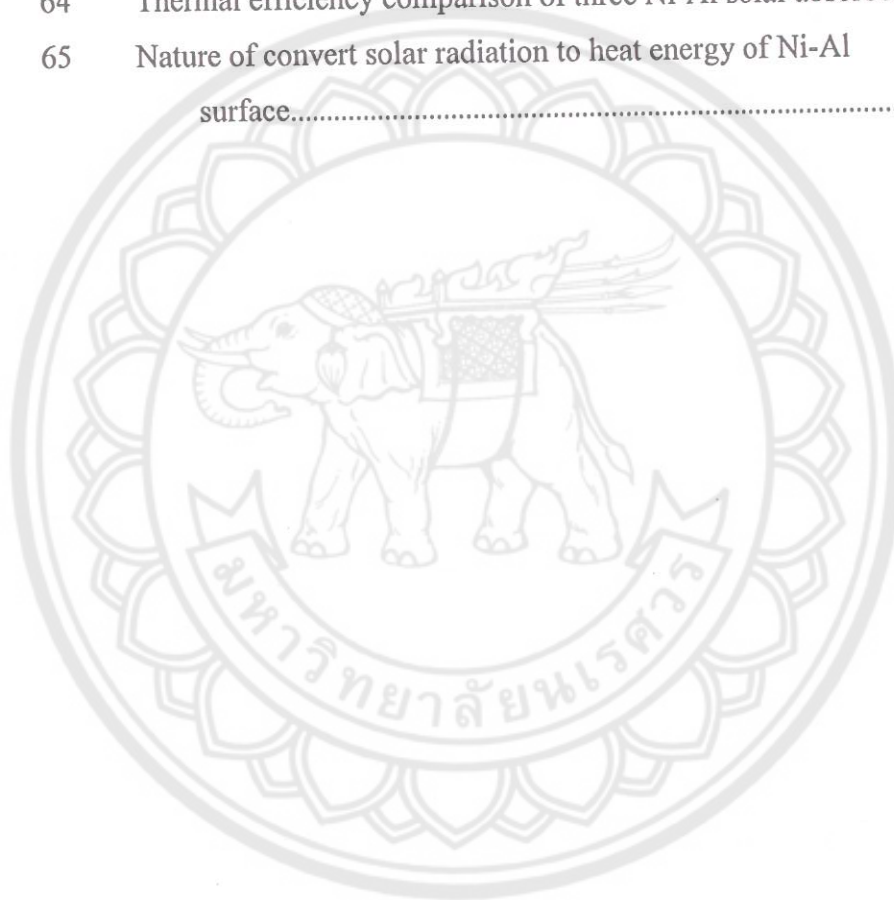
Figures		Page
23	Stainless steel 316L pipe substrate.....	42
24	(a) Thermal spray gun, FS, DS-8000 and (b) spraying process....	44
25	(a) number of roughness of AST, (b) air pressure for sand bath, and (c) sandblast room.....	45
26	Roughness of SS316L substrate.....	45
27	Expansion joint.....	46
28	Expansion joint with O-rings.....	47
29	Configurations of expansion joint.....	48
30	Solar receiver pipe for PTC.....	48
31	Steel structures of parabolic trough testing system.....	49
32	Structure of parabola made from wood.....	49
33	(a) Support reflector made from fiber graph, (b) Poly Ethylene Terephthalate film (PET) reflector.....	50
34	Install PET reflector on the parabola curve.....	51
35	PTC testing system.....	52
36	Heat loss testing system.....	53
37	Heater fin for heating absorber pipe.....	53
38	Thermocouple position achieved at parabolic trough receiver.....	54
39	One dimensional heat loss that occurs during laboratory testing.....	54
40	Open-loop thermal performance testing for PTC.....	57
41	(a) Sandblast stainless steel 316L non coated preparation surface, (b) Ni-Al surface.....	59
42	XRD patterns of Ni-Al powder and three thicknesses Ni-Al solar absorber, together with JCPDS of Ni, NiO, Al and Al ₂ O ₃	61

LIST OF FIGURES (CONT.)

Figures		Page
43	The morphology of (a) surface and (b) cross-section of Ni-Al solar selective surface average thickness 195 μm	62
44	The morphology of (a) surface and (b) cross-section of Ni-Al solar selective surface average thickness 215 μm	62
45	The morphology of (a) surface and (b) cross-section of Ni-Al solar selective surface average thickness 299 μm	62
46	EDS mapping analysis of NiAl coating surface.....	64
47	EDS mapping analysis cross section of NiAl cross-section coating.....	65
48	EDS line analysis on the cross-section of Ni-Al solar absorber.....	65
49	Sun spectrum at AM 1.5, Reflectance and solar absorptance of Ni-Al solar absorber average thickness 195 μm	67
50	Sun spectrum at AM 1.5, Reflectance and solar absorptance of Ni-Al solar absorber average thickness 215 μm	67
51	Sun spectrum at AM 1.5, Reflectance and solar absorptance of Ni-Al solar absorber average thickness 299 μm	68
52	Solar absorptance with differences thicknesses.....	68
53	Temperature distribution in the cylinder pipe at 100°C.....	71
54	Heat loss of Ni-Al solar absorber thickness 195 μm	73
55	Heat loss of Ni-Al solar absorber thickness 215 μm	74
56	Heat loss of Ni-Al solar absorber thickness 299 μm	74
57	Heat loss compare with commercial product with three Ni-Al solar absorber thickness of parabolic trough receiver.....	75
58	Emittance of Ni-Al solar absorber thickness 195 μm	77
59	Emittance of Ni-Al solar absorber thickness 215 μm	77
60	Emittance of Ni-Al solar absorber thickness 299 μm	78
61	Thermal efficiency of Ni-Al solar absorber thickness 195 μm	79

LIST OF FIGURES (CONT.)

Figures		Page
62	Thermal efficiency of Ni-Al solar absorber thickness 215 μm	80
63	Thermal efficiency of Ni-Al solar absorber thickness 299 μm	81
64	Thermal efficiency comparison of three Ni-Al solar absorber.....	82
65	Nature of convert solar radiation to heat energy of Ni-Al surface.....	85

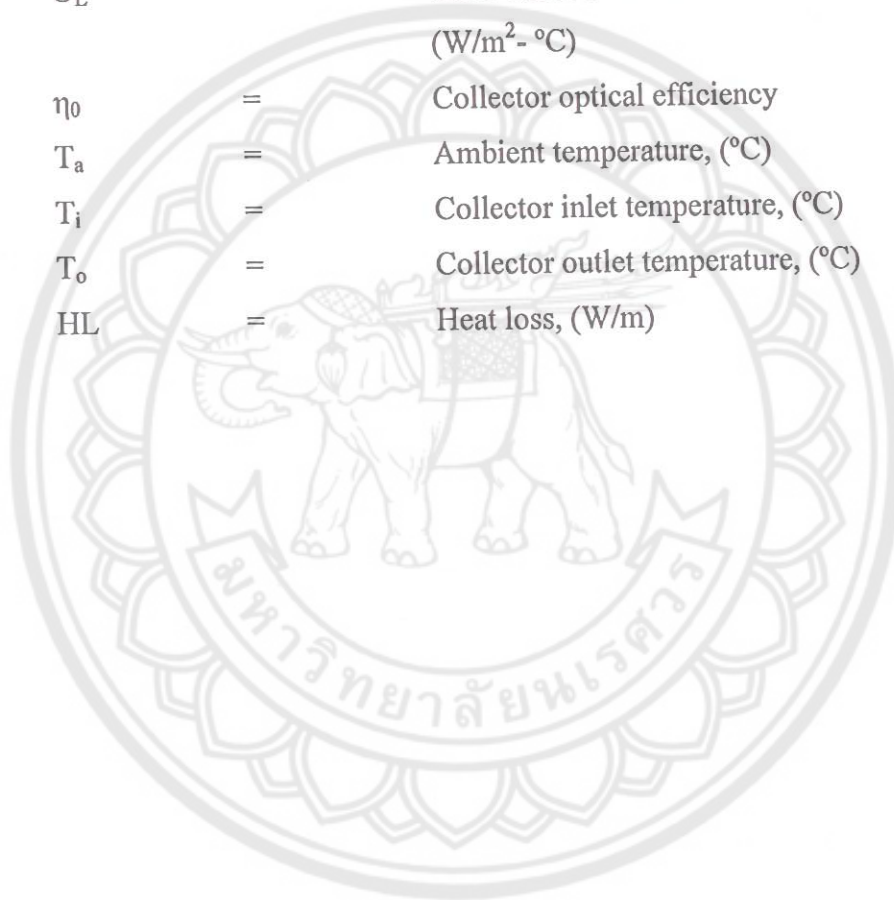


ABBREVIATIONS

α	=	Solar absorptance
R	=	Reflectance
τ	=	Transmissivity
λ	=	Wavelength, (m)
I_{sol}	=	Normal spectral irradiance of the solar radiation wavelength, ($W.m^{-2}.nm^{-1}$)
ε	=	Emittance
c	=	Concentration ratio
θ_{rim}	=	Rim angle
y	=	Horizontal axis
f	=	Focal distance, (m)
x	=	Vertical axis
D	=	Diameter, (m)
r_r	=	Radius, (m)
θ_m	=	A half acceptance
r	=	Radius of parabolic trough reflector, (m)
φ	=	Angle between the collector axis and reflector beam the focus
W_a	=	Collector aperture, (m^2)
h	=	heat transfer coefficient, ($W/m^2.K$)
T	=	Temperature, ($^{\circ}C$ or $^{\circ}K$)
Nu	=	Nusselt number
k	=	Thermal conductivity, ($W/m.K$)
σ	=	Stefan-Boltzmann constant, ($5.67 \times 10^{-8} W/m^2.K^4$)
L	=	Absorber length, (m)
G_B	=	Direct solar irradiance (W/m^2)
A_a	=	Absorber area, (m^2)
η	=	Efficiency

ABBREVIATIONS (CONT.)

\dot{m}	=	Mass flow rate of fluid, (kg/s)
c_p	=	Specific heat at constant pressure, (J/kg- °C)
Q_u	=	Useful energy collector, (J)
F_R	=	Heat removal factor
U_L	=	Solar collector overall heat loss coefficient, (W/m ² - °C)
η_0	=	Collector optical efficiency
T_a	=	Ambient temperature, (°C)
T_i	=	Collector inlet temperature, (°C)
T_o	=	Collector outlet temperature, (°C)
HL	=	Heat loss, (W/m)



CHAPTER I

INTRODUCTION

Background

On average, worldwide, energy from the sun is 1367 W/m^2 daily [1, 2]. Solar radiation can be converted to heat energy by using a solar collector [3]. The efficiency of the solar collector depends on the solar selective materials and typical coating process.

There are many variants of type and size of solar collectors and their use in any specific area or particular application depend on the amount of energy consumption which determines the physical area of the solar collector surface, sufficient to supply the energy consumption requirements. Of particular application is the type of solar collector, called concentrating solar collectors, that convert solar radiation to high heat energy [4, 5]. Concentrating solar collectors was able produced heat energy both flat-plate collectors and evacuated tube collectors because concentrating solar collectors use special reflector film to reflect solar radiation to a point of focus [6, 7]. It has applicate in many industries such as sterilization of food, equipment in the food industry, food drying and steam heating electrical power generating, which requires very high heat [8, 9].

A parabolic trough collector (PTC) system is based on a concentrating solar collector and the structure includes a parabolic trough as the solar collector, a reflector, with a controller mechanism. A PTC reflects the solar radiation collected on its parabolic surface to a point of focus [10]. The directional positioning of the parabola is important to ensure maximum solar radiation falling on the surface of the parabolic collector. This is controlled by the controller in the system. The point of focus of the parabolic collector is some form of tube or reservoir containing a fluid. Water is an appropriate working fluid which can be directly converted to steam [10, 11]. The surface coating of the PTC can comprise a variety of different coating materials, which can be applied by a number of different coating processes, such as sputtering [4, 12, 13, 14, 15, 16, 17, 18, 19], electrochemical application [20, 21, 22,

23, 24], anodization [17], sol-gel [17], electro-plating [17], spraying [17, 25, 26] and thermal spraying [17, 27]). Solar selective materials are often proprietary products sold by different companies, such as Black Crystal, Chrome Coat Energie Solaire, Thermo max, Sunstrip, Tekno Term Energi Showa, Solel, Turbo Sun [17], as listed in the report of C.E. Kennedy (2002). The composition of commercially available solar selective materials varies greatly, and include Ni-Sa, Cr-Cr₂O₃, TiN_xO_y, Ni-NiO_x, Ni, Al₂O₃, Mo-Al₂O₃, W-Al₂O₃, SS-AlN, Mo-AlN, NiAl [14, 15, 16].

Nickel-Aluminum alloy (NiAl) has been used as a surface coating, usually applied by the thermal spray technique [27]. There are many reasons for applying a surface coating of NiAl, such as corrosion resistance and creating a surface that can work in high temperatures. NiAl can sustain temperatures up to 1911 K. It has a density of 5.860 g/m³, giving a high strength surface and has high thermal conductivity (76 W/m. K), high modulus elasticity (193 GPa) and excellent corrosion resistance in high temperature applications [28, 29, 30]. NiAl can be applied as a surface coating by physical vapor deposition (PVD), electroplating or by combustion synthesis [28]. One of properties of NiAl has black color [25, 27] which provides good solar absorptance.

Flame spraying is a thermal spraying surface engineering technique which can be used for the application of NiAl which provides a coating thickness range of 50 μm upwards, on to many kinds of material; ferrous metal, metal alloys including aluminum alloys, ceramics and some polymers. The principle of thermal spraying is melting the material to be applied to a liquid or semi-liquid stage, then spraying the liquid onto the surface of the substrate with high pressure gas. The fast hardening particles form a structure of stacked layers called a lamellar structure. The melted or semi-melted coating being applied to the substrate disperses when hitting the surface and forms bonds among the coating particles which is an interlocking of the reflected and hardened particles known as mechanical bond [31]. One advantage of the thermal spray technique is a simple technique and is commonly used in industry. As well, it can be used to apply a surface coating to large surfaces.

Therefore, this work have objective to used Ni-Al as a solar absorber on stainless steel 316L pipe, prepared by the flame spray technique. The Ni-Al solar absorber was characterized by phase, morphology and chemical composition. The

solar absorptance (α) was also investigated and measured. The thermal analyzed thermal loss, calculated emittance (ϵ) and thermal performance.

Objectives of study

1. To study the materials, structure, and function of parabolic trough collector including available surface coating methods.
2. To coat the selective materials onto the solar receiver by flame spray and characterize the morphology of the coating surface with thickness variation in 50-300 μm .
3. To design and test the thermal efficiency of the receiver under the outdoor conditions.

Keyword

Flame spray technique, Ni-Al composite, solar collector, parabolic trough collector, solar absorber, Heat collecting element (HCE)

Limitation of the study

1. Coating Ni-5wt.%Al on the surface of 316L stainless steel pipe (long 1 m and thickness <3 mm) by flame spray technique.
2. Investigation of physical properties and thermal efficiency of new receiver prototype under the outdoor conditions.

Expectation of the study

1. To obtain the prototype of the solar collector's receiver with local cost and high efficiency.
2. To achieve the guidelines of flame spray technique for development the solar selective materials coating onto absorber pipe of the receiver.
3. To obtain the influence and characteristic of solar absorber material to surface coating of the receiver.

CHAPTER II

THEORIES AND RELATED LITERATURE

The Sun has an effective black body temperature of 5762 K. The biggest clean energy source is the sun. The sun's total energy output is $(1367 \text{ W/m}^2 \text{ every day } 3.8 \times 10^{20} \text{ MW})$, and the earth's receives only a tiny fraction of the total radiation emitted, equal to $1.7 \times 10^{20} \text{ kW}$ [1, 2]). The radiation which is most important to us is that emitted from the sun. The earth and its atmosphere lie within the ultraviolet, visible and infrared spectral regions [2, 3].

Solar radiation data are used in several forms and for a variety of purposes. The most detailed information available is beam and diffuse solar radiation on a horizontal surface, by hours, which is useful in simulations of solar processes [1]. The earth's orbit around the sun is such that the sun-earth distance varies only by 1.7% and since the solar radiation outside the earth's atmosphere is nearly of fixed intensities, the radiation energy flux received per second by a surface of unit area held normal to the radiation of sun ray at the mean earth-sun distance, outside the atmosphere, is practically constant throughout the year [32].

The solar energy collectors are special kinds of heat exchange that transform solar radiation energy to internal energy of the transport medium [9]. The solar absorbers on the substrate that absorbs the incoming solar radiation, converts radiation into heat, and transfer the heat to fluids (usually air, water, or oil) flowing through the collector. The most efficiency thermal solar collectors for hot water or steam production use a spectrally selective surface [33].

The two types of solar collector are divided two groups in motion design as stationary and tracking [34]. The solar collector as flat-plate collector (FPC), evacuated tube collector (ETC), compound parabolic collector (CPC), and parabolic trough collector (PTC) et al.

Solar selective materials and Coating technique

1. Solar selective material

The most efficient thermal solar collectors for hot water production are indicated by a spectral selective surface, which absorbs and converts solar radiation into heat energy [1, 35]. The requirements for coatings that control spectral selectivity are high solar absorptance (α) in solar wavelength (0.3-2.5 μm) [36] and low thermal emittance (ϵ) in the near-infrared (NIR) and far-infrared (FIR) [37, 38, 39, 40], as shown in Figure 1.

The higher or lower cutoff is dependent on the temperature. The operational temperature range of these materials for solar applications can be categorized as low temperature ($T < 100^\circ\text{C}$), middle temperature ($100^\circ\text{C} < T < 400^\circ\text{C}$), and high temperature ($T > 400^\circ\text{C}$) [40].

The beam of thermal radiation is incident on the surface of a body, it has the phenomena of reflection, absorption and transmission on the absorber surface, and part of transmitted through the body. The various properties associated with this beam incident is a fraction of the radiation reflected, called reflectivity (R); the fraction of radiation absorbed; called solar absorptance (α); and the fraction of radiation transmitted, called transmissivity (τ). The three quantities are related by the following Equation 1 [3].

$$R + \alpha + \tau = 1 \quad 1$$

Where

- R = Reflectivity
- α = Solar absorptance
- τ = Transmissivity

This study uses stainless steel 316L, an opaque material of high thickness. Solar radiation cannot transmit through this material. The transmissivity of stainless steel is, therefore, zero, $\tau = 0$

$$R + \alpha = 1 \quad 2$$

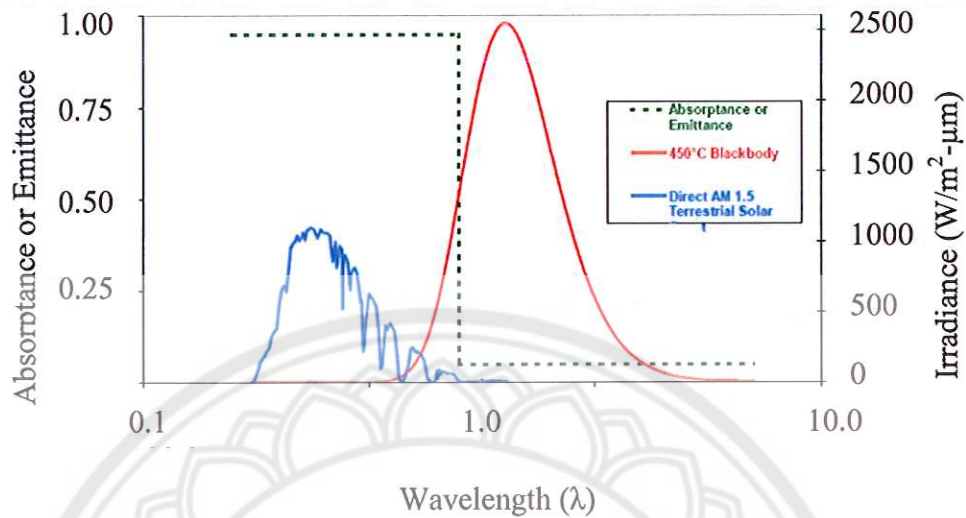


Figure 1 Spectral performance of an ideal selective solar absorber [40]

In Figure 1, the efficient photothermal conversion solar absorber surface must have high solar absorbance and low thermal emittance (ϵ) at operational temperature. A low reflectance ($R \approx 0$) at wavelengths (λ) $\leq 3 \mu\text{m}$ and a high reflectance ($R \approx 1$) at $\lambda \geq 3 \mu\text{m}$ characterize the spectrally selective surface [40].

T. Tuquabo, (2000), reports the standard spectral solar flux incident on the surface of the earth, after atmospheric absorption, is limited to the range between 0.3 and 2.5 μm UV (0-0.38 μm) / VIS (0.38-0.78 μm) / NIR ($> 0.78 \mu\text{m}$) wavelength ranges [3, 8, 41].

The solar absorbance (α) of a surface was one parameter that characterizes the performance of the absorber and defined as the weight fraction of the absorber radiation to incident on the surface, and give by Equation 3 [41, 42, 43, 44, 45].

$$\text{Solar absorbance, } \alpha = \frac{\int_{0.3 \mu\text{m}}^{2.5 \mu\text{m}} I_{\text{sol}}(\lambda)(1 - R(\lambda)) d\lambda}{\int_{0.3 \mu\text{m}}^{2.5 \mu\text{m}} I_{\text{sol}}(\lambda) d\lambda}$$

Where

λ = Wavelength, (nm)

I_{sol} = The normal spectral irradiance, ($\text{W}\cdot\text{m}^{-2}\cdot\text{nm}^{-1}$)

$R(\lambda)$ is the spectral reflectance of the surface and $I_{sol}(\lambda)$ is the normal spectral irradiance of the solar radiation wavelength (λ) [46-48] and using ASTM G173-03 Air Mass 1.5 [39] reference spectra derived from SMARTS v. 2.9.2 (Figure 2).

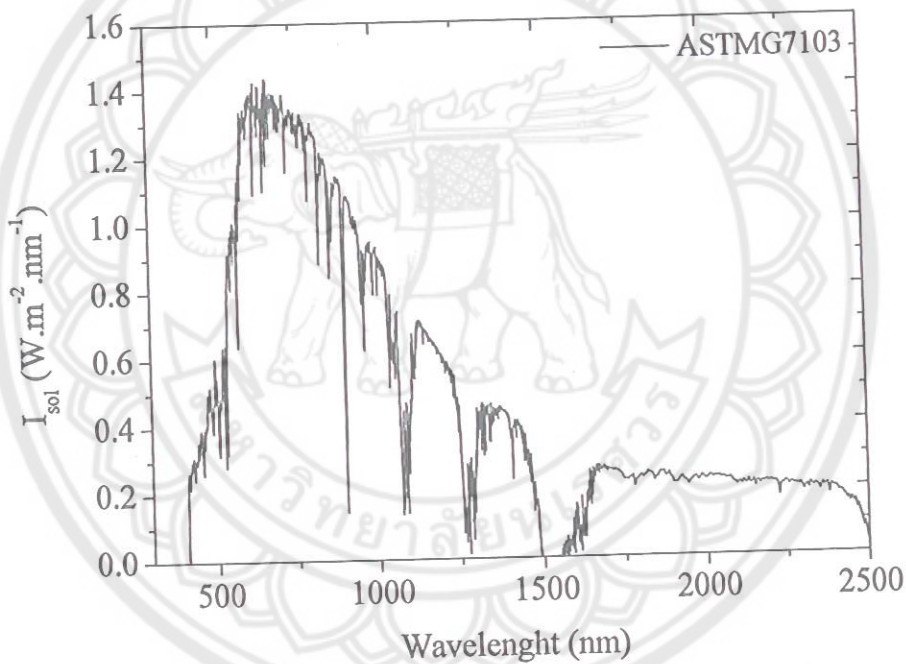


Figure 2 ASTM G173-03 Air Mass 1.5 reference spectra derived from SMARTS v. 2.9.2 [39]

Ni-Al composite coating is one of the intermetallic compounds used for special applications requiring a high melting point (1911 K), low density (5890 kg/m^3), excellent oxidation resistance up to 1573 K, high thermal conductivity and fabrication of a coating with a uniform composition [14, 49, 50]. Ni-Al composite coating have been extensively observed as having thermal and spectral selective properties. Nickel displays high solar absorptivity, good corrosion resistance, heat

resistance and durability, while aluminum exhibits high reflectivity in the IR region, which indicates low thermal emission from the solar absorber surface to the ambient environment [14].

NiAl-Al₂O₃ cermet coating is one of the solar selective absorber materials with high optical performance (α/ϵ) on Cu substrate (0.94/0.07) and stainless steel (SS) substrate (0.95/0.078) [51].

Al Shamaileh E. [14]. reported the thermal efficiency of different solar selective surfaces of two systems. She compared black paint mixed with Ni-Al and black paint coating on the surfaces of solar water heating systems (SWHSs). The result indicated that the optimum composition considered for further testing was 6% NiAl alloy by mass. The applicability of the NiAl alloy coating was tested over one year, spanning all four seasons. Two SHWS systems were used. One used the NiAl alloy coating, while the other used black paint as a coating. The test found that the new coating showed better performance when compared to ordinary black paint by an average of 5°C, over the experimental period of 1 year.

Xu, et al. [52]. observed that the corrosion resistance of the Ni-Al composite coating decreased with increasing Al content. They demonstrated by a galvanic corrosion test that a Ni-5wt%Al coating, prepared by plasma spray process, exhibited no surface corrosion, indicating that the formation of Al₂O₃ on the surface of the Ni-Al composite coating was the best anti-corrosion material [50, 53].

The solar collector must have high solar absorptance for radiation in the solar energy spectrum. At the same time, they lose energy through a combination of mechanisms, including thermal radiation from the absorber surface. It is desirable to have the long-wave emittance of the surface as low as possible to reduce loss. The temperature of this surface in most flat-plate collectors is less than 200°C, while the effective surface temperature of the sun is approximately 6000°C. Thus the wavelength range of the emitted radiate solar radiation is at the wavelength range of the emitted radiation, overlapping only slightly, from the solar spectrum. Under these circumstances, it is possible to devise a surface with high solar absorptance and low long-wave emittance, that is a selective surface [1].

Table 1 Solar selective materials and coating techniques review

Material	Substrate	Fabrication	Solar absorptance	Emittance	Reference
TiAlN/TiAl ON/SiO ₂	Cu	Magnetron sputtering	0.95	0.05	[54]
M-AlN	SS	DC-sputtering	0.92-0.96	0.04-0.05	[55]
CuO	Cu	Chemical conv.	>0.95	<0.07	[43]
AlNi-Al ₂ O ₃	Cu	Magnetron	0.94	0.07	[51]
	SS	sputtering	0.95	0.07	
Colored SS	SS	Chemical conv.	0.62-0.93	0.1	SEL, INCO [40]
Black Ni	Al		0.92	0.14	[56]
	iron	Spray pyrolysis	0.90	0.13	
	Steel	Electrodeposition	0.88-0.96	0.03-0.10	Maxorb [40]
Ni-Sn	Cu	Electrodeposition /Sol-gel	0.92-0.98	0.08-0.25	Black Crystal [40]
NbAlN/NbAl ON/Si ₃ N ₄	Cu	Magnetron sputtering	0.95	0.07	[5]
TiN _x O _y	Cu	ARE	0.92	0.06	Thermomax [40]
Al-N	Cu	DC magnetron sputtering			[57]
Ni-NiO _x	Al	Reactive sputtering	0.96	0.10	Sunstrip [40]
Al/Al ₂ O ₃ /Ni O _x	Al	Spray pyrolysis deposition	0.92	0.03	[58]
Ni-Al ₂ O ₃	Al	Chemical conv.	0.85	0.03	[59]
Ni	Al	Electrodeposited			[60]
NiAl	SHWSs	Paint			[14]

SS = Stainless steel

SHWSs = Solar Hot Water System

A list of solar selective materials are shown in Table 1. The table indicates difference types of surfaces that have increased thermal stability for solar collectors. The application of solar selective surfaces are used in absorber surfaces to absorb solar intensity in global and direct radiation of non-concentrating solar collectors and concentrating solar collectors. Many solar selective materials use different types of collector and substrate as, shown in Table 1.

The materials can absorb solar intensity of all wavelengths of sun rays. The optical performance of the collector is determined by its solar absorptance. The optical properties of the material are measured and present in its solar absorptance properties. Emittance, that is, optical loss from the surface, is low. Emittance refers to optical losses due to all causes, including heat radiation, reflection, the neon effect, etc.

All collectors, regardless of type, use solar selective materials. All the materials used, have high solar absorptance and low emittance. The materials selected due to their reported efficiency in absorbing solar radiation of the solar selective surface. There are no reports, at present, relating to the optical properties of Ni-Al prepared using a flame spray coating technique and applied to parabolic trough collector surfaces.

2. The solar selective coating techniques

Target of papering the selective surface for optical properties were required the highest α and ϵ . The selective surface can be obtained by difference method, i.e. chemical, physical and electrochemical [61]. In Table 1, the solar selective materials were coated by difference technique. All process coated selective surface are required high solar absorptance and decrease thermal emittance. The techniques such as sputtering coating technique, Chemical process, Spray pyrolysis and Paint.

Jeffery Gordon [62]. reported the technique for coating surface as vacuum technique, chemical and electrochemical process. The coating surface as electroplating, anodization, chemical conversion, evaporation, sputtering and paints.

Electroplating process coated, process of sample passing electric current in metallic salts solution. The positive ions moving to negative ions (Cathode). The coating surface consist overlays of position ions get to coating surface. The most

widely used selectively solar-absorbing surface seems to be “black chrome”, which is a complex composite of metallic chrome and dielectric Cr_2O_3 . The metal concentration is graded, as described in the previous section. The selective solar absorption appears to be a result of the combination of the effect of the metal-dielectric composite and of the pronounced surface roughness that has been observed in these films. Black chrome has a high void fraction and consists of rounded particles with size of about 100 nm. The chrome crystallites are smaller, though, with size of the order of 10 nm, and are probably embedded in the oxide phase. The original work on black chrome for solar energy applications was carried out by McDonald, who modified the procedure for making decorative electroplated layers. Several commercial coating are presently produced by MTI Inc., Energies Solaire AS and Batec A/S. The MTI and Batec black chrome coating are deposit on nickel plated copper, and the Energie Solaire coating is backed by stainless steel. The spectral selectivity is large and approximately matches the ideal property. The MTI coating has $\alpha_{\text{sol}} \approx 0.97$ and $\epsilon_{\text{therm}}(100^\circ\text{C}) = 0.09$ [62].

Anodization and electroplating, the commercially produced selectively solar-absorbing coating comprise metallic Ni particles embedded in anodic Al_2O_3 . The initial work was by Andersson, et al. [62]. These coating are made in a two-step process with an initial anodization of aluminum sheet in dilute phosphoric acid. This treatment transforms the surface layer of the metal into porous Al_2O_3 with pore channels perpendicular to the surface which extend through the oxide layer. Subsequently metal is precipitated inside the pores by AC electrolysis in a bath containing nickel sulphate. Metal particles are formed as rods in the pore channels with diameter of about 30-50 nm and a length of about 300 nm. The pore volume fraction is about 30%. By using other metal sulphates in the second step, one can precipitate particles of other metals. A detailed study of the relation between deposition conditions. The coating comprises a nickel pigmented Al_2O_3 layer located under a porous Al_2O_3 layer. The porosity is highest at the outer surface. The bottom of the coating consists of a thin compact Al_2O_3 sheath serving as diffusion barrier [62].

Chemical conversion, the coating that have been commercially produced, one should note a chemically treated rough nickel surface, know under the trade name MAXORB. The spectral selectivity of this absorber is very good with solar absorptance $\alpha_{\text{sol}} \approx 0.93$ and emittance $\epsilon_{\text{therm}}(100^\circ\text{C}) \approx 0.13$ [62].

Evaporation, a selective solar absorber consisting of a cermet of TiN_xO_y on copper and AR coated with silicon dioxide is produced by activated reactive evaporation. The titanium oxynitride has a columnar structure, and the thickness of the optimized coating is in total 150 nm including the AR layer of 95 nm. The German company TiNO_x GmbH has commercialized this absorber and uses roll coating in their manufacturing process. The spectral selectivity is characterized $A_{\text{sol}} = 0.95$ and a thermal emittance of 0.05 at 100°C . The absorber is thermally stable up to 400°C [62].

Sputtering, sputtering coating technique deposited molybdenum-based composite coating for use on large-scale tubular solar collectors designed to operate at $\tau > 300^\circ\text{C}$. The microstructure of the absorber, embodies two graded Mo-dielectric composite layers backed by an infrared reflecting molybdenum layer. An anti-reflecting SiO_2 layer at the top and a diffusion barrier of Al_2O_3 at the bottom complete the design [62]. P. R. Gordo, et al. [57], using sputtering coating technique coated the Al-N on outside of tubular and long substrate. A hollow magnetron cathode and its vacuum system has been designed and constructed to coat 2 m long heat pipe absorbers and fluid pipe absorber tubs with a selective film of aluminum nitride. The technique was optimized to get maximum absorbance of the film in the solar spectrum substrate. Reflectivity of less than 1% at the wavelength of 550 nm and excellent adhesion were obtained.

Paints, selective solar absorbing paints have also recently reached commercialization, and there are at least two such products on the market: the Solarect-ZTM paint developed at the National Institute of Chemistry in Ljubljana, Slovenia, and the SolkoteHI/SORB-IITM paint sold by SOLEC, USA [62].

In solar selective process, many technique were used and reported in Table 1 bur one of interesting coating process is thermal spray coated technique. The thermal spray technique is not a complicated process, allows a high production rate, is a rapid process and has low environmental impact and low cost. As well, this technique can be used as a coating application in an open environment and can also be used for recoating cracked surfaces. The major coating processes: flame, plasma arc, and electric arc, with many of their subsets. Each of these processes encompasses many more subsets, and each has its own characteristic range of temperature, enthalpy, and velocity. These attributes in turn develop coating characteristics that are unique to each process; in the

simplest terms these include coating bond strength, porosity, inclusions, and hardness [13].

S. Sampath, et al. [63]. Study examines three thermal spraying techniques (air plasma spraying; APS, twin-arc spraying; TWA and high velocity oxy-fuel; HVOF) with significantly different particles temperatures and velocities. For comparison purpose the recently developed cold spray processed materials. Each method, in-flight particles.

O. Culha, et al. [64]. Study the microstructural, thermal and mechanical properties of NiAl coating fabricated on 316L stainless steel substrate by using-velocity oxygen fuel (HVOF) method. The effect of thermal cycling on the failure behavior of the Ni-Al based coating has been carried out without an external load at temperature between 47°C and 600°C for the period of 303s cycles. XRD pattern revealed that Ni-Al based coating had Ni₃Al phase on surface, cross-sections demonstrated excellent homogeneity and uniformity. The coating processed low oxide content, low porosity and superior contact with the substrate. The thickness of the Ni-Al based layer is 595 μm.

Coating can be thought of as engineering solutions to enhance surfaces against wear, corrosion, thermal degradation and other surface phenomena. Acceptable coating are generally characterized by good adhesion, substrate compatibility, and low porosity. An acceptable coating process must also be compatible with physical substrate constraints such as temperature and geometry. These coating/substrate attributes include coefficient of thermal expansion (CTE) matching, appropriate edge radii, substrate melting point, and chemical compatibility during deposition and service. Thermal spray can be tailored to meet many of these requirements. Key aspects of the process are illustrate, which shows particles impacting a prepared surface and building up a lamellar structure characteristic of the thermal spray process [13], shown in Figure 3.

3. Thermal spray coating techniques

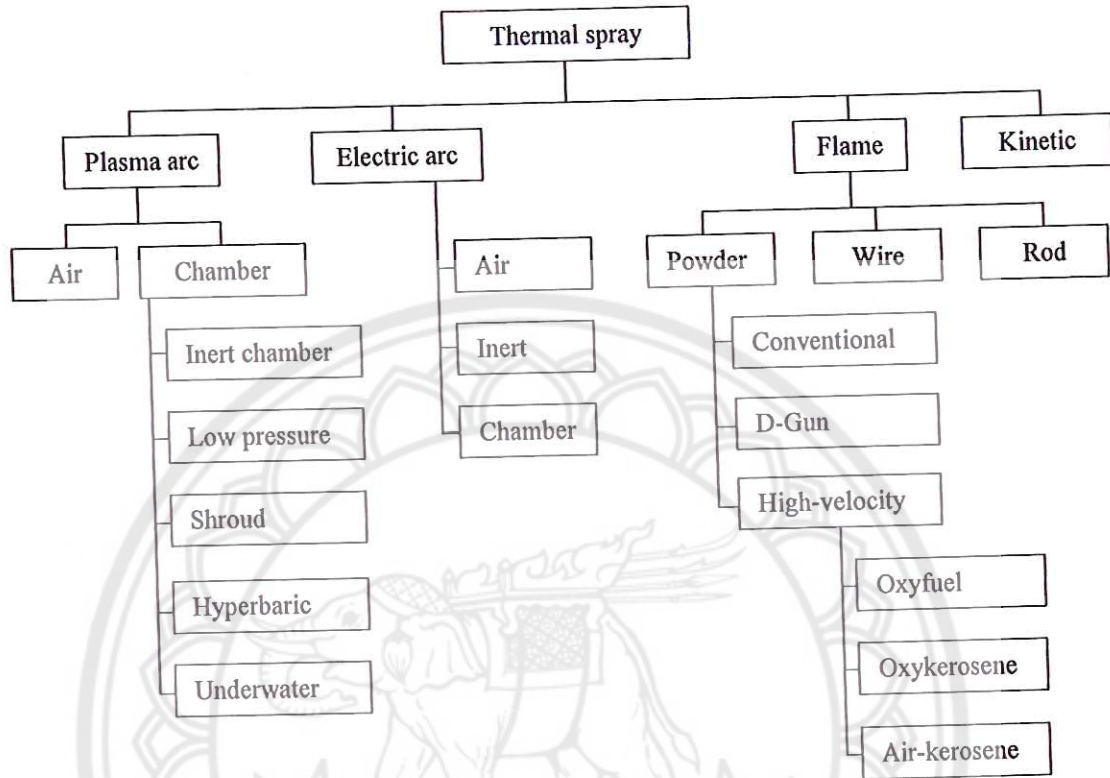


Figure 3 Thermal spray process [13]

Table 2 Thermal spray process comparisons [13]

Process	Gas flow	Temperature	Velocity	Relative adhesive strength	Oxide content, %
	m ³ /h	°C	m/s		
Flame Spraying	11	2200	30	3	6
Atmospheric Plasma Spraying	4.2	5500	240	6	0.5-1
ARC Spraying	71	5500	240	6	0.5-3
High-Velocity Oxy-Fuel	28-57	3100	610-1060	8	0.2
Vacuum Plasma Spraying	8.4	8300	240-610	9	-
1(low) to 10 (high)					

Thermal spray technique was a process in which molten, semi-molten or solid particles are deposited on substrate. The spraying technique was a way of generating a “stream” of such particles. Coating can be generated if the particles can plastically deform at impact with the substrate, which may only happen if they are molten or solid and sufficiently rapid. Their heating and/or acceleration are practical if they occur in a stream of gas. Thus, an academic classification of spray technique is based on the way of generation of such streams [13].

Flame spraying (FS)

Conventional flame spray was the first thermal spray process developed (~1910s) and is still in common use. Modern torches have changed little since the 1950s. Flame spray uses the chemical energy of combusting fuel gases to generate heat [65].

Flame spraying was chronologically the first spraying technique. Powder Flame Spraying (FS-Powder), the chemical energy of combustion of the fuel gas in oxygen was used to generate a hot flame. The gas inlet is axial (1) and powder (2) can be introduced axially or perpendicularly to the torch (3). The particles become molten in the flame (6) and accelerated in the direction of the work piece (4). The modern powder flame spraying trough, [65] was shown in Figure 4 and Table 2

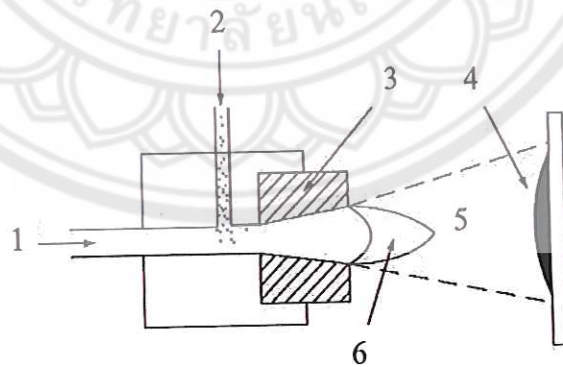


Figure 4 Schematic of flame spraying of a powder [65]

Atmospheric Plasma Spraying (APS)

The plasma generator, consists of a circular anode (1), usually of copper, and a cathode of throated tungsten (2). The cathode is made of graphite in a water-stabilized torch. The electric arc discharge, supported by a generator through the connectors (3, 4) heats up the working gases (5), which expand in the atmosphere, forming a jet. The powder (6), suspended in a carrier gas, is injected into the jet. The particles of the powder after being melted and accelerated in the jet impact the substrate and form the coating [65], are shown in Figure 5 and Table 2.

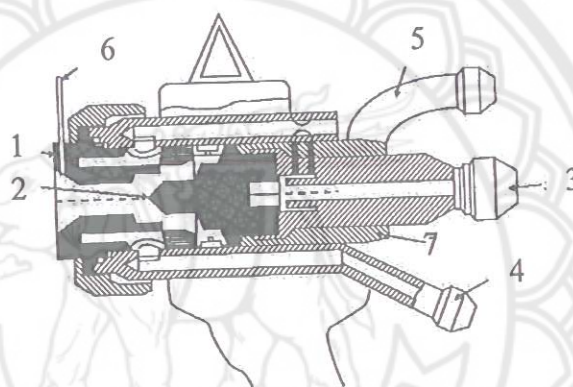


Figure 5 Schematic of a section of a plasma torch [65]

ARC Spraying (AS)

A schematic of an AS installation. Two wires (5), being consumable electrodes, are drawn from spools and form a liquid droplet due to arc heating (4). The droplet is blown by the atomizing gas (1). The gas atomizes the molten droplet and propels fine particles (3) towards a substrate. If the wires are made of different metals, a 'pseudo-alloy' coating can be produced [65], was shown in Figure 6 and Table 2

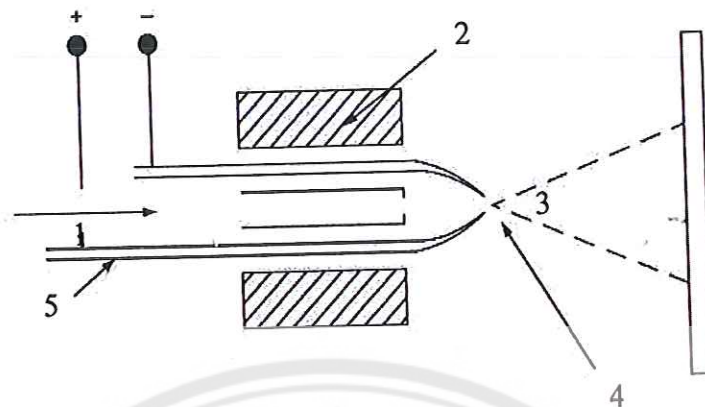


Figure 6 Schematic of an arc-spraying installation [65]

High-Velocity Oxy-Fuel (HVOF) spraying

In HVOF process, the fuel gas or liquid is introduced into the combustion chamber with oxygen. An ignition initiates the combustion and the exhaust gas, formed by a nozzle, passes through a barrel and emerges into the open atmosphere. The powder is introduced radially or axially into the jet. The combustion chamber, nozzle and barrel are intensively cooled by water [65], was shown in Figure 7 and Table 2

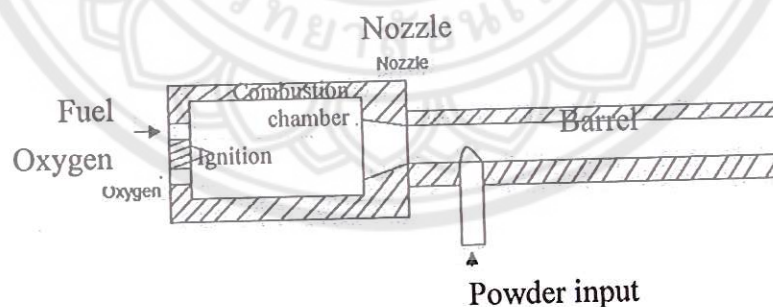


Figure 7 Schematic of an HVOF torch [65]

Vacuum Plasma Spraying (VPS)

A vacuum plasma spraying installation was composed of a plasma torch with in nozzle (2) supplied by the working gases (1) and an electric arc generated (6). Powder is introduced by a port (5) to a plasma jet working in a vacuum (3). An

additional transfer arc (4) is used to clean up and heat the surface prior to spraying [65], was shown in Figure 8 and Table 2.

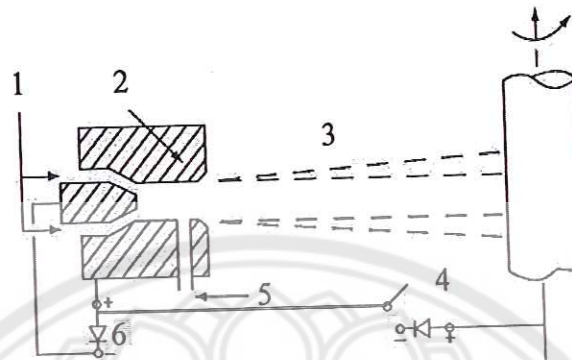


Figure 8 Schematic of the vacuum plasma spraying process [65]

Solar collector

Solar energy collectors are special kinds of heat exchange that transform solar radiation energy to internal energy of the transport medium. The major component of any solar system is the solar collector. This is a device that absorbs the incoming solar radiation, converts it into heat, and transfers the heat to a fluid flowing through the collector. The solar energy collected is carried from the circulating fluid either directly to the hot water or space conditioning equipment or to a thermal energy storage tank, from which it can be drawn for use at night or on cloudy days [9].

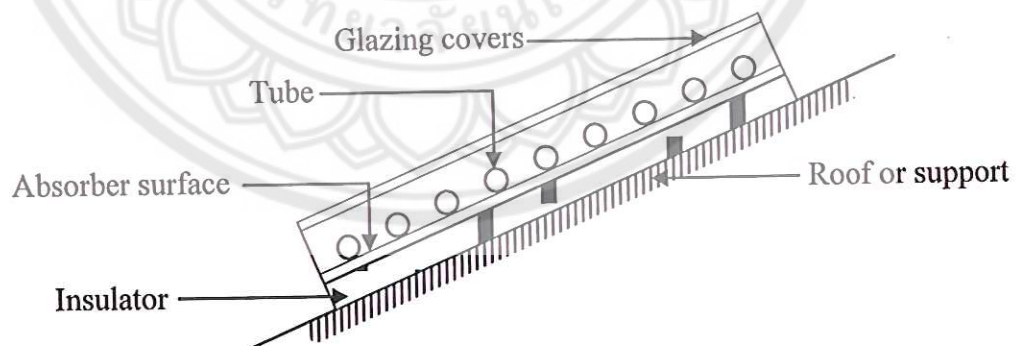
There are basically two types of solar collector: non-concentrating and sun-tracking concentrating solar collector. A non-concentrating collector has the same area for intercepting and absorbing solar radiation. Solar collector can also be distinguished by the type of heat transfer liquid used and whether they are covered or uncovered. A large number of solar collectors are available on the market [9], as shown in Table 3.

Table 3 Two types of solar collector [3, 9]

Motion	Collector type	Absorber type	Concentration ratio	Indicative temperature range (°C)
Stationary	Flat plate collector (FPC)	Flat	1	30-80
	Evacuated tube collector (ETC)	Flat	1	50-200
	Compound parabolic collector (CPC)	Tubular	1-5	60-240
Sun tracking	Liner Fresnel reflector (LFC)	Tubular	10-40	60-250
	Parabolic trough collector (PTC)	Tubular	14-45	60-300
	Cylindrical trough collector (CTC)	Tubular	10-50	60-300
	Parabolic dish reflector (PDR)	Point	100-1000	100-500
	Heliostat field collector (HFC)	Point	100-1500	150-2000

Table 3 shown sun tracking collector as Liner Fresnel reflector (LFC), Parabolic trough collector (PTC), Cylindrical trough collector (CTC), Parabolic dish reflector collector (PDR) and Heliostat field collector (HFC). There are concentrating collectors, concentration ratio between 10-1500, indicative temperature range 60-2000°C [3].

1. Flat-Plate solar Collector (FPC)

**Figure 9 Cross-section of flat plate solar collector**

“Flat-plate” solar collector is an energy conversion device that absorbs solar radiation and transfer the energy to a working fluid passing through the collector, shown in Figure 9. A flat-plate collector does not concentrate incident energy before

absorption, hence, it is able to collect both direct and diffuse components of radiation. Flat-plate collectors are used primarily for air and water heating [62].

The advantages of flat-plate collectors are inexpensive to manufacture, they collect both beam and diffuse radiation, and they are permanently fixed and position, so no tracking of the sun is required. The collector should be oriented directly toward the equator, facing south in the Northern Hemisphere and north in the Southern Hemisphere. The optimum tilt angle of the collector is equal to the latitude of the location, with angle variations of 10° to 15° more or less, depending on the application [34].

2. Evacuated Tube Collector (ETC)

Evacuated tube collector consist of an absorbing surface mounted in a vacuum to eliminated convection heat loss. Two forms of evacuated tubular absorbers are used: all-glass Dewar type and the single glass envelop metal-fin-in vacuum type [62], as shown in Figure10.

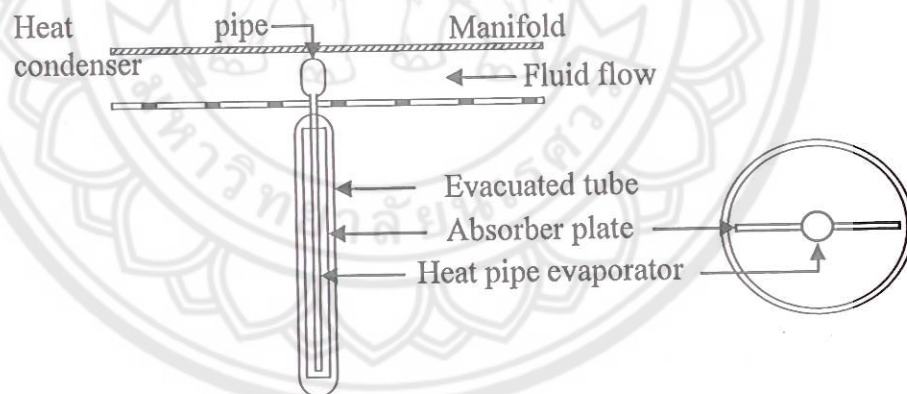


Figure 10 Diagram of an evacuated tube collector

3. Compound Parabolic Collector (CPC)

Compound parabolic collector are non-imaging concentrators. They have the capability of reflecting to the absorber all of the incident radiation within wide limits. Their potential as collectors of solar energy was pointed. The necessity of moving the concentrator accommodate it change solar orientation can be reduced by using a trough with two sections of a parabola facing each other [34], as shown in Figure 11.

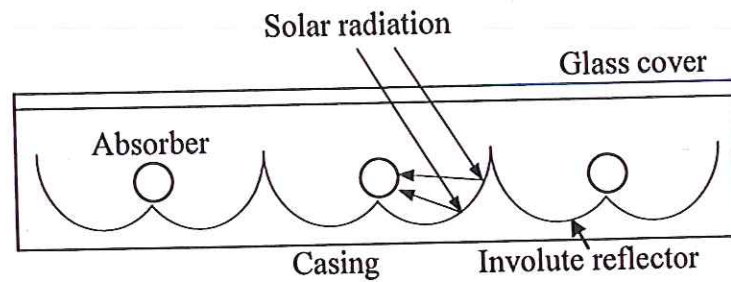


Figure 11 Diagram of compound parabolic collector

4. Liner Fresnel reflector (LFR)

Fresnel collectors are two variations: the Fresnel lens collector (FLC) and the linear Fresnel reflector (LFR) are shown in Figure 12 (a). The focus made from a plastic and shaped in the way show to focus the solar rays to point receiver, whereas the latter relies on an array of linear receiver. The LFR collector can be imagined as a broken-up parabolic trough reflector, showed in Figure 12(b) but difference parabolic troughs, the individual strips need not be for parabolic shape [34].

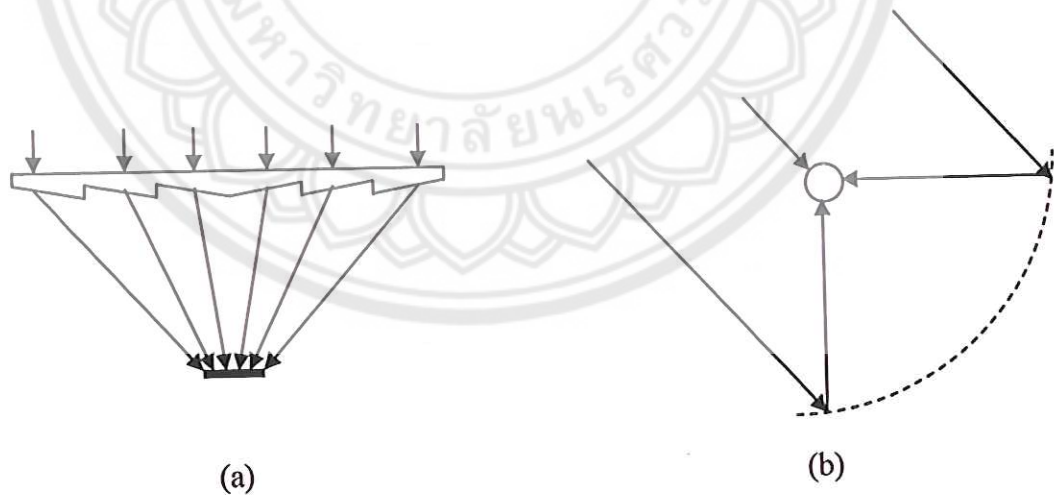


Figure 12 Fresnel collector, (a) Fresnel lens collector (FLC),
(b) Liner Fresnel-type parabolic trough collector

5. Parabolic Dish Reflector (PDR)

A parabolic dish reflector (PDR), shown in Figure 13, is a point-focus collector that tracks the sun in two axis, concentrating solar energy onto a receiver located the focus point of the dish. The dish structure must fully track the sun to reflect the beam into the thermal receiver. For this purpose, tracking mechanisms similar to the ones described in the previous section are employed in double, so the collector is tracked two axis. The receiver absorbs the radiant solar energy, it converted into thermal energy in a circulating fluid. The thermal energy can transfer to electricity using an engine-generator coupled directly to the receiver or transported through pipes to a central power conversion system. Parabolic dish systems can achieve temperature 1500°C. It was replayed that the receiver distributed throughout a collector field. The parabolic dishes are often called distributed receiver systems. Parabolic dishes have several important advantages [9].

The main use of this type of concentrator is for the parabolic dish engine. A parabolic dish engine system is an electric generator that used sunlight instead of crude oil or coal to produce electricity. A Parabolic dish system that generates electricity from a central power convertor the absorbed sunlight from individual receiver and deliver it via a heat transfer fluid to the powder conversion systems. The need to circulate heat transfer fluid throughout the collector field raises design issues such as piping layout, pumping requirement, and thermal losses [9].

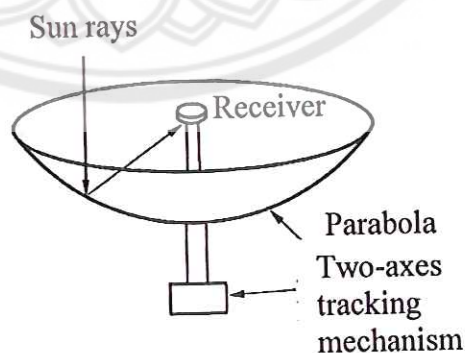


Figure 13 Parabolic dish collector [9]

6. Heliostat Field Collector (HFC)

For extremely high inputs of radiant energy, a multiplicity of flat mirrors, or heliostats, using altazimuth mount can be used to reflect their incident direct solar radiation onto a common target, shown in Figure 14. This is called the heliostat field or central receiver collector. By using slightly concave mirror segments on the heliostats, large amounts of thermal energy can be directed into the cavity of a steam generator produce steam at high temperature and pressure. The concentrated heat energy absorbed by the receiver is transferred to a circulating fluid that can be stored and later used to produce power. Central receivers have several advantages [9].

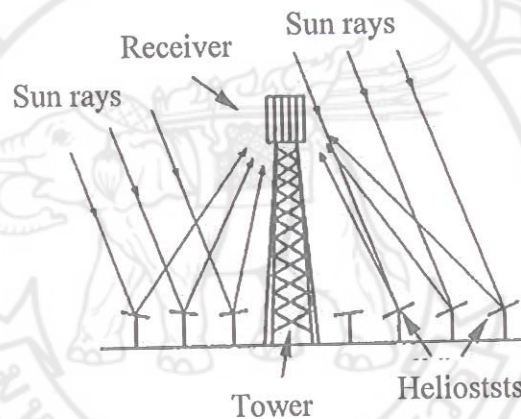


Figure 14 Schematic of central receiver system [9]

Each heliostat at a central receiver facility has from 50 to 150 m² of reflective surface, with four mirrors installed on a common pillar for economy. The heliostats collect and concentrate sunlight onto the receiver, which absorbs the concentrated sunlight, transferring its energy to a heat transfer fluid. The heat transfer system, which consists primarily of pipes, pumps, and valves, directs the transfer fluid in a closed loop among the receiver, storage, and power conversion system. A thermal storage system typically stores the collected energy as sensible heat for later delivery to the power conversion system. The storage system also decouple the collection of solar energy from its conversion to electricity. The power conversion system consists of a steam generator, turbine generator, and support equipment, which convert the thermal energy into electricity and supply it to the utility grid [9].

7. Parabolic Trough Collector (PTC)

Parabolic trough collector are made by bending a sheet of reflective material into parabolic shape. A black metal tube, covered with a glass tube to reduce heat losses, is place along focal line of receiver. Shown in Figure 15. When the parabola pointed toward the sun, parallel rays incident on the reflector are reflected onto receiver tube. The concentrated radiation reaching the receiver tube heats the fluid that circulates through it, thus transforming the solar radiation into useful heat. It is sufficient to use a single-axis tracking of the sun [34].

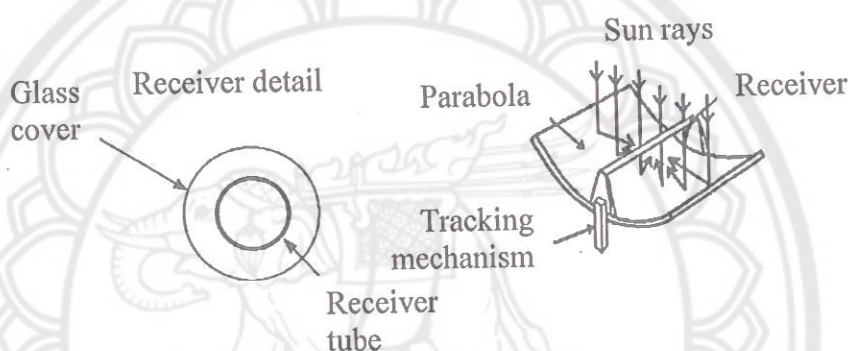


Figure 15 Parabolic trough collector (PTC) [34]

Soteris A., (2009) reported about stationary of solar collector as flat plate collector (FPC), Evacuated tube collector (ETC) and Compound parabolic trough collector (CPC), all of stationary have concentration ratio (c), (Concentration ratio is rasion between absorber area and reflected area) 1-15 can indicative temperature range 30°C - 240°C up to concentration ratio. There stationary collectors are permanently fixed in position and do not track the sun [3].

Parabolic trough collector designs

Cross-section of parabolic trough was showed in Figure 16, and characteristics of the parabolic trough collector system in Table 1 for design parabolic trough collector. The incident radiation on the reflector at the rim of the collector makes an angle (θ_{rim}) with the center line of the collector. The equation of the parabola in terms of the coordinate system is [34].

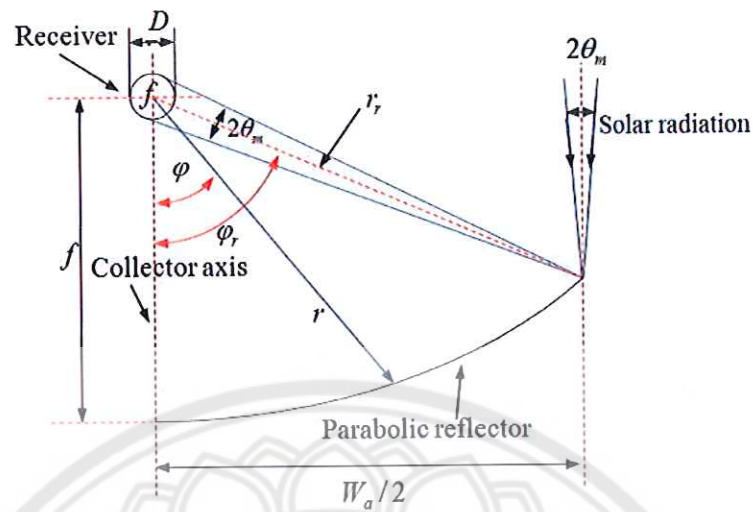


Figure 16 Cross-section of a parabolic trough collector with circular receiver [34]

$$y^2 = 4fx$$

4

Where

f = Parabola focal distance, (m)

y = Horizontal axis

x = Vertical axis

For specular reflector of perfect alignment, the size of the receiver (diameter, D) required to intercept all the solar image can be obtained from trigonometry, given by

$$D = 4 r_r \sin \theta_m$$

5

Where

θ_m = A half acceptance angle, (degree)

D = Diameter of the receiver, (m)

r_r = Radius of θ_m , (m)

For a parabolic reflector, the radius, r is given by

$$r = \frac{2f}{1 + \cos(\varphi)} \quad 6$$

Where

φ = Angle between the collector axis and a reflector beam the focus,
(degree)

r = Radius of parabolic reflector, (m)

As φ varies from 0 to φ_r , r increase from f to r_r and the theoretical image size increase from $2f \sin(\theta_m)$ to $2r_r \sin(\theta_m) / \cos(\varphi_r + \theta_m)$. Therefore, there is an image spreading on a plane normal to the axis of the parabola

$$r_r = \frac{2f}{1 + \cos(\varphi_r)} \quad 7$$

Another important parameter related to the rim angle is the aperture of the parabola, W_a

$$W_a = 2r_r \sin(\varphi_r) \quad 8$$

$$W_a = \frac{4f \sin(\varphi_r)}{1 + \cos(\varphi_r)} \quad 9$$

$$W_a = 4f \tan(\varphi_r/2) \quad 10$$

Where

W_a = Collector aperture, (m^2)

Collector thermal analysis

Heat transfer

Parabolic trough collector performance model is based on energy balance about the collector. The energy balance includes the direct normal solar irradiation incident on the collector, optical losses from collector.

One-Dimensional energy balance model

The parabolic trough collector (PTC) model uses an energy balance between the heat transfer fluid and the atmosphere, and includes all equations and correlations necessary to predict the terms in the energy balance, which depend on the collector type, PTC condition, optical properties, and ambient conditions [66]. The Figure 17(a) shown the one-dimensional steady-state energy balance for a cross-section of parabolic trough collector and (b) shown the thermal resistance model and subscript definitions.

Convection heat transfer between the heat transfer fluid and absorber, from Newton's law of cooling, the convection heat transfer from the inside surface of the absorber pipe to the heat transfer fluid is

$$q_{12\text{conv.}} = h_1 D_2 \pi (T_2 - T_1) \quad 11$$

With

$$h_1 = \text{Nu}_{D_2} \frac{k_1}{D_2} \quad 12$$

Where

- h_1 = Heat transfer fluid convection heat transfer coefficient at T_1 ,
($\text{W}/\text{m}^2 \cdot \text{K}$)
- D_2 = Inside diameter of the absorber pipe, (m)
- T_1 = Mean (bulk) temperature of the heat transfer fluid, ($^{\circ}\text{C}$)
- T_2 = Inside surface temperature of absorber pipe, ($^{\circ}\text{C}$)
- Nu_{D_2} = Nusselt number based on D_2
- k_1 = Thermal conductivity of heat transfer fluid at T_1 , ($\text{W}/\text{m} \cdot \text{K}$)

In these equations, both T_1 and T_2 are independent of angular and longitudinal parabolic trough collector, as will be all temperature and properties in the one-dimensional energy balance model.

The Nusselt number depend on the type of flow through the parabolic trough collector. At typical operating conditions, the flow in a PTC is well within the turbulent flow region. However, during off-solar hour or when evaluating the PTC heat loss on a test platform, the flow in the PTC at lower temperature. Therefore, to model the heat losses under all conditions, the model includes conditional statements to determine type of flow. The Nusselt number used for each flow condition is outlined [66].

Conduction heat transfer through the absorber wall, Fourier's law of conduction through a hollow cylinder describes the conduction heat transfer through the absorber wall.

$$q_{23\text{cond.}} = \frac{2\pi k_{23}(T_2 - T_3)}{\ln\left(\frac{D_3}{D_2}\right)}$$

13

Where

k_{23} = Absorber thermal conductance at the average temperature $(T_2+T_3)/2$, (W/m. K)

T_2 = Absorber inside surface temperature, (K)

T_3 = Absorber outside surface temperature, (K)

D_2 = Absorber inside diameter, (m)

D_3 = Absorber outside diameter, (m)

Heat transfer from the absorber to the glass envelope, convection and radiation heat transfer occur between the absorber and the glass envelop. The convection heat transfer mechanism depends on the annulus pressure. At low temperature ($< \sim 1$ torr), the heat transfer mechanism is molecular conduction. At higher pressure ($> \sim 1$ torr), the mechanism is free convection. The radiation heat transfer occurs because of the difference in temperature between the outer absorber

surface and the inner glass envelop surface. The radiation heat transfer calculation is simplified by assuming the glass envelope is opaque to infrared radiation and assuming gray ($\rho = \alpha$) surface [66].

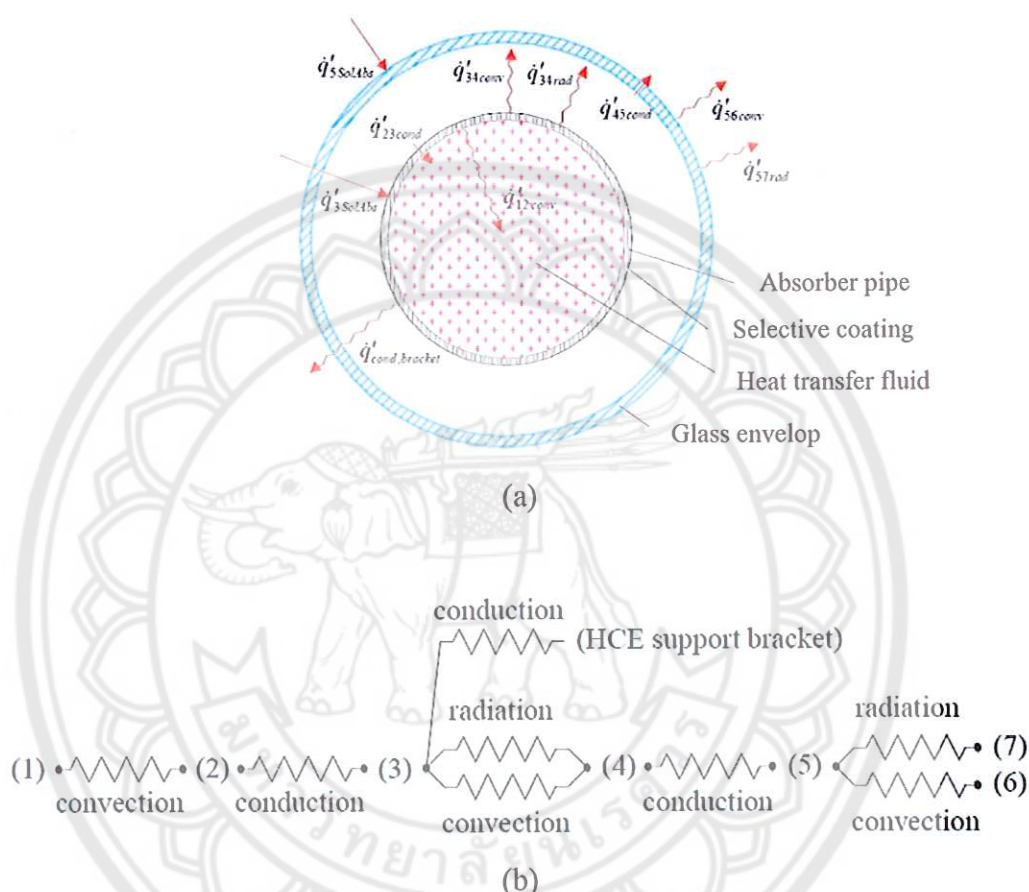


Figure 17 (a) One-dimensional steady-state energy balance and (b) thermal resistance model [66]

Figure 17 (a) shown the one-dimensional steady-state energy balance for a cross-section of parabolic trough collector with glass envelope, and Figure 17 (b) shown the thermal resistance model and subscript definitions. For clarity, the incoming solar energy and optical losses have been omitted from the resistance model. The optical losses are due to imperfections in the collector mirrors, tracking errors, shading, and mirror and parabolic trough collector cleanliness. The effective incoming solar energy is an absorbed by the glass envelope and the absorber selective coating.

Some energy that was absorbed into the selective coating was conducted through the absorber and transfer to the heat transfer fluid by convection; remaining energy is transmitted back to the glass envelope by convection and radiation and lost through the parabolic trough support bracket through conduction. The energy from the radiation and convection then passes through the glass envelop by conduction and along with the energy absorbed b glass envelop was lost to the environment by convection and radiation [66].

Radiation heat transfer, the radiation heat transfer between the absorber and glass envelope (q_{34rad}) is estimated with the following Equation 14

$$q_{34rad} = \frac{\sigma \pi D_3 (T_3^4 - T_4^4)}{\left(\frac{1}{\epsilon_3} + (1 + \epsilon_4) D_3 / (\epsilon_4 D_4) \right)} \quad 14$$

Where

- σ = Stefan-Boltzmann constant, ($W/m^2 \cdot K^4$)
- D_3 = Outer absorber diameter, (m)
- D_4 = Inner glass envelop diameter, (m)
- T_3 = Outer absorber surface temperature, (K)
- T_4 = Inner glass envelop surface temperature, (K)
- ϵ_3 = Absorber selective coating emissivity
- ϵ_4 = Glass envelope emissivity

Conduction heat transfer through the glass envelop, it use the same equation as the conduction through the absorber wall described. The anti-reflective treatment on the inside and outside surface of the glass envelope is assumed to introduce no thermal resistance and to have no effect on the glass emissivity. This should be fairly accurate since the treatment is a chemical etching and does not add additional elements to the glass surface. As in the absorber case, the temperature distribution is assumed to be liner [66].

Heat transfer from the glass envelop to atmosphere. The heat will transfer from the glass envelop to the atmosphere by convection and radiation. The convection due to the temperature difference between the glasses envelop and sky [66].

1. Heat loss analysis

When a certain amount of solar radiation falls on the surface of a collector, most of it is absorbed and delivered to the transport fluid, and it is carried away as useful energy. In all thermal systems, heat losses to the environment by various modes of heat transfer are inevitable. The thermal network for a single-cover, in terms of conduction, convection and radiation [3].

Focusing concentrator has another set of losses called optical losses, which by proper design and choice of material and workmanship can decrease but not eliminated. The optical efficiency of PTC (or concentrator) is the product of eight parameters [67].

2. Thermal efficiency analysis

The thermal performance (η) of solar collector can be determined by the detailed analysis of the optical and thermal characteristics of the solar collector materials and collector design. Experimental performances testing under control condition. Conditions in test as direct solar radiation (W/m^2 , G_B), collector aperture (A_a , m^2), air speed (m/s), ambient temperature ($^\circ\text{C}$), Fluid inlet temperature (T_i , $^\circ\text{C}$), Fluid outlet temperature (T_o , $^\circ\text{C}$), Fluid flow rate (\dot{m}) [9], given by Equation 15.

$$\eta = \frac{\dot{m}c_p(T_o - T_i)}{A_a G_B} \quad 15$$

Where

- η = Collector efficiency
- \dot{m} = Fluid flow rate, (kg/s)
- c_p = Specific heat at constant pressure, (kJ/kg. $^\circ\text{C}$)
- A_a = Collector aperture, (m^2)
- T_o = Fluid outlet temperature, ($^\circ\text{C}$)
- T_i = Fluid inlet temperature, ($^\circ\text{C}$)
- G_B = Beem solar radiation, (W/m^2)

The performance test on steady-state conditions, with steady fluids flow rate, constant wind speed and ambient temperature. When a constant inlet fluid temperature is supplied to the collector, it is possible to maintain a constant outlet fluid temperature from collector. The useful gain from the collector is calculate from Equation 16.

$$Q_u = \dot{m}c_p(T_o - T_i) \quad 16$$

Where

$$Q_u = \text{Useful energy collector, (J)}$$

and have seen that the useful energy collector from collector is gave by Equation 17.

$$Q_u = A_a F_R [G_B (\tau\alpha)_n - U_L (T_o - T_i)] \quad 17$$

Where

$$A_a = \text{Absorber area, (m}^2\text{)}$$

$$F_R = \text{Heat removal factor}$$

$$U_L = \text{Solar collector overall heat loss coefficient, (W/m}^2 \cdot \text{°C)}$$

During testing, the collector is mounted in such a way as to face the sun perpendicularly; as a result, the transmittance-solar absorptance product for the collector corresponds to that of beam radiation at normal incidence. Therefore, the term $(\tau\alpha)_n$ is used in Equation 17 to denote that the normal transmittance-solar absorptance product is used.

Concentrator collector can used for the useful energy collector and collector efficiency.

$$Q_u = F_R [G_B \eta_0 A_A - A_r U_L (T_i - T_a)] \quad 18$$

$$\eta = F_R \eta_0 - \frac{F_R U_L (T_i - T_a)}{C G_B} \quad 19$$

Where

η_0 = Collector optical efficiency

C = Collector concentration ratio

A_r = Receiver area, (m²)

Parabolic trough collector, retain high efficiency, even at higher collector inlet temperature. It should be noted that the radiation levels examined are considered as beam radiation. The heat loss coefficient, U_L in Equation 19 is not constant but is a function of the collector inlet and ambient temperature.

$$F_R U_L = c_1 + c_2 (T_i + T_a) \quad 20$$

Where

c_1 = First-order coefficient of the collector efficiency, (W/m². °C)

c_2 = Second-order coefficient of the collector efficiency, (W/m². °C)

T_a = Ambient temperature, (°C)

Apply Equation 20 in 18 for concentrating collector

$$Q_u = F_R [G_B \eta_0 A_a - A_r c_1 (T_i - T_a) - A_r c_2 (T_i - T_a)^2] \quad 21$$

For concentrating collector, the efficiency can be written as

$$\eta = F_R \eta_0 - \frac{c_1(T_i - T_a)}{CG_B} - \frac{c_2(T_i - T_a)^2}{CG_B} \quad 22$$

Application of solar collector

The applications of solar collector can apply to a lot activity as life, industrial and energy. The steam of 100-250°C can be used in industrial plants [10]. The most important industrial processes using heat at a mean temperature level are sterilizing, pasteurizing, drying, hydrolyzing, distillation and evaporation, washing and cleaning, and polymerization [3].

Table 4 Heat process using in industrials [3]

Industry	Process	Temperature, (°C)
Dairy	Pressurization	60-80
	Sterilization	100-120
	Drying	120-180
	Concentrates	60-80
	Boiler feed water	60-90
Tinned food	Sterilization	110-120
	Pressurization	60-80
	Cooking	60-90
	Bleaching	60-90
Textile	Bleaching, dyeing	60-90
	Drying, decreasing	100-130
	Dyeing	70-90
	Fixing	160-180
	Pressing	80-100

Table 4 (cont.)

Industry	Process	Temperature, (°C)
Paper	Cooking, drying	60-80
	Boiler feed water	60-90
	Bleaching	130-150
Chemical	Soaps	200-260
	Synthetic rubber	150-200
	Processing heat	120-180
	Pre-heating water	60-90
Meat	Washing, sterilization	60-90
	Cooking	90-100
Beverages	Washing, sterilization	60-80
	Pasteurization	60-70
Flours by-products	Curing	60-140

CHAPTER III

RESEARCH METHODOLOGY

The absorber of parabolic trough collector used Ni-Al particles prepared by flame spray technique on stainless steel 316L pipe. The Ni-Al solar absorber was characterized by phase, morphology, chemical composition. The solar absorptance (α) was also investigated and measured. The thermal analyzed thermal loss, calculated emittance (ϵ) and thermal performance.

Experimental procedures

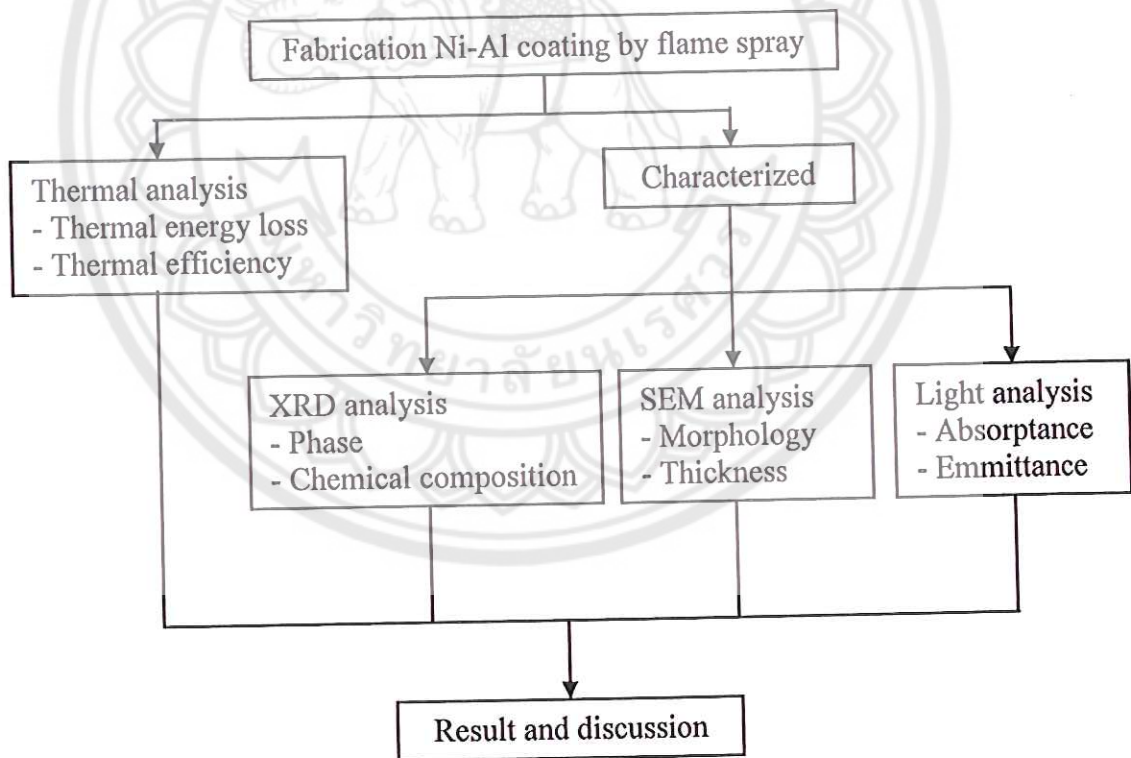


Figure 18 Experimental procedures

Equipment

1. X-Ray diffraction, XRD



Figure 19 Rigaku miniflex II X-ray diffractometer

X-Ray diffraction, every substrate has a unique X-Ray powder pattern because line position depends on the unit cell size, and line intensity depends on the type of atoms presents and on their arrangement in the crystal. Thus, in much the same way that you and I can be identified by our characteristic fingerprints, so an unknown solid can be identified from its unique powder pattern. The first sight, the most straightforward way of identifying a way of identifying an unknown solid would be to compare its powder its powder pattern with a library of standards. However, this is usually too inconvenient for literally tens of thousands of powder patterns are currently known. A system of classifying powder patterns so that unknown pattern can quickly be identified was devised by Hanawalt in 1936. A powder pattern is characterized by line positions and relative intensities. However, line positions depend on the wavelength of the X-ray used. Since interplanar spacings (d) derived from the line positions are independent of X-ray wavelength, Hanawalt used lists of d values and relative intensities to characterize powder patterns [68].

In case study using X-ray diffraction Rigaku miniflex II, shown in Figure 19.

$$2d \sin\theta = n\lambda$$

2. Scanning electron microscopy, SEM



Figure 20 JEOL JSM-5910 LV scanning electron microscope

Scanning electron microscope (SEM) is a type of electron microscope that produces images of a sample by scanning electron beam. The electrons interact with the atoms in the sample, producing various signals that can be detected and contain information about the sample's surface topography and composition. The electron beam is generally scanned in a raster scan pattern, and the beam's position combines with the detected signal to produce an image. SEM can achieve resolution better than 1 nanometer. Specimens can be observed in high vacuum, in low vacuum, in wet conditions (in environmental SEM), and in a wide range of cryogenic or elevated temperatures, shown in Figure 20.

3. Energy dispersive spectrometer, EDS

Energy dispersive spectrometer (EDS) uses the X-ray spectrum emitted by a solid sample bombarded with a focused beam of electron to obtain a localized chemical analysis. All elements from atomic number 4 (Be) to 92 (U) can be detected in principle, though not all instruments are equipped for 'light' elements ($Z < 10$). Qualitative analysis involves the identification of the lines in the spectrum and is fairly straightforward owing to the simplicity of X-ray spectra. Quantitative analysis (determination of the elements present) entails measuring line intensities for each element in the sample and for the elements in calibration standards of knowing the composition [69].

4. Ultraviolet-Visible-Near Infrared spectrophotometer, UV-Vis Near IR

The Ultraviolet-Visible-Near Infrared Spectrometer measured in wavelength 300-2500 nm, it's shown in Figure 21. The samples measured a reflectance (R) in wavelength and calculated a solar absorptance (α) base on Equation 3.



Figure 21 UV-3101PC Ultraviolet-Visible-Near Infrared Spectrophotometer

Preparation

1. Sample preparation

Commercially available Ni-5wt.%Al particles. The surface used 450NS of Oerlikon Metco, Switzerland for a starting material. The Metco 450NS was general purpose materials for restoration of worn or mismachined components. They are also used as bond coats for OEM-specified and general industrial applications under top coats such as ceramics and compressor abrasives. Nickel aluminum coating has good oxidation resistance up to 800°C. Metco 450NS was designed to be applied using

atmospheric plasma spray or combustion powder Thermospray processes. The material specifications presented in Figure 22 and Table 5.



Figure 22 Nickel-5% Aluminum thermal spray powders

Table 5 Specification of Ni-5wt.%Al powder

Ni-5wt%Al material information		
Chemical composition (wt. %)	Ni	Weight balance
	Al	4.5-5.5
	Other (max)	2.5
Particle size distribution	Nominal Range (μm)	45-90
	Apparent density (g/cm^3)	3.7 ± 0.3
Physical properties	Manufacture	Mechanically Clad
	Morphology	Spheroidal
Macro hardness		65-80 HRB
Max service temp.	$^{\circ}\text{C}$	800

Note: Data from Oerlikon Metco, Switzerland

The stainless steel substrate is an austenitic chromium-nickel stainless steel containing molybdenum. This addition increases general corrosion resistance, resistance pitting from chloride ion solution, and provides increased strength at elevated temperatures. In type 316L is an extra-low carbon. Typical uses include exhaust manifolds, furnace parts, heat exchangers, jet engine part, pharmaceutical and photographic equipment, valve and pump trim, chemical equipment, digests, tank, evaporators, pulp, paper and textile processing equipment, parts exposed to marine atmospheres and tubing.

The stainless steel 316L (SS316L) was made a spiral top and bottom side for connecting expansion joint, showed in Figure 23. The physical properties of SS316L are summarized in Table 6.



Figure 23 Stainless steel 316L pipe substrate

Table 6 Chemical composition, Mechanical and Physical properties of stainless steel 316L pipe

Stainless steel 316L material information		
Chemical composition (%)	Carbon	0.03 max.
	Manganese	2.00 max.
	Phosphorous	0.045 max.
	Sulfur	0.03 max.
	Silicon	0.75 max.
	Chromium	16.00-18.00
	Nickel	10.00-14.00
	Molybdenum	2.00-3.00
	Nitrogen	0.10 max.
	Iron	balance
Mechanical properties	UTS ksi (MPa)	81(558)
	0.2% YS ksi (MPa)	42(290)
	Hardness Roeckwell	B79
Physical properties	Density	7.99 g/cm ³
	Specific heat	0.12 kJ/kg. K
	Thermal conductivity (100°C, 500°C)	16.2, 21.4 (W/m. K)
	Melting Range	1371-1399 °C

Note: Data from AK steel corporation

The Ni-Al coating prepared by the flame spray technique at Advance surface technology (ATS) Co., Ltd; AST. Substrate preparation, sandblast in 4S70, 3S70 (AST condition) and protect grease by plastic cover all substrates, set up on the rotation podium (rotation 50 RPM). Flame spray gun is model DS-8000 from Switzerland, Castolin S.A. Case postale 360 CH-1001 Lausanne, as shown in Figure 24. The condition parameter of coating was recommended by the gun manufacturers in Table 7.

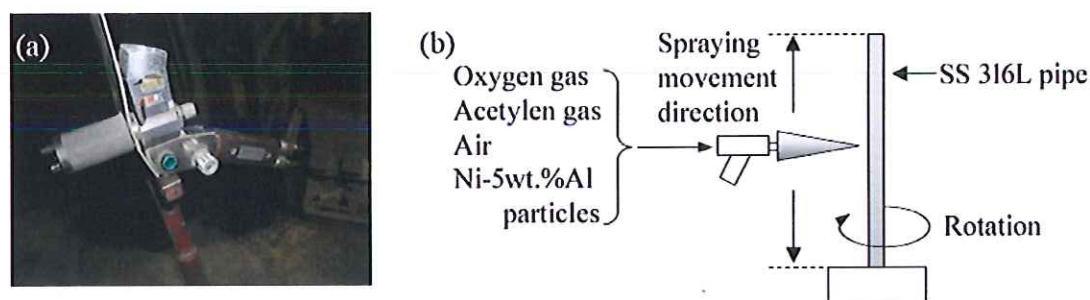


Figure 24 (a) Thermal spray gun, FS, DS-8000 and (b) spraying process

Table 7 Condition parameter of flame spraying process

Method	Parameters flame spray
Oxygen	4.0 bar
Acetylene	0.7±0.1 bar
Air	0.6 bar
Spraying distance	150 mm
Substrate rotation speed	50 rpm
Substrate material	Stainless steel 316L

Substrate surface preparation

Stainless steel 316L pipe was a substrate for parabolic trough absorber. The dimensions were outer diameter 33.33 mm, inner diameter 27.90 mm, thickness 2.71 mm. The length of absorber area was 1000 mm. Total area of the absorber was 0.104 m². The end of absorber pipe top and bottom were 100 mm free space length. It was made spiral for connecting expansion joint to support glass envelope. The pipe substrate was coated in process of Advance Surface Technology (AST).

Sandblast, standard of AST used roughness number 3S70 or 4S70, it was shown in Figure 25(a). The worker was sandblasted with air pressure 6 kg/cm³ in close-door, shown in Figure 25(b-c). In the preparation process of SS316L, the worker must set-up process of sand bath outer working room and spraying in the close-room unit 3S70 or 4S70 roughness on SS316L surface and cover by plastic. Plastic was cover for protection fat from hand in working process.

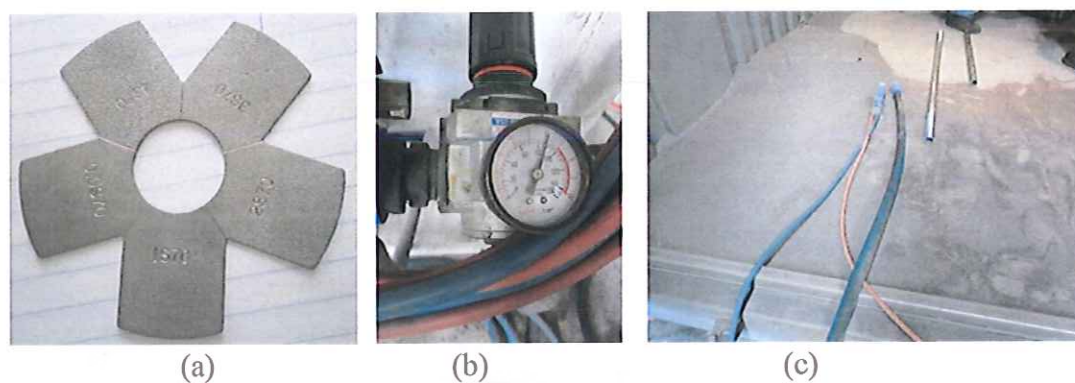


Figure 25 (a) number of roughness of AST, (b) air pressure for sand bath, and (c) sandblast room

After surface cleaning preparations, the 316L pipe was a higher surface roughness in Figure 26.



Figure 26 Roughness of SS316L substrate

2. Parabolic trough collector

Parabolic trough collector is designed for generating heat energy. The complement of parabolic trough collector as absorber pipe, expansion, glass envelope and a parabolic trough reflector. The structure and dimensions of the parabolic trough collector and the parabolic trough testing stand were shown in Table 8.

Table 8 Structure and dimensions of parabolic trough receiver and parabolic trough testing stand

Description	Material	Dimension
Structure stand	steel	50.8 cm
Parabola curve	Fiber graph	0.02 (thickness)
Reflector aperture	PET	1.569 m ²
Parabolic trough aperture		1.569 m ²
Concentrating ratio		15
Rim angle		75
Tracking	DC motor	12V
Solar selective material	Ni-Al	
Absorber pipe	SS316L	OD/ID 33.33/29.99 mm
Glass envelop	Borosilicate glass	OD/ID 65/55 mm

Expansion joint support glass envelope, and protect vacuum loss were made from aluminum material, shown in Figure 27.

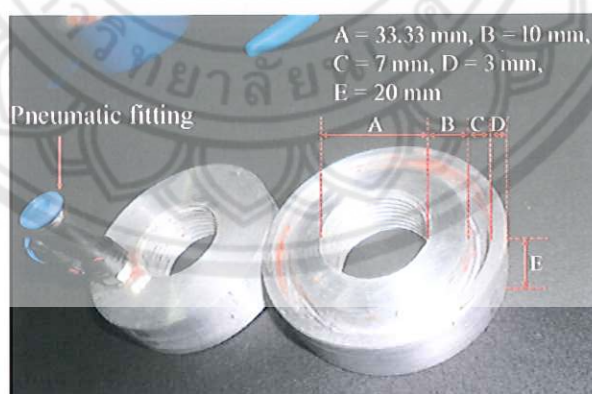


Figure 27 Expansion joint

For this research used aluminum cylinder pipe outer diameter 53.33 mm and 20 mm thickness. The aluminum center, making a hold and spiral for connecting absorber pipe. The thickness of the gap between the outer of spiral hold and outer

aluminum 3 mm, it was gutter of the glass envelope. The glass envelop thickness 5 mm was inserted to gutter of aluminum expansion joint. One of the aluminum was made a hold and install pneumatic fitting. The fitting was connected vacuum tube and pump air out of parabolic trough collector.

Install O-rings in gap of expansion joint, shown in Figure 28.

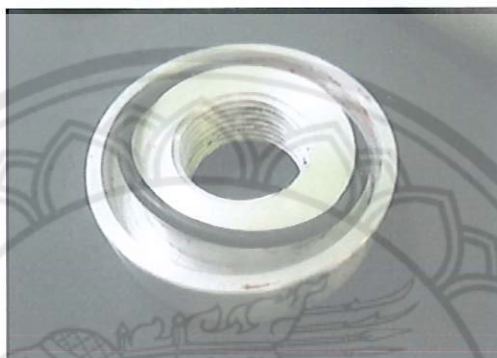


Figure 28 Expansion joint with O-rings

The expansion joint was installed in the absorber pipe until the end of the spiral. Install glass envelop cover absorber surface, glass envelop insert into the gutter of expansion joint and install other expansion joint cover glass envelope again. The glass envelope was installed to cover the absorber pipe and install in the center of expansion. Air and vacuum loss between absorber pipe, glass envelop and expansion were covered with high temperature silicone gel. In the complete process of parabolic trough receiver can checking by vacuum pumping or air pressure does not leak from inside to outside of the parabolic trough collector, the complete parabolic trough receiver was shown in Figure 29.

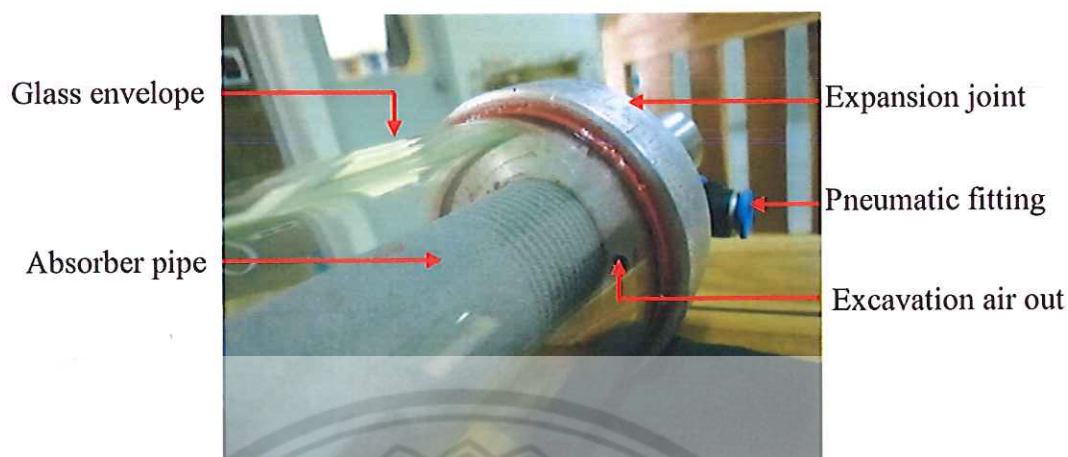


Figure 29 Configurations of expansion joint

Figure 30 it's shown a diagram of parabolic trough collector (one of all model). The absorber pipe using stainless steel 316L for the substrate and coating solar selective material on the top of the surface. The solar selective material was coated on the surface, it's a high solar absorptance of radiation in the solar spectrum, and low emittance in the long wave energy spectrum to reduce thermal radiation loss.

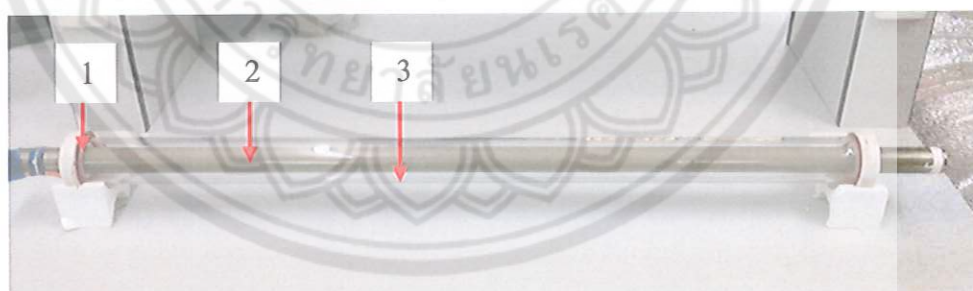


Figure 30 Solar receiver pipe for PTC

The supports testing stand using carbon steel 2 in, width \times long \times high (180 \times 180 \times 120 cm) and coating white color for decrease temperature impact of high solar radiation. The support installed DC motor drive tracking, rotate, position, and bearing, shown in Figure 31.

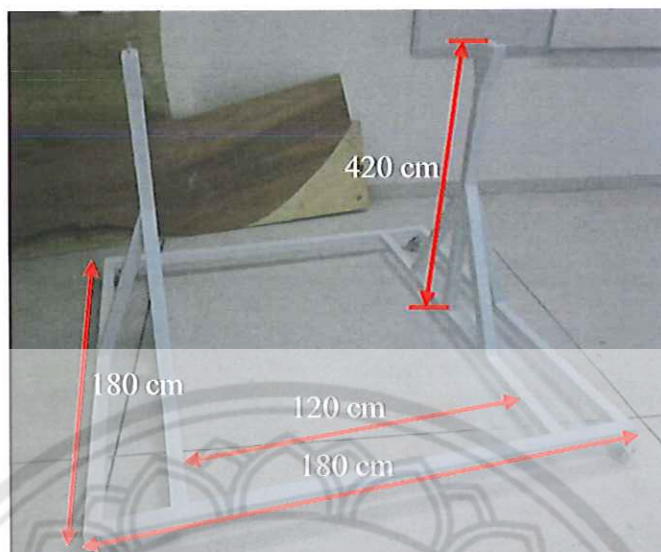


Figure 31 Steel structures of parabolic trough testing system

The parabola curve and reflector were used wood and fiber graft material for decrease weight. The three parabola curve woods were installing in left, right and center. There are fixed with the resin glue and screws. The wood supports the focus position was making a hold diameter 33.33 mm and integrate with wood parabola curves. All of wood structure was covered with resin again. The resin can protect humanity, water and wood structure broken, shown in Figure 32.

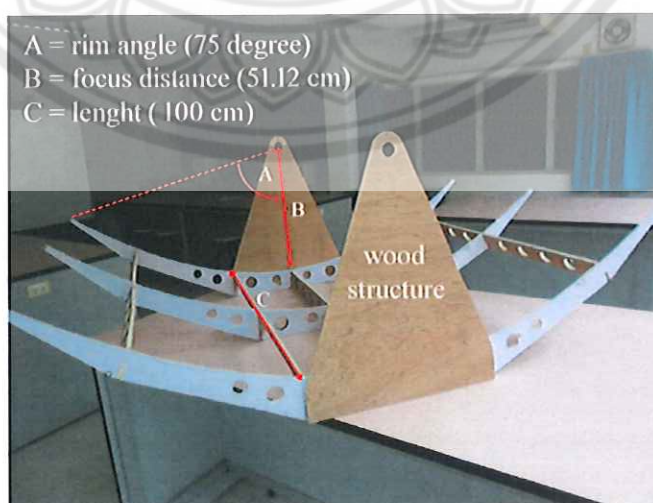


Figure 32 Structure of parabola made from wood

The reflector was PET reflector film, shown in Figure 33(a). This film can reflect solar radiation more than 95% (from material information) and it can deposit on curve supporter. Table 8, rim angle of parabola curve was 75 degrees. So, the curve of a parabola is not interesting for use glass for reflector and PET reflector film was a good way. The supports PET reflector was made from fiber graph with 200 g/in² strand fiber and coordinate resin. Fiber graph was made each layer until 3 mm thickness and cutting width 100 cm length 180 cm, shown in Figure 33(b). Install fiber graph on wood curve structure and fixing at the top of a structure with resin and scrubbed surface until smooth all areas. PET reflector was deposited on the 1 mm steel sheet with spray glue after install on the top of fiber graph supports

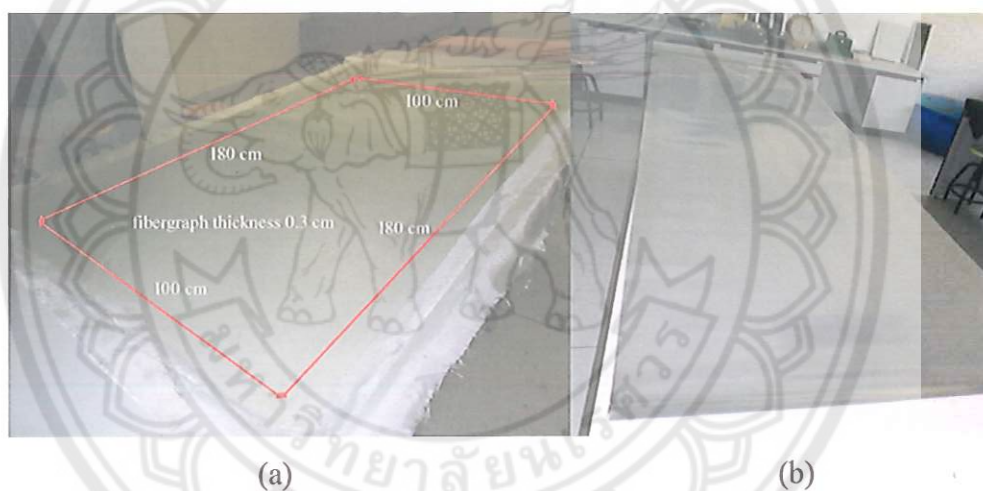


Figure 33 (a) Support reflector made from fiber graph, (b) Poly Ethylene Terephthalate film (PET) reflector

PET reflector was attached installer on the top of parabola supports, shown in Figure 34. The reflector was smooth all of surface. The fiber graph support was installed and attach to wood structure by fiber graph resin and all wood structure were shrouded by fiber graph resin again for protect humidity from environmental.

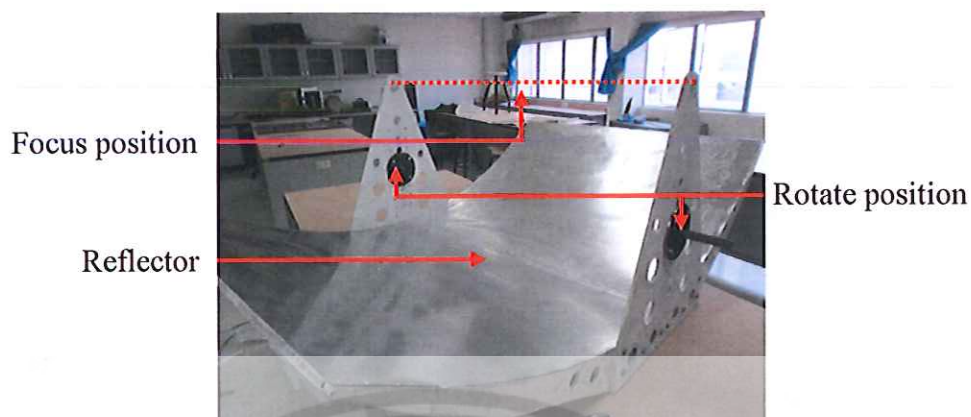


Figure 34 Install PET reflector on the parabola curve

The configuration of parabolic trough testing stand as parabola curve was installed reflector, the steel supports of the parabolic trough testing system, working fluid control and sensor measurement. There are shown Figure 35. The parabola was connected with the bearing position for rotating tracking with the sun. The parabolic trough collector was installed at the focus point, insert the absorber pipe into the hold of wood plate and throw out of them. Motor drive tracking was installed on the steel supporters and back of parabola reflector. Connected water joint and waterspout to the absorber both two ways of absorber pipe. Waterspout connected with flow control, heater and water pump. This research chooses to continue water supply thermal performance testing. So, this test could have a water tank for water backup in the test time. The measurement as ambient temperature, inlet-outlet absorber temperature and direct solar radiation measurement.

During the test, water was continued pumping into the parabolic trough collector and increasing 10°C every 10 min or (stable) between 40°C - 80°C . Flow meter was control mass flow rate kg/min. Temperature sensors were measured water inlet to absorber and outlet absorber, ambient temperature in the testing area. At test time, direct radiation was reflected to the focus point. Intensity of them can observe on the parabolic trough receiver. Solar tracking was depending on that, if the sun move to another area intensity light on the parabolic trough receiver move too. So, solar tracking was using this factor for track parabolic reflector to the high intensity all the time test.

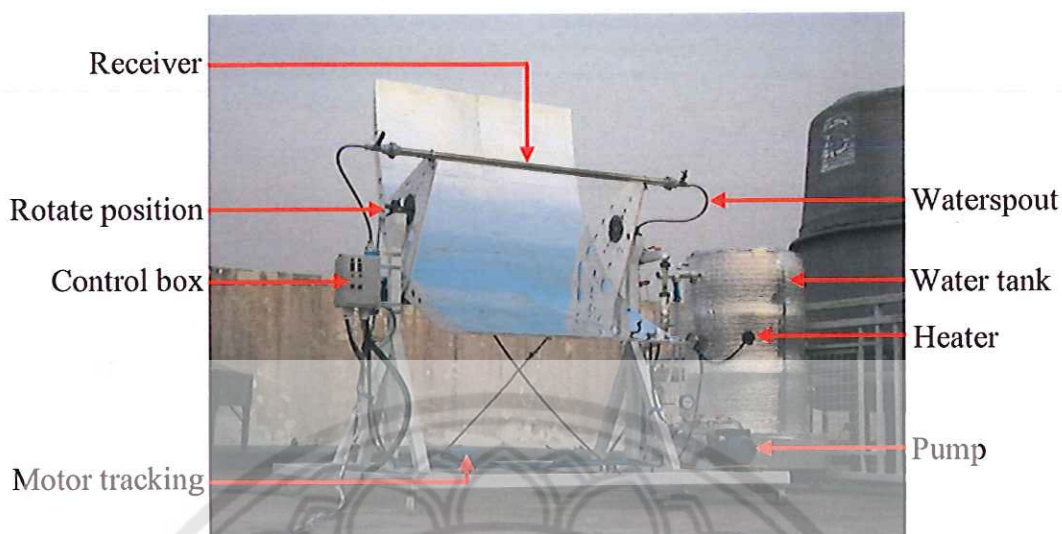


Figure 35 PTC testing system

Surface and thermal analysis

1. Surface

The Ni-Al coating was investigated the surface morphology and analysis element by scanning electron microscope (SEM) and energy dispersive X-ray (EDX). The reflection and solar absorptance of surface coating were determined by Ultraviolet-visible-near infrared spectrophotometer at wavelength 300-2500 nm. The phase and chemical composition of the coating was analyzed using X-ray diffraction meter.

2. Thermal loss of parabolic trough collector

The parabolic trough collector was operated at high temperature with a long time. The thermal energy can losses from that to the atmosphere. In this test process was imitate parabolic trough collector operating temperature in 30-200°C. The test was gave-up heat energy from inside, the vacuum space between absorber pipe and glass envelop were protect heat energy loss out of that. The temperature parameter was measured for analyzing thermal energy loss out of the collector. The method flowing National Renewable Energy Laboratory (NREL) of the U.S. Department of Energy Office of Energy Efficiency & Renewable Energy. The test described here is that same as the test described in [70, 71] and thermal loss was set-up tested at School of Renewable Energy Technology (SERT) of Naresuan University.

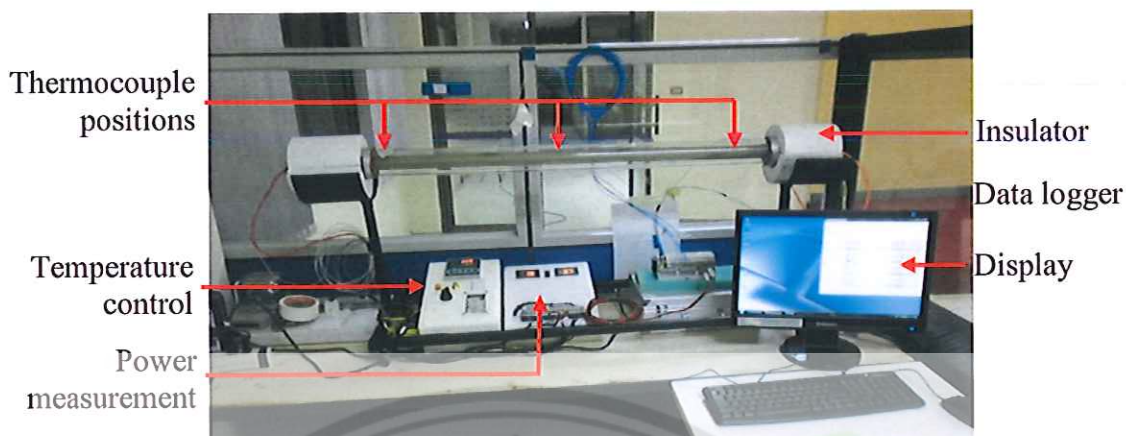


Figure 36 Heat loss testing system



Figure 37 Heater fin for heating absorber pipe

The heat loss process of parabolic trough receiver was shown in Figure 36. A parabolic trough collector was installed to the cylinder insulator on the station. Connecting vacuum pumps continuous pumping air out of the collector during tested. Insert fin heater (shown in Figure 37) to absorber pipe. Temperature sensors were installed to the position on the parabolic trough collector, there are shown in Figure 38.

Temperature sensors were installed inside of absorber pipe 200 mm, 400 mm, 600 mm and 800 mm, outer glass envelope 200 mm, 400 mm, 600 mm and 800 mm from the edge and ambient temperature. Temperature of heater was measure similar thermal conductivity testing. All parameter measurements were recorded to the data recorder every second.

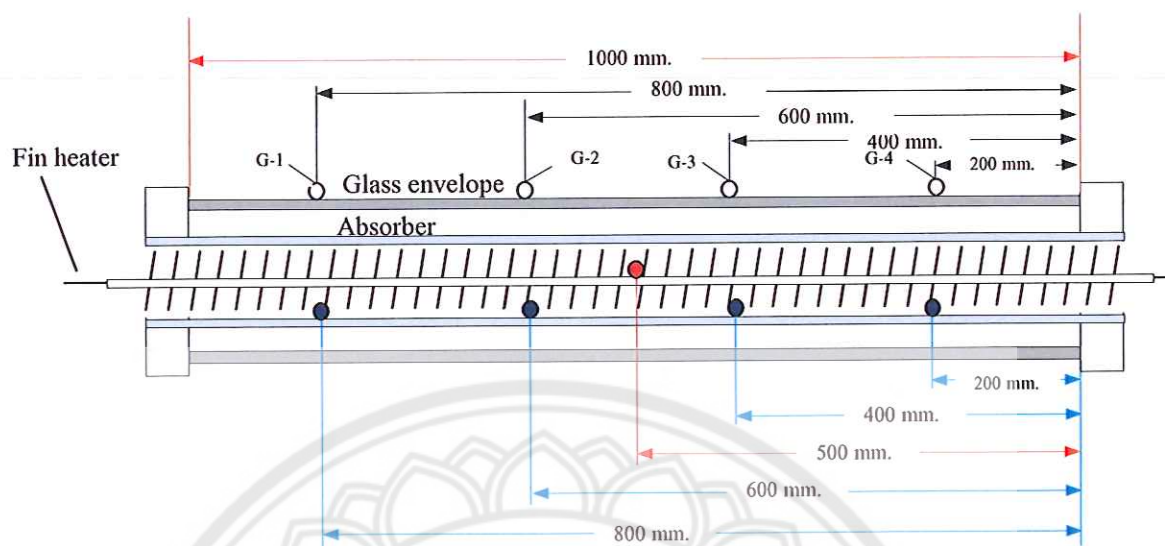


Figure 38 Thermocouple position achieved at parabolic trough receiver

Calculating absorber emittance

The inner absorber surface was heated to a uniform temperature of the internal heaters. The energy then conducts through the absorber, radiates across the annulus, and conducts through the glass envelope. At steady-state the temperatures are constant, and the conducted and radiated power are equal to the measured heat loss [70, 71]. As shown in Figure 39.

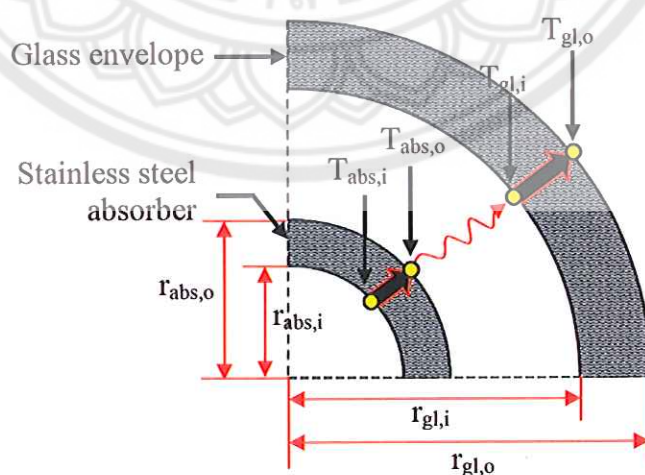


Figure 39 One dimensional heat loss that occurs during laboratory testing

The absorber emittance, ϵ_{abs} , is calculated from an iterative solution of the following equations [70, 71].

$$\text{Heat loss, (W/m)} = \frac{2\pi r_{abs,i} (T_{abs,i} - T_{abs,o})}{\ln\left(\frac{r_{abs,o}}{r_{abs,i}}\right)} \quad 24$$

$$\text{Heat loss, (W/m)} = \frac{2\pi r_{abs,o} \sigma (T_{abs,o, Kelvin}^4 - T_{gl,i, Kelvin}^4)}{\frac{1}{\epsilon_{abs}} + \frac{1 - \epsilon_{gl}}{\epsilon_{gl}} \left(\frac{r_{abs,o}}{r_{gl,i}}\right)} \quad 25$$

$$\text{Heat loss, (W/m)} = \frac{2\pi r_{gl} (T_{gl,i} - T_{gl,o})}{\ln\left(\frac{r_{abs,o}}{r_{abs,i}}\right)} \quad 26$$

Where

$r_{abs,i}$	=	inner radius absorber pipe, (m)
$r_{abs,o}$	=	outer radius absorber pipe, (m)
$r_{gl,i}$	=	inner radius glass envelop, (m)
$r_{gl,o}$	=	outer radius glass envelop, (m)
ϵ_{gl}	=	emittance glass envelop (0.89 [70, 71])
ϵ_{abs}	=	emittance absorber pipe
$T_{abs,i}$	=	inner temperature absorber, ($^{\circ}\text{C}$, K)
$T_{abs,o}$	=	outer temperature absorber, ($^{\circ}\text{C}$, K)
$T_{gl,i}$	=	inner temperature glass envelop, ($^{\circ}\text{C}$, K)
$T_{gl,o}$	=	outer temperature glass envelop, ($^{\circ}\text{C}$, K)
σ	=	Stefan-Boltzmann constant ($5.6703 \times 10^{-8} \text{ W/m}^2 \cdot \text{K}^4$)

3. Thermal efficiency of parabolic trough receiver

In testing process from standard of ISO 9806-1: 1994 and ASHRAE standard 93: 2003 give information on testing solar energy collector using single-phase fluids [3]. A PTC three Ni-Al thicknesses had been test under steady state conditions. The method allows ambient conditions and continuous measurements over the test. This is a three Ni-Al coating thickness on absorber pipe of PTC were used to account the efficiency collector capacity as well as the diffuse irradiance on the aperture area. The tests were design all structure and conditions shown in Table 9.

Table 9 PTC hot water generation system specification

Items	Value
Receiver diameter (absorber pipe)	33 mm
Receiver length	1000 mm
Glass envelope diameter	65 mm
Concentration ratio	15
Water flow rate	1.88 kg/min
Aperture area	1.569 m ²

Testing process

PTC test system for hot water generations. The parabolic trough structure makes from fiberglass, aperture area has a PET reflectance (>95%) on wood structure. Stand made from steel and tracking by DC motor 12V, receiver at the focus point, measurements temperature water inlet and outlet, fix flow late by flow meter and water constant by temperature control.

The thermal performance of the parabolic trough collector is determined in part of obtaining values of instantaneous efficiency for a combination of values of incident radiations, ambient temperature and inlet fluid temperature. This requires experimentally measuring the rate of direct solar radiation onto the parabolic trough collector as well as the rate of energy addition to the transfer fluids as it passes through the collector, all under steady-state. In additions, tests are performed to determine the time response characteristic of the collector as well as how its study-state thermal

efficiency varies with incident angles between the direct beam and the thermal collector aperture area at various sun and collector positions. The testing diagram is shown in Figure 40.

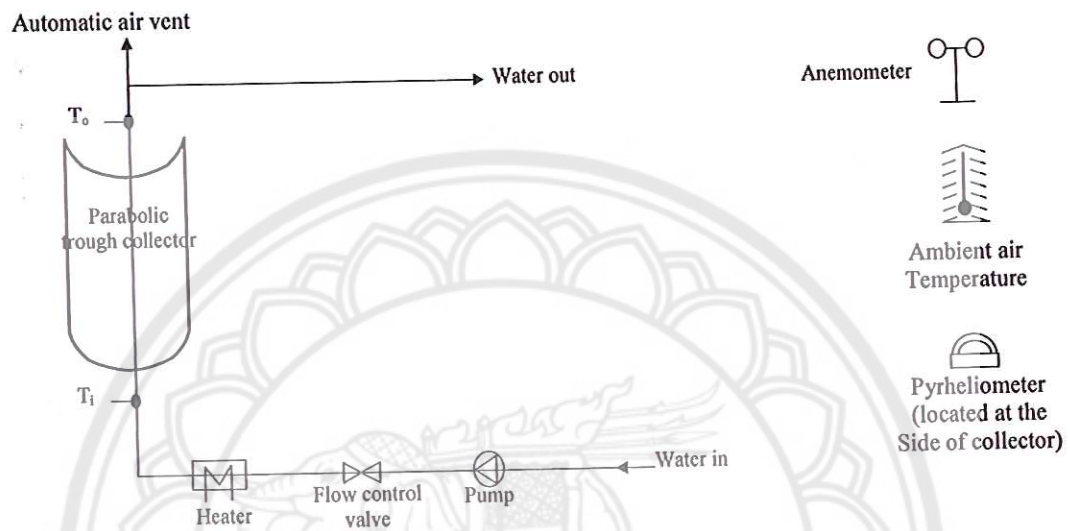


Figure 40 Open-loop thermal performance testing for PTC

CHAPTER IV

RESULT AND DISCUSSION

In this section, the result of the surface coating of stainless steel 316L applied with the flame spray coating technique on the solar absorber was analyzed and presented in terms of the surface and thermal characteristics. The surface analysis was focused on phase, chemical compositions, morphology, structure, thickness, and solar absorptance (α). The thermal loss, thermal emittance (ϵ) and thermal efficiency.

Surface coating with flame spray technique

A stainless steel 316L pipe with outer diameter of 33.33 mm, inner diameter of 27.9 mm, and length of 1000 mm was applied as the substrate material for the solar absorber. The outer surface of the stainless steel pipe was firstly prepared by sandblasting and the roughness of the sandblasted surface was compared with the standard conditions of 3S70 or 4S70 published by the Advance Surface Technology Company (AST). The sandblasted substrate is shown in Figure 41(a) which illustrates the finished rough surface with gray tone and was able to reflect the light. The sandblasted surface of the substrate was then coated with Ni-Al by using a flame spray gun (DS-8000) with the support of AST. In the coating process, the Ni-Al particles were melted at a temperature greater than 1500°C by acetylene gas combustion and the melted particles then sprayed on the prepared surface at a distance of 10-15 cm. The adherence between the melted particles and the surface depended on the roughness of the stainless surface. The features of the coated surface were similar to that of the uncoated sandblasted surface, but now had the dark color of the Ni-Al. The Ni-Al coated surface is shown in Figure 41(b).

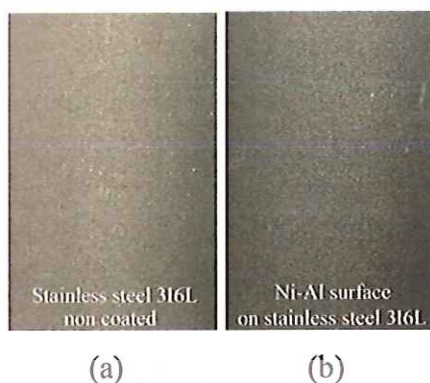


Figure 41 (a) Sandblast stainless steel 316L non coated preparation surface, (b) Ni-Al surface

The thickness of the NiAl coating was controlled and measured using a micrometer. The NiAl particles were agglomerated and melted during the spray process and deposited to substrate. The thickness of the Ni-Al coating was measured by taking a number of measurements of the diameter of the coated pipe at various points along its length, averaging those readings, and comparing against the initial diameter of the absorber pipe substrate. The diameter of the absorber pipe was considered to be constant at ambient temperatures thus not affecting the final diameter measurements.

Surface analysis

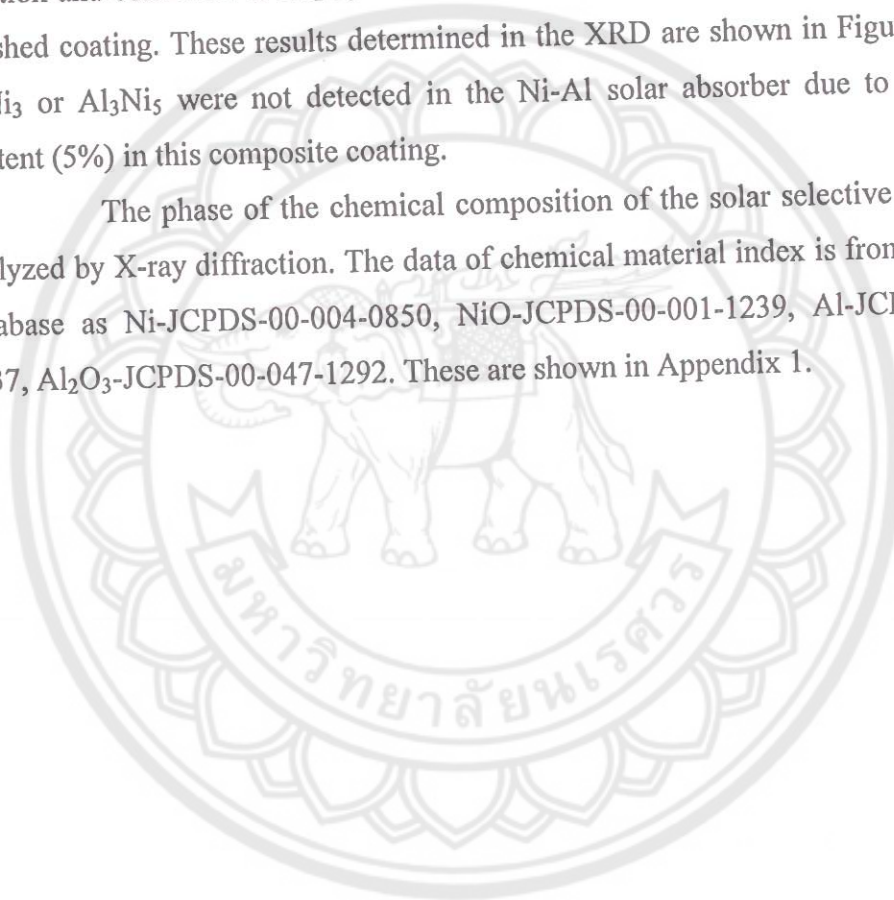
1. XRD

Flame spray techniques, working at a high temperature greater than 2000°C, can utilize oxygen from the air during the process of melting the Ni-Al particles. This ambient oxygen combines with the Ni and Al when it is deposited on the substrate surface.

Analysis of the phase of the Ni and Al was carried out. This was done by comparing the XRD patterns on the coated surface of each of the substrates that had been coated with different thicknesses of Ni-Al particles (three different thicknesses of coating had been prepared). The results of this comparison were that phase of the Ni and Al on starting material. After coating, the pattern was presented the major phase of Ni and new phase NiO and Al₂O₃, shown in Figure 42.

In the flame spray coating process ambient oxygen combines with the Ni and Al to form NiO and Al₂O₃ can participate with feedstock in the coating. The XRD patterns on the coated surfaces show this new phase. Of the Al₂O₃ and NiO resulting from the coating process, the nickel feedstock showed the highest phase on the new surface. In the feedstock for the spray coating process, 95% of the content was Ni, and only 5% was Al. However, the Al feedstock component had the major oxidation reaction and converted to Al₂O₃. Some Ni oxidated resulting in the NiO phase in the finished coating. These results determined in the XRD are shown in Figure 42. NiAl, AlNi₃ or Al₃Ni₅ were not detected in the Ni-Al solar absorber due to the low Al content (5%) in this composite coating.

The phase of the chemical composition of the solar selective surface was analyzed by X-ray diffraction. The data of chemical material index is from the JCPDS database as Ni-JCPDS-00-004-0850, NiO-JCPDS-00-001-1239, Al-JCPDS-01-085-1237, Al₂O₃-JCPDS-00-047-1292. These are shown in Appendix 1.



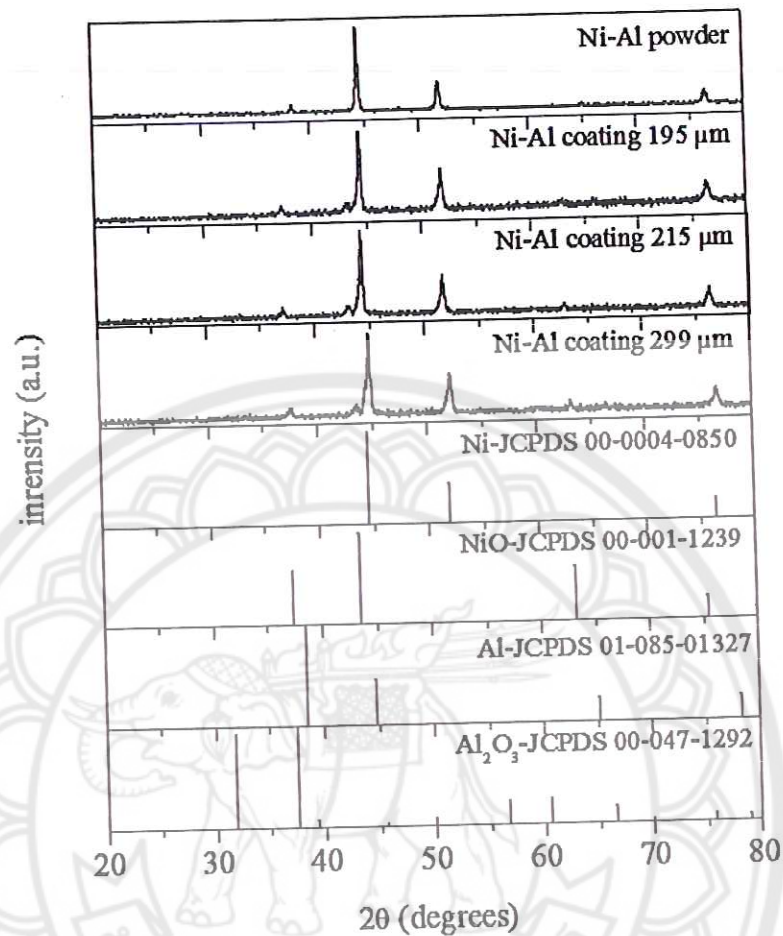


Figure 42 XRD patterns of Ni-Al powder and three thicknesses Ni-Al solar absorber, together with JCPDS of Ni, NiO, Al and Al₂O₃

2. SEM Imaging

The surface was imaged by a scanning electron microscope (SEM) and the surface morphology and thickness were characterized.

The typical SEM images of the surface of the NiAl solar absorber are shown in Figures 43-45. The SEM image indicated that the three samples had a similar morphology. In each sample the surfaces had been built up layer by layer in the spraying process, to a different thickness in each sample (thin, medium, thick).

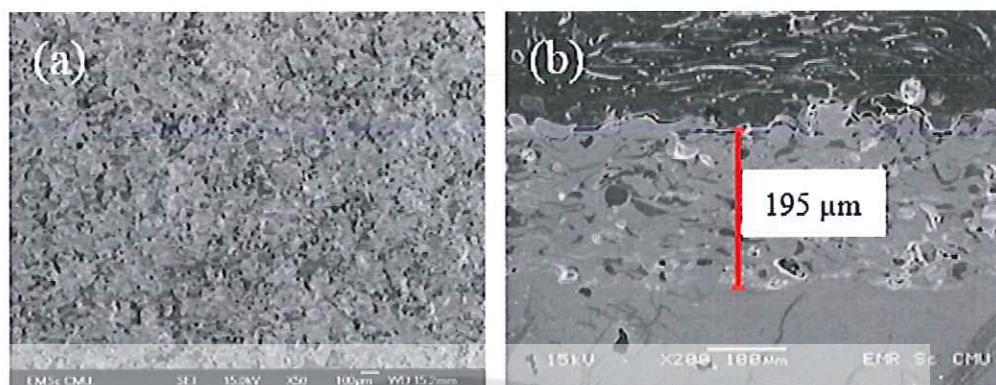


Figure 43 The morphology of (a) surface and (b) cross-section of Ni-Al solar selective surface average thickness 195 μm

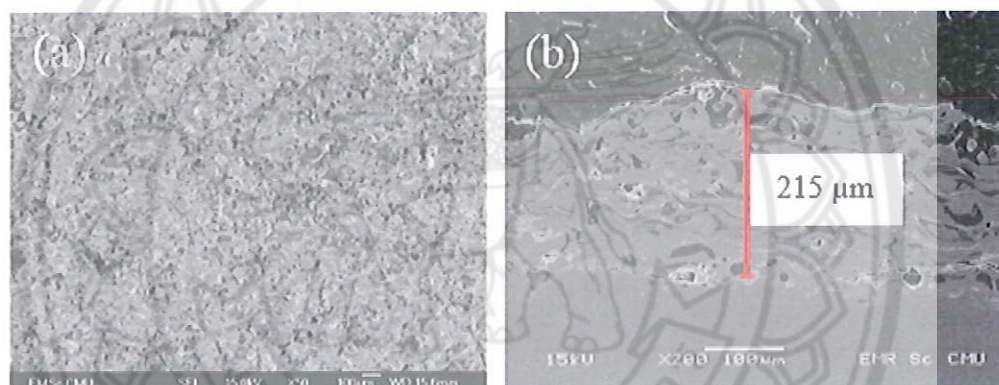


Figure 44 The morphology of (a) surface and (b) cross-section of Ni-Al solar selective surface average thickness 215 μm

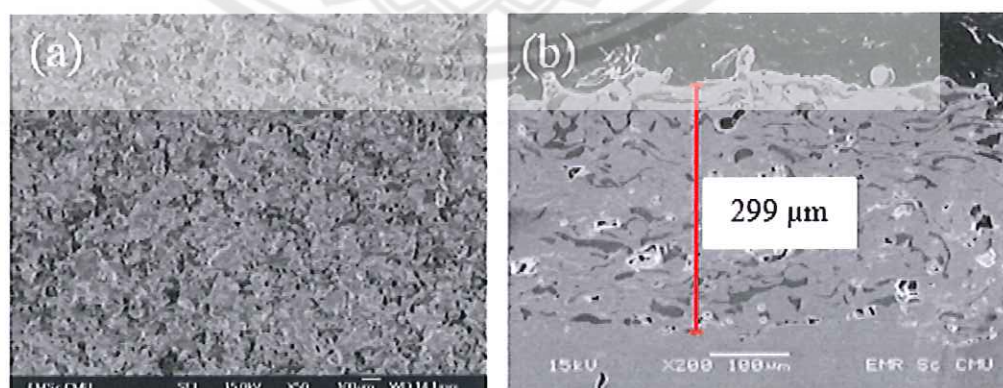


Figure 45 The morphology of (a) surface and (b) cross-section of Ni-Al solar selective surface average thickness 299 μm

Table 10 The thickness from flame spray coating

Model	Thickness (average) (μm)
1	195
2	215
3	299

The structure of each of the NiAl solar absorbers with different thicknesses was shown in cross-section using SEM imaging. Each was similar to the others in all three thicknesses. The coatings had overlapping layers with each layer parallel to the surface of the stainless steel 316L pipe substrate. This layered structure was similar to the microstructure of the Ni-Al composite prepared by other techniques [27, 52, 63]. The layers in each sample exhibited a similar level of roughness of the surface with a different average thickness in the three models. The coating surface and average thickness of the layers in the three models are shown in Figure 45b-47b. Model 1 had an average thickness of 195 μm , model 2, 215 μm and model 3, 299 μm , as shown in Table 10.

The coating had high adhesion contact with the substrate, indicating a good bonding between the melted Ni-Al particles and the substrate. The rough surface of NiAl solar absorber provided a good bonding to the top coating [52].

3. SEM-EDS analysis

An Energy Dispersive Spectrometer (EDS) is used to characterize the chemical composition of materials. Flame spray coating techniques can be used 'in the open air' without the requirement for special sealed rooms or cabinets. Apart from the making flame spraying a cheaper technique, it has the advantage of utilizing oxygen from the surrounding air in the chemical process involved in the coating process, converting Ni, for example, to NiO and the Al to Al_2O_3 . The EDS confirms the chemical composition of the new surface.

The SEM imaging of the surface of the coated material was analyzed for its chemical composition using the Energy Dispersive Spectrometer (EDS) which characterized the surface chemical composition, as illustrated in Figure 46. The EDS mapping shows the chemical composition of the fundamental elements of the sample

as Ni 72.94 wt%, Al 11.76 wt%, and O 15.29 wt%. According to the XRD pattern of the Ni-Al solar absorber, the melted Ni and Al particles on the stainless steel 316L pipe substrate had reacted with the environmental oxygen during the rotation of the pipe when it was being cooled to room temperature. In addition, the formation of Al_2O_3 and NiO on the surface of the Ni-Al solar absorber is able to offer an increasing anti-corrosion on the surface [50, 53, 72].

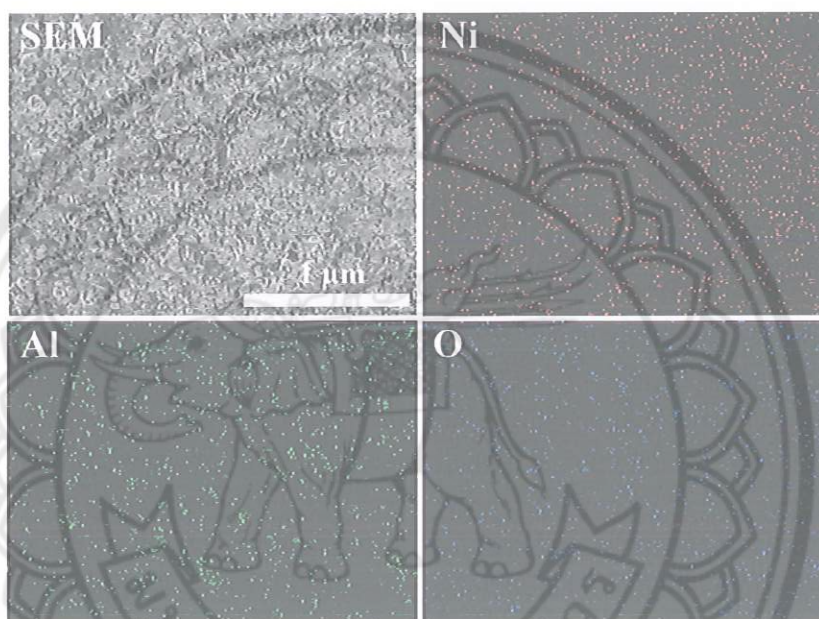


Figure 46 EDS mapping analysis of NiAl coating surface

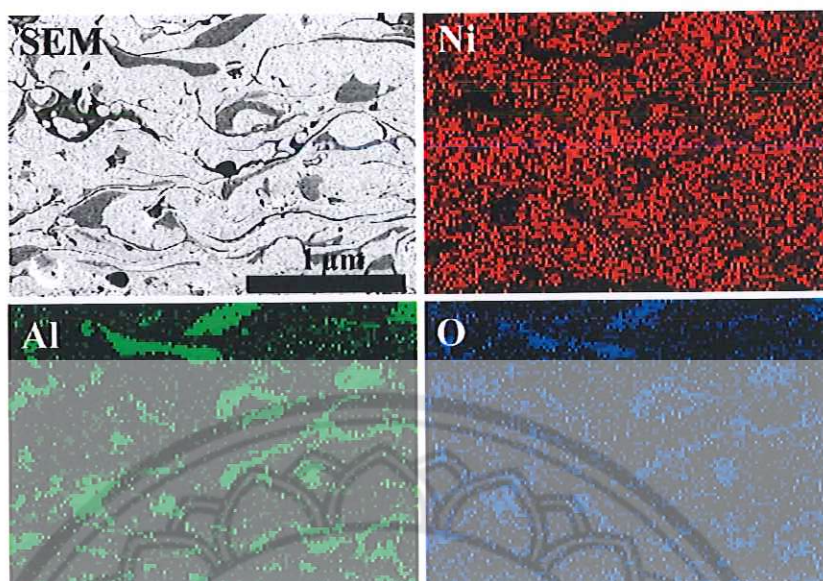


Figure 47 EDS mapping analysis cross section of NiAl cross-section coating

Figure 47 shows the cross section of the SEM image of the Ni-Al solar absorber. It can be observed that the surface coating has overlapped each layer as a parallel structure. The chemical composition of the fundamental elements of the cross section included Ni 80.26 wt.%, Al 8.93 wt.% and O 10.81 wt.%. According to the result of XRD pattern and EDS mapping of NiAl solar absorber. The Ni and Al particles on the substrate had reacted with oxygen in the environment, as has been previously discussed.

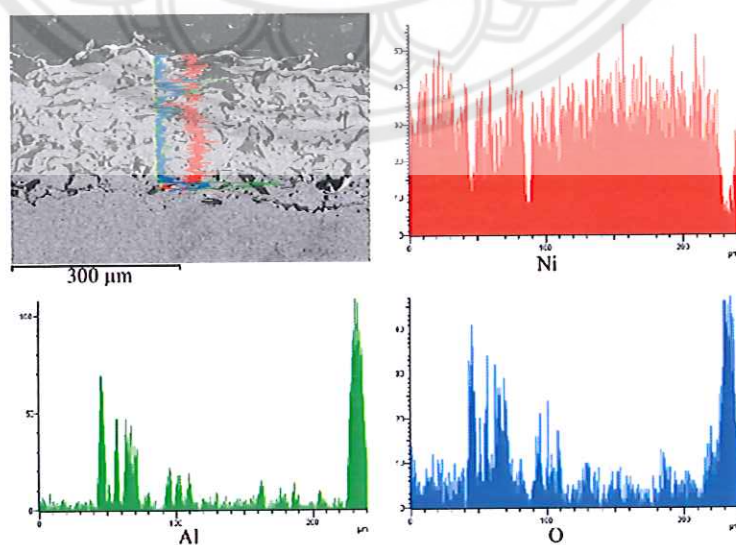


Figure 48 EDS line analysis on the cross-section of Ni-Al solar absorber

The EDS line scan image of the cross-section of the Ni-Al solar absorber is shown in Figure 48. The chemical composition of the fundamental elements of the Ni-Al solar absorber cross-section was Ni 87.53 wt.%, Al 5.04 wt.% and O 7.43 wt.%.

According to the reported analysis of the XRD pattern, SEM image and EDS surface, the cross section and line scan cross section of the Ni-Al solar absorber had a chemical composition comprising Ni, Al and O in a ratio similar to the weight percent of each of the three chemical elements.

The starting materials Ni and Al were found on the surface and in the cross-section, together with oxygen which created the oxidization during the flame spray process. When the Ni and Al particles were melted and deposited on to the substrate the oxygen from the environment was sufficient to transform the Ni and Al on the surface into the NiO and Al₂O₃ phase.

4. Ultraviolet-Visible-Near Infrared Spectrophotometer

Ultraviolet-Visible-Near Infrared Spectrophotometer was used to measure the reflectance (R) and the solar absorptance (α) for the spectra with different thicknesses of the NiAl solar absorber. The R and α values were calculated and compared with the sun spectrum of AM 1.5 in the wavelength range of 300-2500 nm, as shown in Figure 49-51. Each of the Ni-Al solar absorbers; with average thicknesses of 195 μm , 215 μm and 299 μm , were found to have slightly increased R with the increase in the wavelength. In the UV-Visible spectrum region (300-800 nm) the R was relatively low while in the near infrared region it was high and close to 1 at 2450 nm. The solar absorptance (α) of the Ni-Al solar absorber gradually decreased with the increase in the wavelength. Over the entire wavelength of the solar spectrum, the calculated α were found to be 0.75, 0.74 and 0.74.

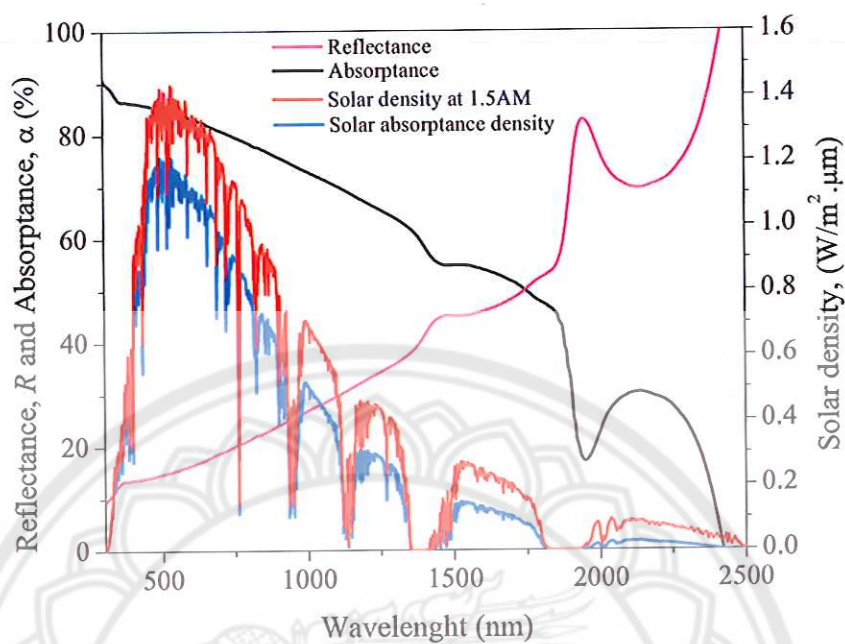


Figure 49 Sun spectrum at AM 1.5, Reflectance and solar absorptance of Ni-Al solar absorber average thickness 195 μm

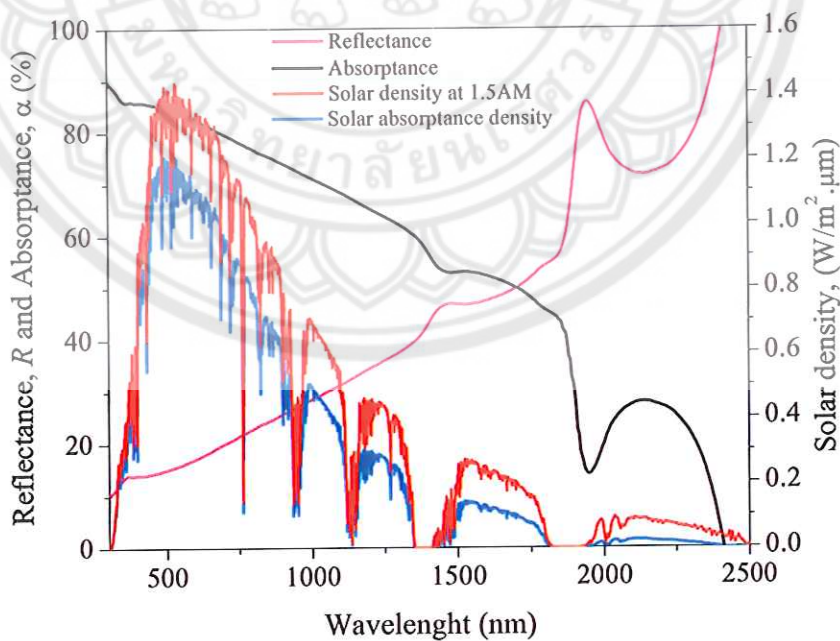


Figure 50 Sun spectrum at AM 1.5, Reflectance and solar absorptance of Ni-Al solar absorber average thickness 215 μm

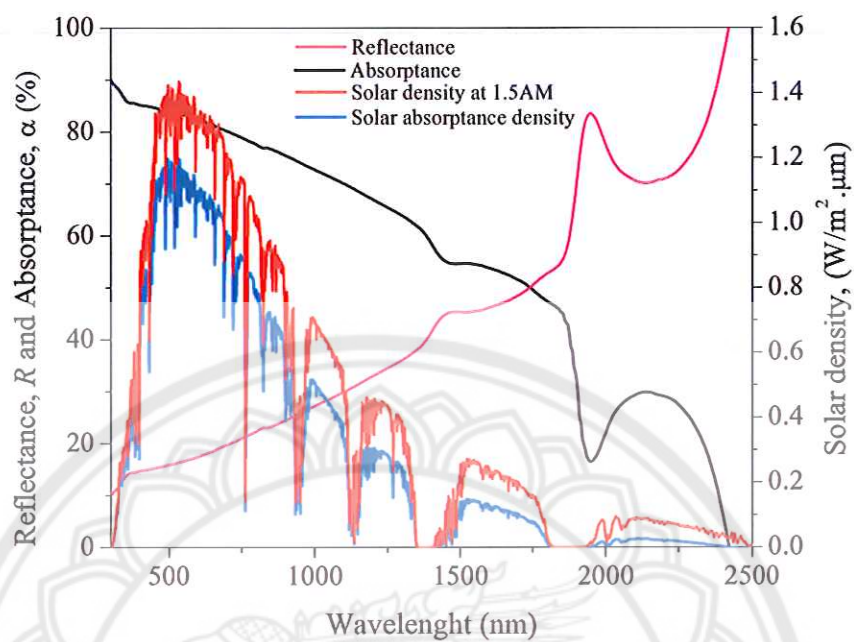


Figure 51 Sun spectrum at AM 1.5, Reflectance and solar absorptance of Ni-Al solar absorber average thickness 299 μm

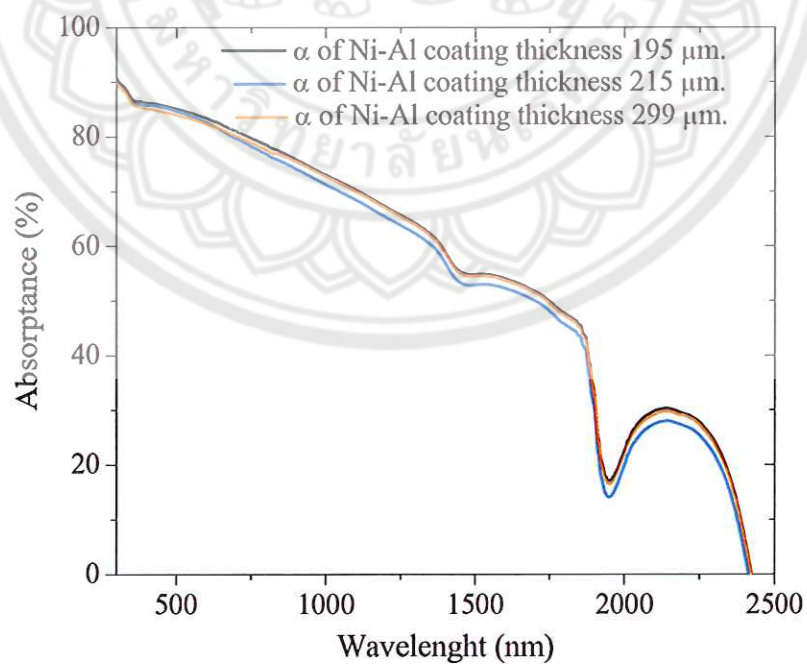


Figure 52 Solar absorptance with differences thicknesses

Table 11 Solar absorptance and reflectance with difference thickness

The average thickness of solar selective surface (μm)	Reflectance (R)	Solar absorptance (α)
195	0.33	0.75
215	0.34	0.74
299	0.33	0.74

The measured reflectance was in the long wavelength range of 300-2500 nm as shown in Table 11. The average reflectance of the Ni-Al solar absorber of each coating thickness was, for the average thickness of 195 μm , 0.33, for the average thickness of 215 μm , 0.34 and for 299 μm , 0.33. The reflectance was calculated with Equation 3 at all wavelengths and the solar absorptance and reflectance were plotted for the three different thicknesses of the absorber, as shown in Figure 52. The trend of solar absorptance of the Ni-Al solar absorber gradually decreases with the increasing wavelength. Over the entire wavelength of the solar spectrum, the calculated average solar absorptance of the three Ni-Al solar absorbers are shown in Table 11. This demonstrates that the flame spray technique can successfully coat Ni-5 wt.% Al particles onto a 316L stainless steel substrate pipe. Even with the different thicknesses, the Ni-Al surface showed high solar absorptance. However there was little difference in the solar absorptance level between the three surfaces of different thickness.

Table 12 Solar absorptance of Ni-Al compare with another materials and coating technique

Solar absorptance, α	Coating method	Reference
0.92	Spray pyrolysis	[26]
92-0.96	DC sputtering	[73]
0.97	Sol-gel	[74]
0.91	DC sputtering	[75]
0.747-0.754	Flame spray	In present study

Table 12 compares the Ni-Al solar absorber materials, and the flame spray techniques used in this research with other solar materials and coating techniques. For example, Al/Al₂O₃/NiO_x is applied using the spray pyrolysis technique, metal-aluminium nitride (M-AlN) is applied by DC sputtering, Ni-Al₂O₃/SiO₂ with Sol-gel technique. These other materials and coating techniques have been reported to have higher solar absorptance than the solar absorptance of the Ni-Al applied using the flame spray technique used in this research. However, some coating techniques use toxic chemicals in the process of applying the solar absorber materials. For example, the sputtering technique used a toxic chemical in the process, which requires the coating to be applied in a vacuum space. The DC sputtering uses a high voltage electrical current, therefore being high cost and requires a high volume of output. The flame spray technique used in this research uses no toxic chemicals, uses free oxygen from the air. Although the materials used (Ni and Al) result in a coating with lower solar absorptance than the other materials applied with the other techniques, the advantages of Ni-5 wt.% Al particles are obvious; it is a simple process, with non-toxic application of the coating, is cheap, and results in high anti-corrosion protection, and the coating has strong adhesion to the substrate.

The flame spray coating technique has been clearly demonstrated to be a good choice, perhaps the best choice, for the application of solar selective surface coatings in the field of high-temperature solar collectors.

Thermal analysis

1. Heat loss

The three different thicknesses of Ni-Al coating were tested for energy loss. The parabolic trough receiver with the varying thicknesses Ni-Al absorber coating was tested for heat loss in the temperature range of 40-200°C with a 10°C increase for every steady state. Temperatures and power values were recorded every second. Steady state was achieved when the glass and absorber temperature reached a constant value. The average temperatures, taken at three positions over the length of the glass and the absorber were calculated. The parabolic trough receiver was 1 m long at 25°C, with absorber inner diameter 2.79 cm/outer diameter 3.33 cm and glass envelope inner diameter 5.5 cm/outer diameter 6.5 cm. Laboratory testing of the heat

loss in the parabolic trough receiver, normalized per meter of receiver length, is summarized and illustrated in Figure 36 (Chapter 3: Methodology).

For the heat loss testing a parabolic trough collector was constructed with a Ni-Al solar absorber material coated on stainless steel 316L pipe, similarly to previous activities. The parabolic trough collector was situated in an evacuated glass tube, thus being surrounded by a vacuum. The whole device is termed an evacuated receiver for the purpose of this discussion. For the test a stainless steel fin heater with inner diameter of 25 mm was inserted into one end of the parabolic trough collector. A power transducer was used to measure the heater consumption. The total heat loss was calculated based on the power of the heater. The average temperature of the glass envelope and absorber, and the ambient temperature, together with the power consumed by the heater, were used for the calculation of heat loss, which was calculated for every steady state temperature of the absorber and the glass envelope. The data are shown in Appendix 2.

Instead of showing the heat loss for Ni-Al solar absorber of the entire parabolic trough collector, heat loss per meter (100 cm) of parabolic trough collector was calculated and is presented on the y-axis. The x-axis is the average absorber temperature at the time of testing. The heat loss results are not presented with the average absorber temperature, which are above the ambient temperature. This is due to the heat loss in the evacuated receivers being primarily due to radiation and is therefore more dependent on the absorber temperature only rather than the difference between the absorber temperature and the ambient temperature.



Figure 53 Temperature distribution in the cylinder pipe at 100°C

Figure 53 illustrates the heat distribution along the length of the pipe and over the profile of the pipe, including inner and outer surface temperatures. The imaging was done using an IR thermometer FLIR TG165 with the resistance heater temperature at 100°C.

Equation 27 is the equation for the fixed curve process and was used to calculate heat loss.

$$Q_{\text{loss}} \text{ (W/m)} = 0.423 - 0.002T_{\text{abs}} + (9.236 \times 10^{-4})T_{\text{abs}}^2 \quad 27$$

Figure 54 shows the heat loss trend of the Ni-Al coating thickness of 195 μm on the solar selective surface. The heat loss of the parabolic trough collector per meter over the length of the collector was calculated and is shown on the y-axis (W/m). The x-axis is the average absorber temperature at the time of the test. The heat loss result is shown for the absorber temperature range of 40°C to 200°C. Heat loss at ambient temperature was lower than 5 W/m and increased to 40 W/m as the temperature increased. The resulting heat loss is shown in Appendix 2.

Equation 28 was used to calculate the heat loss for the Ni-Al coating thickness of 215 μm on the solar selective surface.

$$Q_{\text{loss}} \text{ (W/m)} = 0.001 - 0.007T_{\text{abs}} + 0.001T_{\text{abs}}^2 \quad 28$$

and the trend is showed in Figure 55. The calculated heat loss of the parabolic trough collector per meter length is shown on y-axis (W/m). The x-axis is the average absorber temperature at the time of the test. The heat loss result is shown for the absorber temperature range of 40°C to 200°C. Heat loss at ambient temperature was lower than 4 W/m and increased to 43 W/m as the temperature increased. The resulting heat loss is shown in Appendix 2.

Equation 29 was used to calculate the heat loss for the Ni-Al coating thickness of 299 μm on the solar selective surface.

$$Q_{\text{loss}} \text{ (W/m)} = -1.178 + 0.033T_{\text{abs}} + (8.66 \times 10^{-4})T_{\text{abs}}^2 \quad 29$$

and the trend is showed in Figure 56. The calculated heat loss of the parabolic trough collector per meter length is shown on y-axis (W/m). The x-axis is the average absorber temperature at the time of the test. The heat loss result is shown for the absorber temperature range of 40°C to 200°C. Heat loss at ambient temperature was lower than 3 W/m and increased to 40 W/m as the temperature increased. The resulting heat loss is shown in Appendix 2.

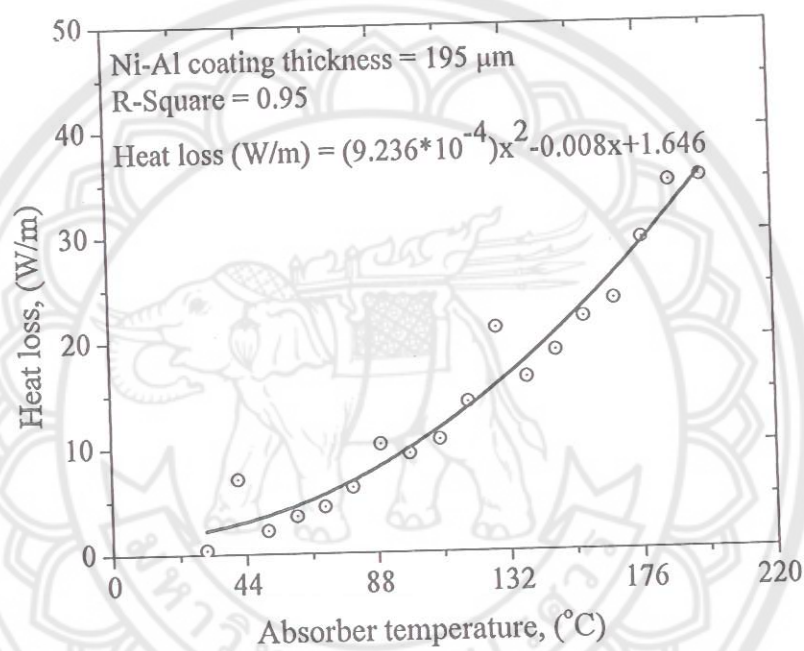


Figure 54 Heat loss of Ni-Al solar absorber thickness 195 μm

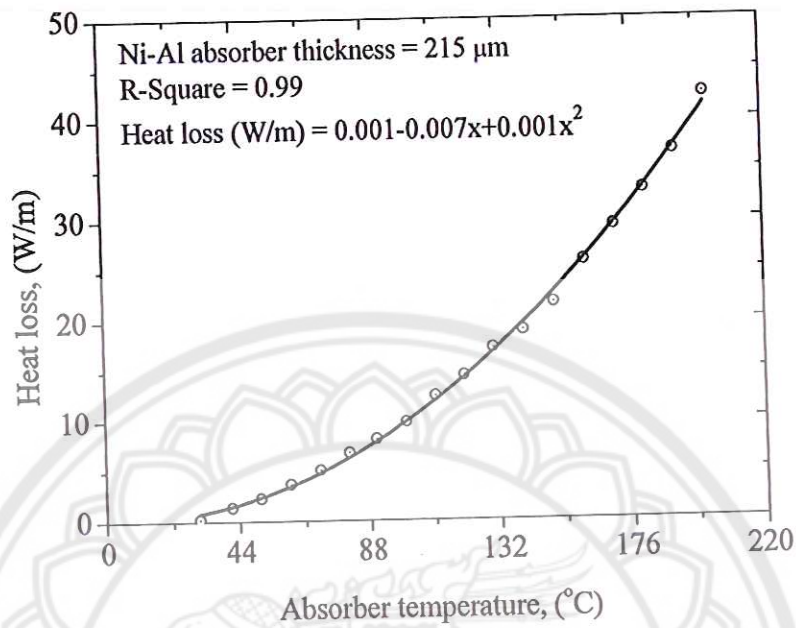


Figure 55 Heat loss of Ni-Al solar absorber thickness 215 μm

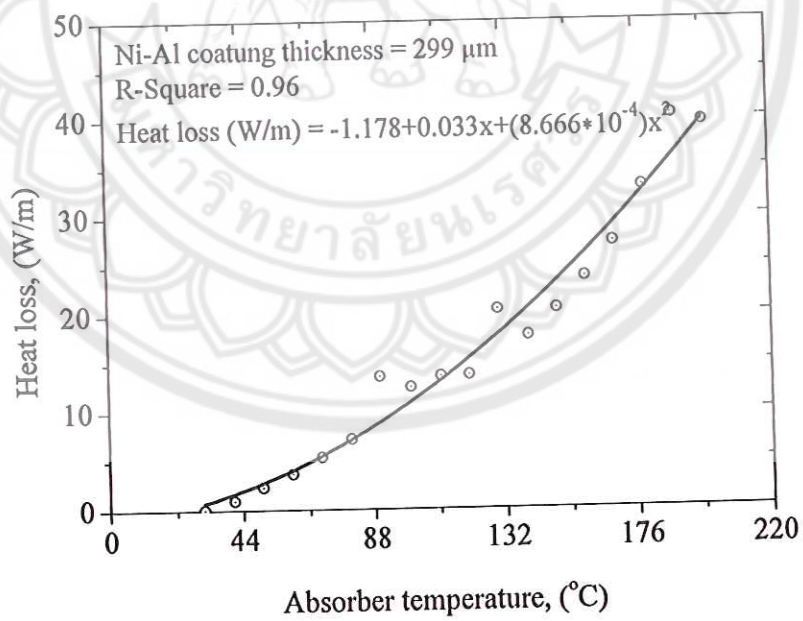


Figure 56 Heat loss of Ni-Al solar absorber thickness 299 μm

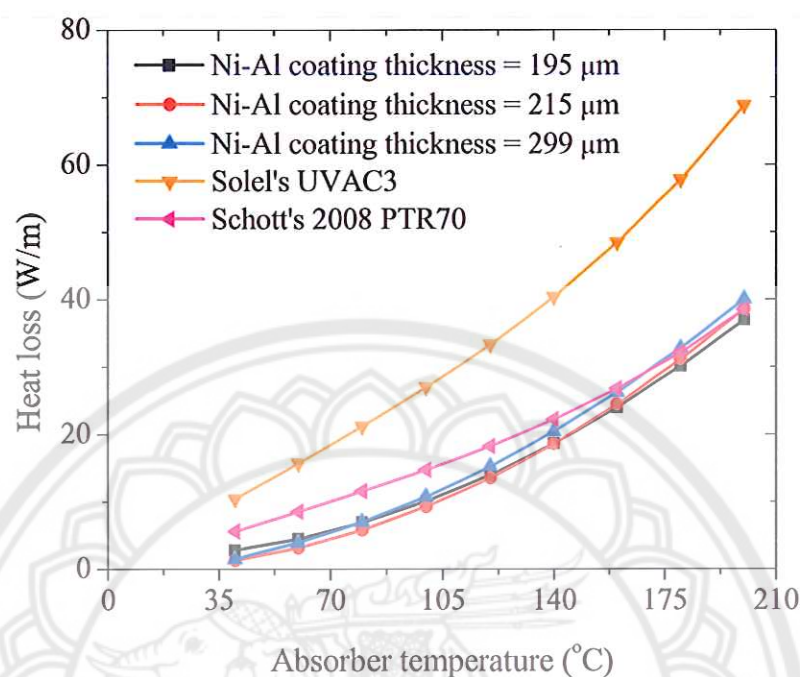


Figure 57 Heat loss compare with commercial product with three Ni-Al solar absorber thickness of parabolic trough receiver

A comparison of heat loss of two commercial parabolic trough receivers is shown in Figure 56. These two commercial units were the Schott 2008 PTR70 and the Solel UVAC3. In the marketplace, it seems that most parabolic trough receivers are coated with expensive solar selective materials which are applied using a very complicated coating technique. Some of these materials do have a negative environmental impact due to some having toxic substances in the coating material, and also because of the coating technique used, which use toxic chemicals.

Both of these commercial parabolic trough receivers selected for the study utilize a very complicated coating technique, such as sputtering, and both do have coatings of expensive solar selective materials. However, notwithstanding their market status as being top of the line, when operating at high temperatures some heat energy is lost from the receiver. The Figure 57 shows the actual and comparative energy loss, with the highest energy loss being from the Solel UVAC3 and the Schott 2008 PTR70 having a lower energy loss. When compared to the Ni-Al solar absorbers constructed and used in the present study, with different coating thicknesses, it was found that the

Ni-Al coatings had the lowest heat loss. In all the units compared both commercial and constructed for the study, there was a vacuum between the outer absorber pipe and the inner glass envelope to protect against energy loss. The vacuum space of the commercial products is generally done by pumping the air out of the vacuum space and when close to the pressure of zero psi, the space is permanently closed, maintaining the vacuum over the long term, which may still be subject to vacuum loss over time, thereby reducing the efficiency of the vacuum space to reduce heat loss. In contrast with this, the vacuum in the vacuum space of the three constructed Ni-Al solar absorbers were continuously maintained by continuous pumping to maintain the vacuum at increasing and higher operating temperatures. These units were designed in this way to ensure a continuous vacuum over time and over the temperature range up to higher operating temperatures. The heat loss propensity of this vacuum factor can therefore be considered in this research as a constant in the constructed units. The Ni-Al surface model was demonstrated as being a lower heat loss model than the commercial Solel UVAC3 and Schott 2008 PTR70 models. An important observation is that there was a similar heat in all three Ni-Al coated models regardless of the different thicknesses of coating, and in each case they had lower heat losses than the commercial units.

Emittance (ϵ) of the parabolic trough receiver absorber was calculated from the Equations 27-29, using the variable values measured in the laboratory heat loss experiments (shown in Figure 57). The following correlation fits the calculated emittance to the absorber temperature. The emittance results are shown in Figures 58, 59 and 60 for each of the three thicknesses of the solar selective surface coatings.

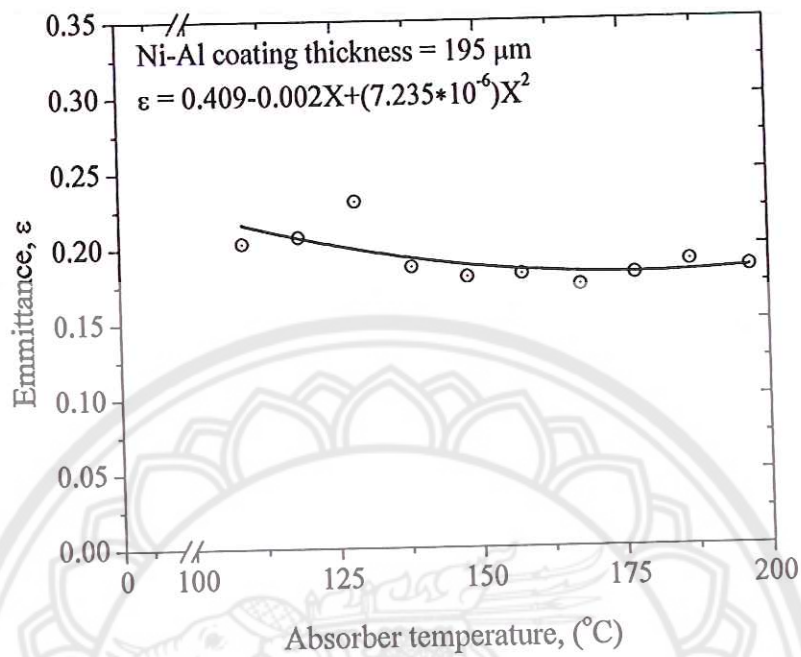


Figure 58 Emittance of Ni-Al solar absorber thickness 195 μm

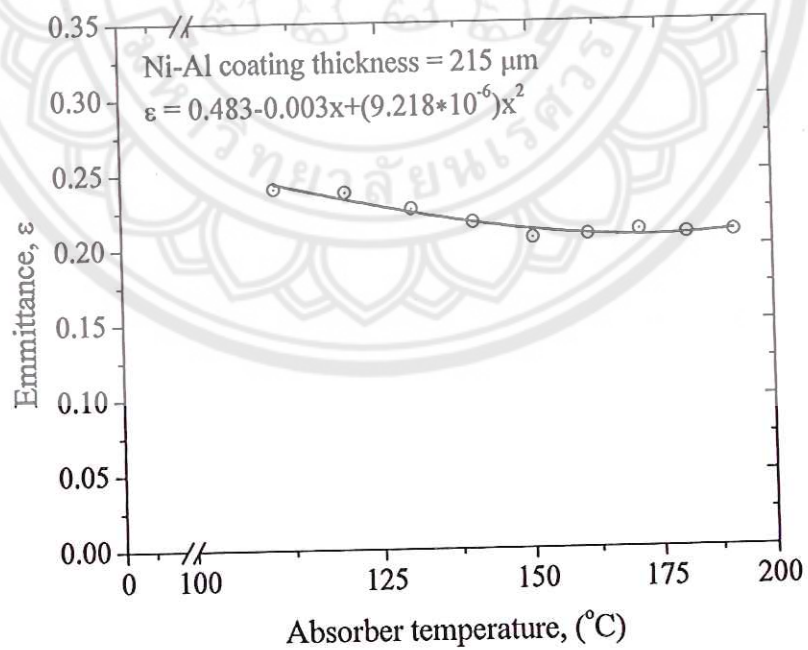


Figure 59 Emittance of Ni-Al solar absorber thickness 215 μm

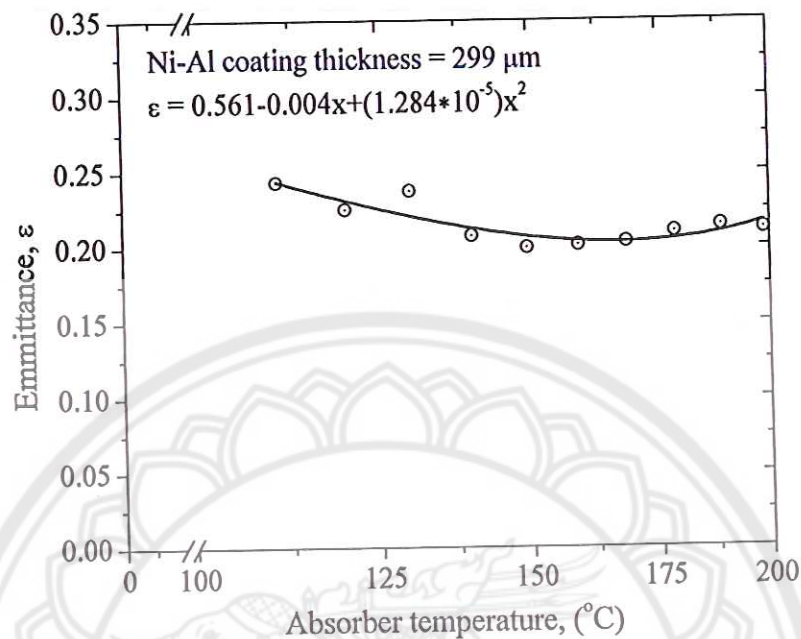


Figure 60 Emittance of Ni-Al solar absorber thickness 299 μm

The Ni-Al solar selective coating has low reflectance at a shorter wavelength giving it greater high temperature solar absorptance. This is demonstrated in Figures 57-59 where we can see that, as the absorber temperature increases, more of the thermal radiation is emitted as shorter wavelengths. However, for all three thicknesses of the Ni-Al solar absorber coating, the fit curve of emittance has a shallow slope. One reason for this is that the proportion of the heat loss that is due to conduction at the end of the parabolic trough receiver increasing with decreasing absorber temperatures. The test results were that thermal emittance starting at 100°C were, for each thickness, 0.22 for thickness 194.79 μm , 0.23 for 215 μm and 0.20 for 299 μm . The emittance was lower for the thin Ni-Al solar absorber and increased when the coating thickness increased. The higher thickness Ni-Al absorbs larger amounts of heat energy and in steady state radiates them out at a higher rate. The large absorber surface area can also increase heat loss.

2. Thermal efficiency of parabolic trough collector.

Combustible powder comprised of Ni-Al particles were coated on stainless steel substrate using the flame spray process. The thermal efficiency of each of the three models with coating thicknesses of 195 μm , 215 μm and 299 μm was calculated using Equations 19. The experimental parameters included ambient temperature (T_a , $^{\circ}\text{C}$), the temperature of the water at the inlet (T_{in} , $^{\circ}\text{C}$) temperature, direct solar radiation (G_B , W/m^2) and the flow rate of the water through the collector pipe (\dot{m} , l/m). These are summarized in Table 9.

For the Ni-Al solar absorber thickness of 195 μm , the thermal efficiency calculation was performed under steady state approximations. The thermal efficiency (η) was compared with the heat loss parameter ($F_R U_L / C$) as shown in Figure 61. For operational purposes, the factors, F_R and U_L , were determined as constant values, and the efficiency of the collector was given by Equation 30:

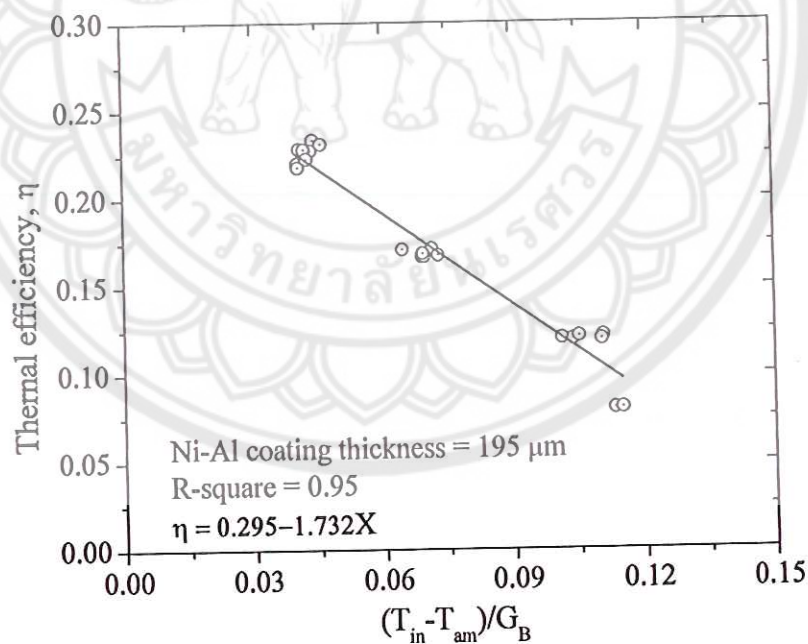


Figure 61 Thermal efficiency of Ni-Al solar absorber thickness 195 μm

$$\eta = 0.295 - 1.732(T_{in} - T_{am})/G_B$$

30

The relationship was formed by the linear equation. Initially, testing was done by feeding water into the system, with the inlet water temperature at about room temperature. For this sample, the maximum efficiency and the intercept ($F_R\eta_0$) was 0.295. The efficiency difference was divided by the corresponding horizontal scale difference; $-F_R U_L/C$, which was -1.732 (the slope of line as shown in Figure 60).

For the Ni-Al solar absorber thickness of 215 μm , the thermal efficiency of the Ni-Al coating was performed under steady state conditions. The thermal efficiency (η) was compared with the heat loss parameter $-F_R U_L/C$, as shown in Figure 62. The factors for operating under steady irradiation, F_R and U_L , were determined as constant values. From this experimental data, the efficiency of the collector can be calculated by Equation 31:

$$\eta = 0.409 - 1.697(T_{in} - T_{am})/G_B$$

31

For this test, the maximum efficiency and the intercept ($F_R\eta_0$) was 0.409, and the slope of line, $-F_R U_L/C$, was -1.697 (Figure 62).

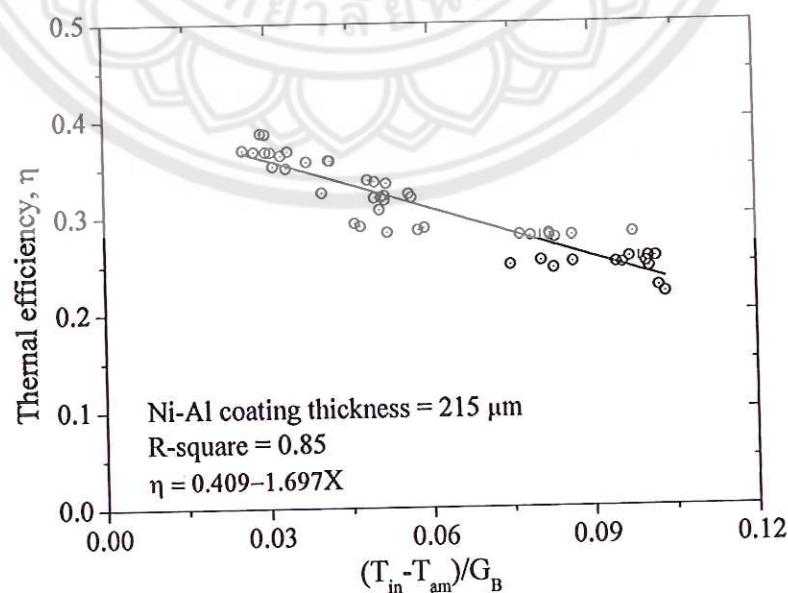


Figure 62 Thermal efficiency of Ni-Al solar absorber thickness 215 μm

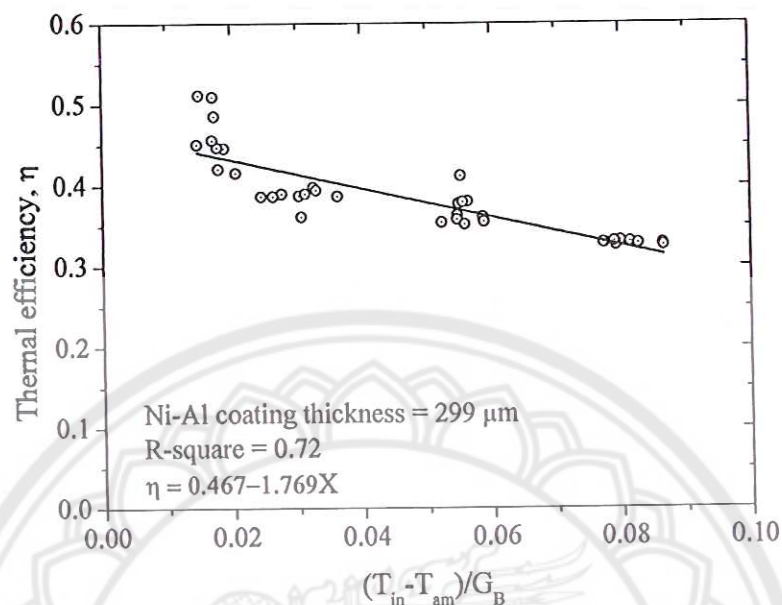


Figure 63 Thermal efficiency of Ni-Al solar absorber thickness 299 μm

For the Ni-Al solar absorber thickness of 299 μm, the thermal efficiency of the Ni-Al coating was performed under steady state conditions. The factors for operating under steady irradiation, F_R and U_L , were determined to be constant values. Therefore, the efficiency of collector for this sample was given by Equation 32:

$$\eta = 0.467 - 1.769(T_{in} - T_{am})/G_B \quad 32$$

The maximum efficiency and the intercept ($F_R \eta_0$) was 0.467, and the slope of line, $-F_R U_L / C$, was -1.769 (Figure 63).

This process was performed the same way for each of the three samples, with different thicknesses, ensuring the results were comparable.

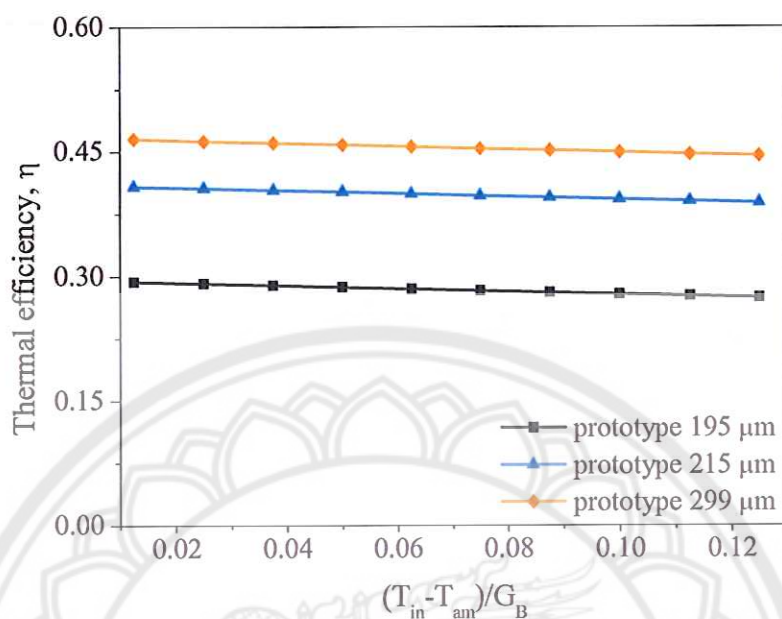


Figure 64 Thermal efficiency comparison of three Ni-Al solar absorber

The three Ni-Al solar absorbers of the parabolic trough collectors were tested under steady state conditions. The collectors in this research were designed with homogeneous parameters and different thicknesses of the solar selective coating material. The many complex parameters involved in determining the optical efficiency of the Ni-Al solar absorbers, and the thermal efficiency results for the three thicknesses are shown in Figure 64. The intercept factors are shown, and compared, in Table 13.

Optical efficiency (η_0) is the ratio of the amount of energy absorbed by the receiver and the amount of energy incident on the collector's aperture, which depends on the optical properties of the material design. The geometry of the collector (A_f) was designed to reduce the ratio of the lost area (A_l) (shadow) to the aperture area (A_a). Thus, the optical efficiency (η_0) was the relationship of the reflectance of the reflector (ρ), the transmittance of the glass cover (τ), the solar absorptance of the collector (α), the intercept factor (γ), geometric factor (A_f), and the angle of incidence. The optical efficiency was calculated by Equation 33 [34].

$$\eta_0 = \rho\tau\alpha\gamma [(1 - A_f \tan(\theta)\cos\theta)]$$

33

The optical efficiency is different for each Ni-Al solar absorber because the values for the reflectance and solar absorptance of each were not equal. Optical efficiency was assumed to be some value of the thermal efficiency calculation as the intercept factor ($\gamma = 1$, is defined as the ratio of the energy intercepted by the receiver to the energy reflected by the focusing device [76, 77], and assuming perfect equipment (indicating a ratio of 1:1, and the geometric factor $A_f = 0$). So, the term of $\tan(\theta)\cos(\theta)$ in the equation was equal to zero (although θ at testing area used 17°).

Table 13 The result of thermal performance and Ni-Al solar selective thickness

Parameter	Thermal performance equation		
	$\eta = 0.295 - 1.732$ $(T_{in} - T_{am})/G_B$	$\eta = 0.409 - 1.697$ $(T_{in} - T_{am})/G_B$	$\eta = 0.467 - 1.769$ $(T_{in} - T_{am})/G_B$
Thickness	195 μm	215 μm	299 μm
η_0	0.61	0.60	0.60
α	0.75	0.74	0.74
τ	0.90	0.90	0.90
$\alpha.\tau$	0.67	0.66	0.66
$F_R U_L$	25.98	25.45	26.53
F_R	0.48	0.68	0.67
U_L	54.12	37.43	39.59

Note: τ of borosilicate glass 0.9

Thermal efficiency is the capability of transferring heat energy into a fluid. From our experimental results, we have demonstrated that the thickness of the solar selective surface is an important factor that influences the performance of the collector. The intercept ($F_R \eta_0$) parameter represents the maximum thermal efficiency and it varies with the thickness; an increase in thickness resulted in an increase in thermal efficiency. The Ni-Al coating with thickness 299 μm had the highest thermal

efficiency while the thinner surface thickness of 195 μm had the lowest thermal efficiency. This is shown in Figures 61-63. So it has been demonstrated that higher thicknesses absorb higher heat energy and show greater heat gain. The optical efficiency (η_0) of the coatings of different thicknesses were, however, very similar in value.

The test results, as illustrated in Figures 61-63, show the decrease in thermal efficiency over time, for the three thicknesses of coating. The slope of the line ($-F_R U_L / C$) represents the thermal efficiency loss. This shows that the thermal efficiency of the collectors demonstrated the same characteristic of decreasing, over each of the three thicknesses of coating. Generally, the slope of the line ($-F_R U_L$) in a thermal efficiency curve always indicates a decrease in thermal efficiency.

In this research the thermal efficiency of the parabolic trough collector that was coated with Ni-Al particles, applied using the flame spray technique was compared with the parabolic trough collectors that had been coated with different solar selective material, and applied using different techniques, as reported in other research. The comparative values are shown in Table 14 which also indicated the source of the information used in the comparison

Table 14 Comparison of collector efficiency equation

Solar selective material	Coating technique	Absorber substrate	Absorber length	Efficiency	Reference
Black	Paint	Copper	1.3 m	0.69	[76]
Black	Paint	Copper	1.25 m	0.69	[78]
Black	Black chrome	Copper	2 m	0.67	[79]
Ni-Al	Flame spray	SS316L	1 m	0.29	Case study
				0.40	Case study
				0.46	Case study

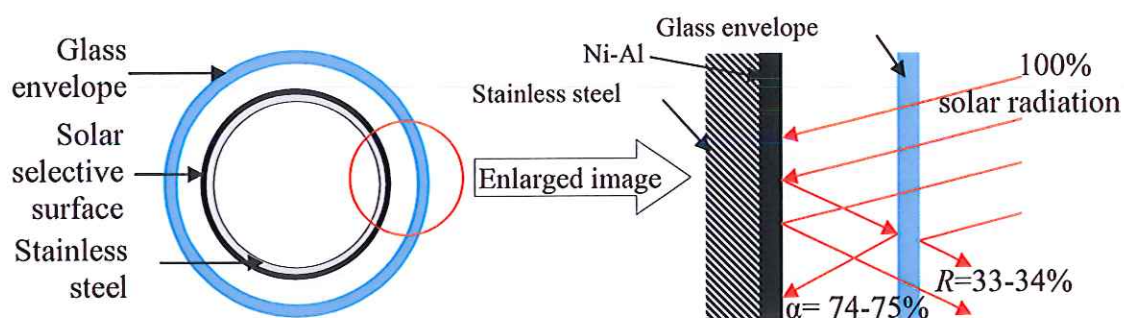


Figure 65 Nature of convert solar radiation to heat energy of Ni-Al surface

Figure 65 explains the mechanism of the heat transfer process, which describes how the solar radiation is converted to heat energy in the parabolic trough collector. In the figure, the cross-section view of the parabolic trough collector shows the stainless steel pipe substrate, the Ni-Al surface deposited on the substrate, and the glass envelope surrounding the coated pipe, which contains a vacuum. Heat transfer occurs when solar radiation falls on the outer surface of the glass envelope (which is made from borosilicate material), transfers through to the outer coating surface of the collector pipe, and is then transferred through the collector pipe to heat the water in the pipe.

The borosilicate glass tube has superior physical properties allowing it to be used in a high temperature situation exceeding 500°C. The glass a high transmittance rate estimated to be 0.9 or better, and a low reflectance of less than 0.4. The vacuum space in the glass envelope, with internal pressure close to 0 psi, reduces heat loss significantly almost to 0.

The glass envelope tube covers the full length of the Ni-Al solar absorber, and space make a vacuum space. Radiation back through the glass cover from the Ni-Al surface is almost insignificant resulting in the Ni-Al surface absorbing close to 100% of the solar radiation transferred from the outer glass surface to the selective surface. The rough surface of the Ni-Al coating also protects against radiation being reflected back to the outer surface. The result of these various physical properties of the materials is that almost 100% of the incidental solar rays are converted to heat energy which is transferred to the fluid with a high level of efficiency. In high temperature operating conditions, the vacuum gap is effective in protecting against heat energy loss from the collector.

CHAPTER V

CONCLUSION AND RECOMMENDATION

Conclusion

Ni-Al solar absorber was successfully coated on a stainless steel SS316L pipe substrate using the flame spray technique. The starting spray material was Ni-Al combustible powder using Ni-5 wt.% Al particles. The different thicknesses of Ni-Al solar absorber with 195, 215 and 299 μm were prepared. The surface of the Ni-Al solar absorber had a dark gray color tone and roughness. The Ni-Al solar absorber coating was composed of Ni, Al, NiO and Al_2O_3 phases. The microstructure of the coating had overlapped layer by layer with the layer structure parallel to the surface of the substrate. Most splats were found predominantly in the Ni and Al-rich area. This technique was used to produce different coating thicknesses. The solar absorptance (α) of all thickness were relatively identical values (0.74-0.75) over the whole wavelength range of the solar spectrum.

The Ni-Al solar absorber coated on a stainless steel SS316L pipe was specifically designed for receiver tube in the Parabolic Trough Collector (PTC) for measuring heat loss and thermal performance. All the receiver tube with different Ni-Al thickness were covered with a glass vacuum tube in order to reduce heat loss to the surroundings. During operating temperature at 100°C , heat loss of each thickness was 17.64, 17.35 and 22.75 W/m.K for thickness 195, 215 and 299 μm , respectively. It is found that heat loss in the receiver tube composed of heat conduction and radiation mechanisms because a vacuum insulator inside of receiver tube cannot totally eliminate heat loss, corresponding to the theoretical of radiation heat transfer. According to the heat loss results at 100°C , the emittance (ϵ) increased with the thickness and reached its highest to 0.28 of 299 μm thick. The thermal performance of PTC is one of the performance indices of the collector which presents the relationship between maximum collector efficiency ($F_R\eta_0$) and thermal loss ($-F_RU_1/C$). The collector efficiency was 0.29, 0.40 and 0.46 with the thicknesses of 195, 215 and 299 μm , respectively, with the thermal loss viz -1.732, -1.697 and -1.769. The increasing Ni-Al thickness was effective on the thermal efficiency and thermal loss due to the

ability of Ni-Al particles melted in Ni-Al solar absorber layers for absorbing and to convert the solar radiation into thermal energy and transferring to the working fluid. The results show that the Ni-Al solar absorber with 299 μm thickness is found to be the suitable choice for the solar absorber materials because of the highest α (0.74) and $F_{R\eta_0}$ (0.49), compared to the other thicknesses considered in this research. Therefore, the Ni-Al solar absorber is a good candidate for a solar absorber material for solar collectors at high operating temperature.

Recommendations

1. Thermal conductivity and heat loss testing needs to be done in high temperature environments in temperatures higher than 200°C , which is usual in large scale solar power plants.
2. The direct solar radiation in testing should follow the thermal efficiency testing standards of direct solar radiation $\geq 790 \text{ W/m}^2$.
3. Testing for thermal efficiency should be carried out with water at an inlet temperature greater than 100°C .



REFERENCES

REFERENCES

- [1] John A. Duffie and W.A. Beckman. (2006). **Solar engineering of thermal process**. New Jersey: John Willey & Sons.
- [2] H P Garg and J. Prakash. (2004). **Solar energy fundamentals and applications**. New Delhi: Tata McGraw-Hill Publishing Company Limited.
- [3] Kalogirou, S.A. (2009). **Solar energy engineering**. N.P.: Elsevier.
- [4] Barshilia, H.C., Selvakumar, N., Rajam, K.S., Sridhara Rao, D.V. and Muraleedharan, K. (2008). Deposition and characterization of TiAlN/TiAlON/Si₃N₄ tandem absorbers prepared using reactive direct current magnetron sputtering. **Thin Solid Films**, 516(18), 6071-6078.
- [5] Barshilia, H.C., Selvakumar, N., Rajam, K. S. and Biswas, A. (2008). Spectrally selective NbAlN/NbAlON/Si₃N₄ tandem absorber for high-temperature solar applications. **Solar Energy Materials and Solar Cells**, 92(4), 495-504.
- [6] Gong, G., Huang, X., Wang, J. and Hao, M. (2010). An optimized model and test of the China's first high mperature parabolic trough solar receiver. **Solar Energy**, 84(12), 2230-2245.
- [7] Valan Arasu, A.T. (2007). Sornakumar, Design, manufacture and testing of fiberglass reinforced parabola trough for parabolic trough solar collectors. **Solar Energy**, 81(10), 1273-1279.
- [8] Beckman, J.A.D.W.A. (2006). **Solar wngineering of thermal processes**. Hoboken, New Jersey: John Wiley & Sons.
- [9] Kalogirou, S.A. (2004). Solar thermal collectors and applications. **Progress in Energy and Combustion Science**, 30(3), 231-295.
- [10] Fernández-García, A., Zarza, E., Valenzuela, L. and Pérez, M. (2010). Parabolic-trough solar collectors and their applications. **Renewable and Sustainable Energy Reviews**, 14(7), 1695-1721.
- [11] Valenzuela, L., Zarza, E., Berenguel, M. and Camacho, F.E. (2005). Control concepts for direct steam generation in parabolic troughs. **Solar Energy**, 78(2), 301-311.

- [12] Wang, Y. and W. Chen. (2004). Microstructures, properties and high-temperature carburization resistances of HVOF thermal sprayed NiAl intermetallic-based alloy coatings. **Surface and Coatings Technology**, 183(1), 18-28.
- [13] Dacis., J.R. (2004). **Handbook of thermal spray technology**. United States of America: ASM International.
- [14] AlShamaileh, E. (2010). Testing of a new solar coating for solar water heating applications. **Solar Energy**, 84(9), 1637-1643.
- [15] Juang, R.-C., Yeh, Y.-C., Chang, B.-H., Chen, W.-C. and Chung, T.-W. (2010). Preparation of solar selective absorbing coatings by magnetron sputtering from a single stainless steel target. **Thin Solid Films**, 518(19), 5501-5504.
- [16] Madhusudana., M. and H.K. Sehgal. (1982). Spary-Deposited black nickel selective absorber surface fot solar thermal conversion. **Applied Energy**, 10, 65-74.
- [17] C.E.Kennedy. (2002). **Review of mid-to high-temperature solar selective absorber materials**. Washington, D.C: National Renewable Energy Laboratory, Technical report NREL/TP-550-45633.
- [18] V.Teixeira a, E.Sousa a, M.F. Costaa, C.Nunes b, L.Rosa b, M.J. Carvalhob and E.R.c. M.Collares-Pereira b, J.Gago c. (2002). Chromium-based thin sputtered composite coatings for solar thermal collectors. **VACUUM**, 64, 299-305.
- [19] Ming-Sheng LeuU, B.F.C., S.Y. Chen, Y.W. Lee and W.C. Lih. (2000). Properties of (Ti,Al)N coatings deposited by the magnetic filter cathodic arc. **Surface and Coatings Technology**, 133-134, 319-324.
- [20] Hawk, J.A. and Alman, D. E. (1999). Abrasive wear behavior of NiAl and NiAl-TiB₂ composites. **Wear**, 225-229(Part 1), 544-556.
- [21] Tharamani, C.N. and S.M. Mayanna. (2007). Low-cost black Cu-Ni alloy coatings for solar selective applications. **Solar Energy Materials and Solar Cells**, 91(8), 664-669.
- [22] Barrera, E., Gonzalez, F., Rodriguez, E. and Ramirez, J.A. (2010). Correlation of optical properties with the fractal microstructure of black molybdenum coatings. **Applied Surface Science**, 256(6), 1756-1763.

- [23] Lira-Cantú, M., Sabio, A.M., Brustenga, A. and Gómez-Romero, P. (2005). Electrochemical deposition of black nickel solar absorber coatings on stainless steel AISI316L for thermal solar cells. **Solar Energy Materials and Solar Cells**, 87(1-4), 685-694.
- [24] S. Surviliene a, L. Orlovskaja a and S. Biallozor b. (1999). Black chromium electrodeposition on electrodes modified with formic. **Surface and Coatings Technology**, 122, 235-241.
- [25] Madhusudana, M. and Sehgal, H.K. (1982). Spray-Deposited black nickel selective absorber surfaces for solar thermal conversion. **Applied Energy**, 10, 65-74.
- [26] Ienei, E., Isac, L., Cazan, C. and Duta, A. (2010). Characterization of Al/Al₂O₃/NiOx solar absorber obtained by spray pyrolysis. **Solid State Sciences**, 12(11), 1894-1897.
- [27] Wang, Y., Wang, Z., Yang, Y. and Chen, W. (2008). The effects of ceria on the mechanical properties and thermal shock resistance of thermal sprayed NiAl intermetallic coatings. **Intermetallics**, 16(5), 682-688.
- [28] Sierra, C. and A.J. Vázquez. (2005). NiAl coatings on carbon steel by self-propagating high-temperature synthesis assisted with concentrated solar energy: mass influence on adherence and porosity. **Solar Energy Materials and Solar Cells**, 86(1), 33-42.
- [29] Songbo, X., Yongda, Z., Xing, H., Bangna, Z. and Zhongxing, Y. (2002). Corrosion resistance of the intermetallic compound, NiAl, in a molten carbonate fuel cell environment. **Journal of Power Sources**, 103(2), 230-236.
- [30] Hawk, J.A. and D.E. Alman. (1999). Abrasive wear behavior of NiAl and NiAl-TiB composites. **Wear**, 225-229, 544-556.
- [31] Pawlowski, L. (2008). **The science and engineering of thermal spray coating** J.W.S. England: Wiley.
- [32] Tiwari, G.N. (1997). **Solar thermal engineering systems**. New Delhi, India: Narosa Publishing House.
- [33] Boström, T.K., E. Wäckelgård and G. Westin. (2005). Durability tests of solution-chemically derived spectrally selective absorbers. **Solar Energy Materials and Solar Cells**, 89(2-3), 197-207.

- [34] Kalogirou, S.A. (2009). **Solar energy engineering processes and systems**. United States of America: Elsevier.
- [35] T. Bostrom, G. Westin and E. Wackelgard. (2007). Optimization of a solution-chemically derived solar absorbing spectrally selective surface. **Solar Energy & Solar Cells**, 91, 38-43.
- [36] Enrique, B., Gonzalez, F., Rodriguez, E. and Alvarez-Ramirez, J. (2010). Correlation of optical properties with the fractal microstructure of black molybdenum coating. **Applied Surface Science**, 256, 1756-1763.
- [37] Yu Liu, Cong Wang and Y. Xue. (2012). The spectral properties and thermal stability of NbTiON solar selective absorbing coating. **Solar Energy Materials & Solar Cells**, 96, 131-136.
- [38] Bostrom, T., Valizadeh, S., Lu, J., Jensen, J., Westin, G. and Wäckelgård, E. (2011). Structure and morphology of nickel-alumina/silica solar thermal selective absorber. **Journal of Non-Crystalline Solids**, 357, 1370-1375.
- [39] G. Katumba, G. Makiwa, T. R. Baisitse, L. Olumekor, A. Forbes and E. Wäckelgård. (2007). Solar selective absorber functionality of carbon nanoparticles embedded in SiO₂, ZnO and NiO matrices. **Phys. stat. sol.**, 5(2), 549-551.
- [40] Kennedy, C.E. (2002). **Review of mid - to high temperature solar selective absorber materials**. United States: National Renewable Energy Laboratory.
- [41] Tuquabo, T. (2000). **Characterization of selective solar absorbers**. Sweden: Uppsala.
- [42] Katumba, G., Olumekor, L., Forbes, A., Makiwa, G., Mwakikunga, B. and Lu, J. (2008). Optical, thermal and structural characteristics of carbon nanoparticles embedded in ZnO and NiO as selective solar absorbers. **Solar Energy Materials and Solar Cells**, 92(10), 1285-1292.
- [43] Karthick Kumar, S., Suresh, S., Murugesan, S. and Paul Raj, S. (2013). CuO thin films made of nanofibers for solar selective absorber applications. **Solar Energy**, 94, 299-304.
- [44] Bostrom, T., E. Wackelgard, and G. Westin. (2005). Durability tests of solution-chemically derived spectrally selective absorbers. **Solar Energy Materials and Solar Cells**, 89(2-3), 197-207.

- [45] Boström, T.K., E. Wäckelgård and G. Westin. (2004). Anti-reflection coatings for solution-chemically derived nickel—alumina solar absorbers. **Solar Energy Materials and Solar Cells**, 84(1-4), 183-191.
- [46] Gueymard, C.A. (2001). Parameterized transmittance model for direct beam and circumsolar spectral irradiance. **Solar Energy**, 71(5), 325-346.
- [47] Gueymard, C.A. (2004). The sun's total and spectral irradiance for solar energy applications and solar radiation models. **Solar Energy**, 76(4), 423-453.
- [48] Gueymard, C.A., D. Myers and K. Emery. (2002). Proposed reference irradiance spectra for solar energy systems testing. **Solar Energy**, 73(6), 443-467.
- [49] Dong, H.X., Jiang, Y., He, Y.H., Song, M., Zou, J., Xu, N.P., et al. (2009). Formation of porous Ni–Al intermetallics through pressureless reaction synthesis. **Journal of Alloys and Compounds**, 484(1–2), 907-913.
- [50] Cai, F. and C. Jiang. (2014). Influences of Al particles on the microstructure and property of electrodeposited Ni–Al composite coatings. **Applied Surface Science**, 292, 620-625.
- [51] Xue, Y., Wang, C., Wang, W., Liu, Y., Wu, Y., Ning, Y., et al. (2013). Spectral properties and thermal stability of solar selective absorbing AlNi–Al₂O₃ cermet coating. **Solar Energy**, 96, 113-118.
- [52] Xu, C., Du, L., Yang, B. and Zhang, W. (2011). The effect of Al content on the galvanic corrosion behaviour of coupled Ni/graphite and Ni–Al coatings. **Corrosion Science**, 53(6), 2066-2074.
- [53] Cai, F., C. Jiang and X. Wu. (2014). X-ray diffraction characterization of electrodeposited Ni–Al composite coatings prepared at different current densities. **Journal of Alloys and Compounds**, 604, 292-297.
- [54] L., R., A. Pitaes, M. Andritschky, P. Capela, M.F. Cerqueira and A. Matilainen, K. (2011). **Pischow, optical characterization of TiAlN/TiAlON/SiO₂ absorber for solar selective applications**. Elsevier: Surface and Coating Technology.
- [55] Zhang, Q.-C. (2000). Recent progress in high-temperature solar selective coatings. **Solar Energy Materials and Solar Cells**, 62(1–2), 63-74.
- [56] M. Madhusudana and H.K. Sehgal. (1982). Spray-deposited black nickel selective absorber surface for solar thermal conversion. **Applied energy**, 10, 65-74.

- [57] Gordo, P.R., Cabaço, J.M.C., Nunes, Y., Paixão, V.M.B. and Maneira, M.J.P. (2002). Cylindrical hollow magnetron cathode. Al–N selective coatings for solar collector absorbers. *Vacuum*, 64(3–4), 315-319.
- [58] Elena, L., Isac, L., Cazan, C. and Duta, A. (2010). Characterization of Al/Al₂O₃/NiOx solar absorber obtained by spray pyrolysis. *Solid State Sciences*, 12, 1894-1897.
- [59] Zhenxiang Li, J.Z. and Lihui Ren. (2012). Aqueous solution-chemical derived Ni-Al₂O₃ solar selective absorbing coating. *Solar Energy Materials and Solar Cells*, 105, 90-95.
- [60] Santiago, S. and A.M. Fernandez. (2014). Electrolytic Nickel Impregnation of Porous Anodic Aluminum Oxide Films Using AC Voltage as Solar Selective Absorber. *Energy Procedia*, 57, 2733-2742.
- [61] Kritsada., B. (2010). **Production and characterization of solar selective surface** (pp. 22-24). Phitsanuloke: Graduate School of Naresuan university.
- [62] Gordon, J. (2001). **Solar energy**. London: James & James (Science Publishers).
- [63] Sampath, S., Jiang, X.Y., Matejicek, J., Prchlik, L., Kulkarni, A. and Vaidya, A. (2004). Role of thermal spray processing method on the microstructure, residual stress and properties of coatings: an integrated study for Ni–5 wt.%Al bond coats. *Materials Science and Engineering: A*, 364(1–2), 216-231.
- [64] Culha, O., CeliK, E., Ak Azem, N.F., Birlik, I., Toparli, M. and Turk, A. (2008). Microstructural, thermal and mechanical properties of HVOF sprayed Ni–Al-based bond coatings on stainless steel substrate. *Journal of Materials Processing Technology*, 204(1–3), 221-230.
- [65] Lech., P. (2008). **The science and engineering of thermal spray coating**. Chichester: John Wiley & Sons.
- [66] Forristall, R. (2003). **Heat transfer analysis and modeling of a parabolic trough solar receiver implemented in engineering equation solver**. Golden, Colorado: National Renewable Energy Laboratory.
- [67] Magal, B.S. (1990). **Solar power engineering**. New Dalhi: Tata McGraw-Hill.
- [68] Whiston, C. (1991). **X-ray methods**. London: John Wiley & Son.

- [69] Hafner, B. (n.d.). **Energy dispersive spectroscopy on the SEM.** USA:
University of Minnesota
- [70] Kutscher, F.B.a.C. (2008). **Heat-loss testing of solel's UVAC3 parabolic trough receiver.** Golden, Colorado: National Renewable Energy Laboratory.
- [71] Kutscher, F.B.a.C. (2009). **Heat loss testing of schott's 2008 PTR70 parabolic trough receiver.** Golden, Colorado: National Renewable Energy Laboratory.
- [72] Rahman, A., Jayaganthan, R., Prakash, S., Chawla, V. and Chandra, R. (2009). High temperature oxidation behavior of nanostructured Ni-Al coatings on superalloy. **Journal of Alloys and Compounds**, 472(1-2), 478-483.
- [73] Zhang, Q.-C. (2000). Recent progress in high-temperature solar selective coatings. **Solar selective materials & solar cells**, 62, 63-74.
- [74] Boström, T., Jensen, J., Valizadeh, S., Westin, G. and Wäckelgård, E. (2008). ERDA of Ni-Al₂O₃/SiO₂ solar thermal selective absorbers. **Solar Energy Materials and Solar Cells**, 92(10), 1177-1182.
- [75] Zhao, S., C.-G. Ribbing and E. Wäckelgård. (2005). New method to optimize a solar absorber graded film profile. **Solar Energy**, 78(1), 125-130.
- [76] A. Valan Arasu, T.S. (2007). Design, manufacture and testing of fiberglass reinforced parabolic trough for parabolic trough solar collectors. **Solar Energy**, 81, 1273-1279.
- [77] A. Valan Arasu and T. Sornakumar. (2006). Performance characteristics of parabolic trough solar collector system for hot water generation. **International Energy Journal**, 7(2), 137-145.
- [78] Sornakumar, A.V.A.a.T. (2006). Performance Characteristics of Parabolic Trough Solar Collector System for Hot water Generation. **International Energy Journal**, 7(2), 137-145.
- [79] Alibakhsh, K., Samaneh, D., Reza, D. and Alimorad, R. (2015). Performance evaluation and nanofluid using capability study of a solar parabolic trough collector. **Energy Conversion and Management**, 89, 368-375.



APPENDIX A JCPDS DATABASE

Name and formula

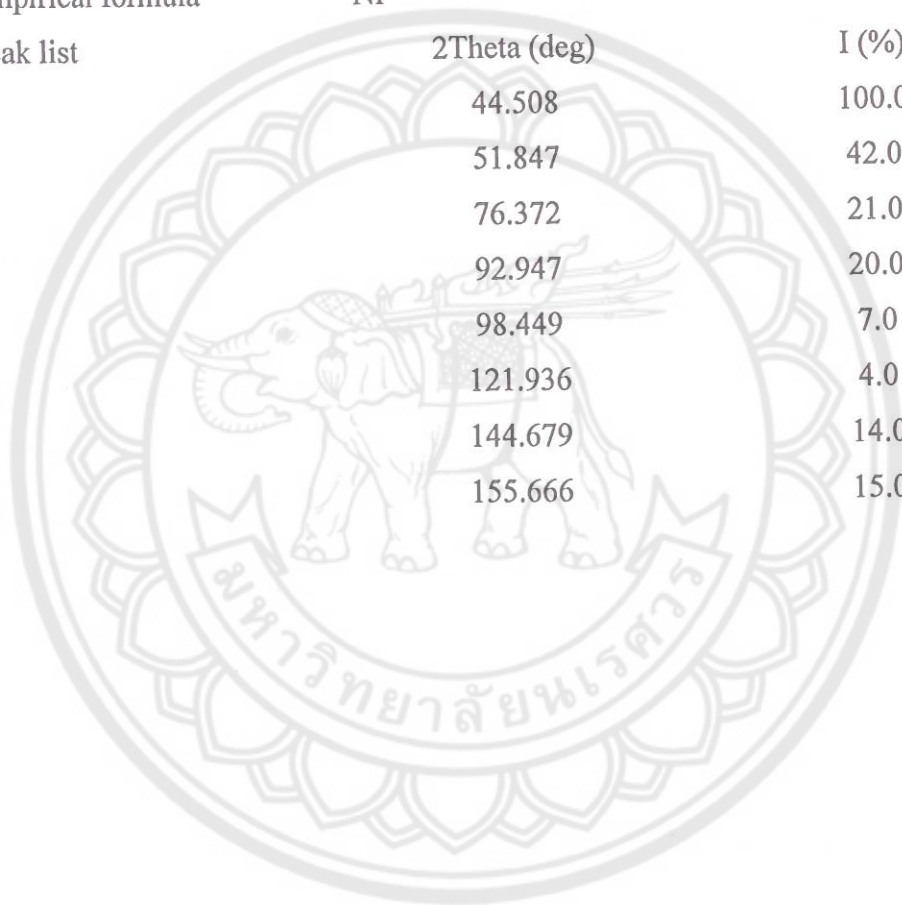
Reference code 00-004-0850

Nickel

Chemical formula Ni

Empirical formula Ni

Peak list	2Theta (deg)	I (%)
	44.508	100.0
	51.847	42.0
	76.372	21.0
	92.947	20.0
	98.449	7.0
	121.936	4.0
	144.679	14.0
	155.666	15.0



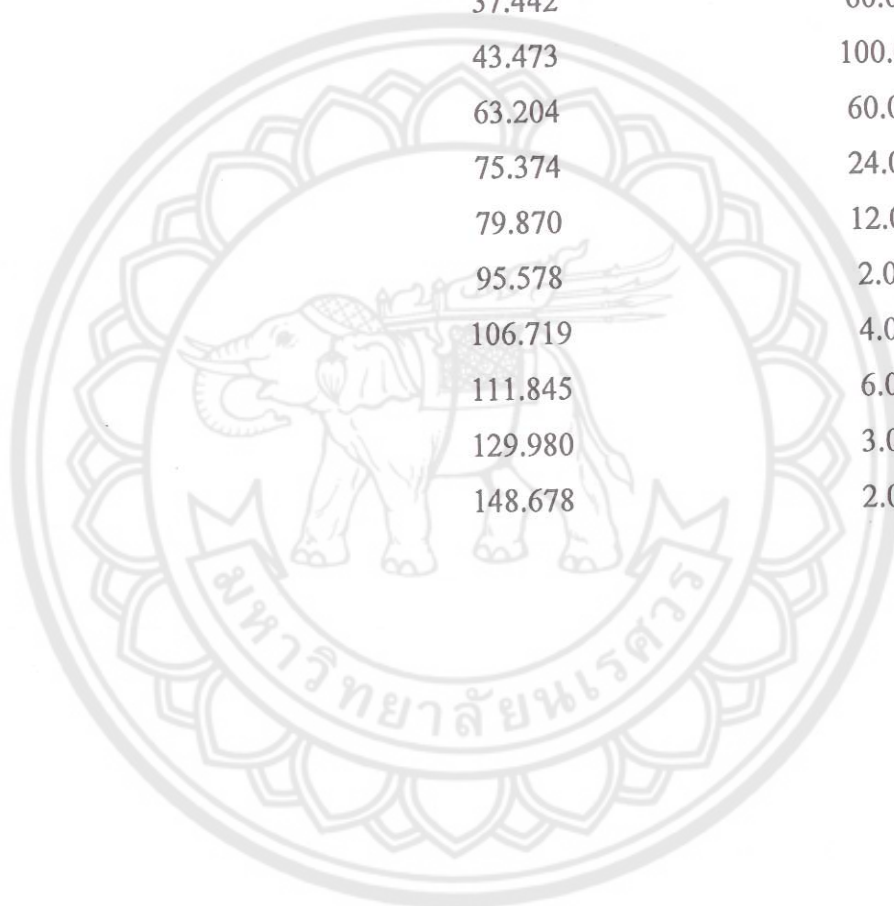
Name and formula

Reference code 00-001-1239
Nickel Oxide

Chemical formula NiO

Empirical formula NiO

Peak list	2Theta (deg)	I (%)
	37.442	60.0
	43.473	100.0
	63.204	60.0
	75.374	24.0
	79.870	12.0
	95.578	2.0
	106.719	4.0
	111.845	6.0
	129.980	3.0
	148.678	2.0



Name and formula

Reference code 00-085-1327

Aluminum

Chemical formula Al

Empirical formula Al

Peak list	2Theta (deg)	I (%)
	38.475	100.0
	44.723	45.5
	65.101	23.3
	78.234	22.8
	82.441	6.3



Name and formula

Reference code 00-047-1292

Aluminum Oxide

Chemical formula Al_2O_3 Empirical formula Al_2O_3

Peak list	2Theta (deg)	I (%)
	19.331	56.0
	31.820	93.0
	37.507	100.0
	39.241	7.0
	45.619	3.0
	49.991	7.0
	56.707	23.0
	60.503	24.0
	66.495	16.0
	69.999	3.0
	75.656	7.0
	78.923	6.0
	92.993	7.0
	96.313	10.0
	114.285	6.0
	130.858	3.0
	135.255	7.0
	143.542	11.0
	162.858	21.0

APPENDIX B HEAT LOSS RESULT

Table 15 Heat loss testing of Ni-Al coated thickness 195 μm

Test	Average absorber temperature (°C)	Average glass temperature (°C)	Average ambient temperature (°C)	Absorber – Ambient temperature (°C)	Heat loss W/m
1	30.75	28.59	26.95	3.80	0.39
2	41.52	30.28	27.41	14.11	7.06
3	51.28	31.72	27.84	23.44	2.21
4	60.96	32.90	28.00	32.96	3.54
5	70.35	34.04	28.29	42.07	4.42
6	79.78	35.43	28.69	51.09	6.21
7	89.30	36.80	28.42	60.87	10.26
8	99.17	38.53	28.64	70.52	9.34
9	109.08	40.40	29.37	79.70	10.61
10	118.80	41.91	29.58	89.22	14.10
11	128.56	43.62	29.57	98.99	21.10
12	138.27	45.87	29.72	108.54	16.37
13	148.00	47.63	28.93	119.07	18.86
14	157.50	49.20	28.89	128.61	22.01
15	167.62	51.28	29.45	138.16	23.66
16	177.14	53.36	28.87	148.26	29.40
17	186.68	65.76	28.18	158.49	34.77
18	196.83	63.79	28.24	168.59	35.20

Table 16 Heat loss testing of Ni-Al coated thickness 215 μm

Test	Average absorber temperature (°C)	Average glass temperature (°C)	Average ambient temperature (°C)	Absorber – Ambient temperature (°C)	Heat loss W/m
1	30.75	27.68	25.35	5.39	0.20
2	41.44	30.16	27.16	14.28	1.41
3	51.14	32.08	27.94	23.19	2.31
4	61.12	34.34	28.75	32.38	3.69
5	71.11	36.13	29.05	42.06	5.10
6	80.96	38.75	30.18	50.78	6.82
7	90.27	41.08	29.99	60.27	8.17
8	100.37	43.81	30.68	69.69	9.87
9	110.31	46.06	30.77	79.53	12.45
10	120.05	48.00	30.87	89.18	14.50
11	130.01	50.02	30.69	99.33	17.22
12	140.04	52.32	30.48	109.56	18.94
13	150.49	54.50	29.92	120.58	21.69
14	160.79	54.93	29.21	131.58	25.87
15	170.88	57.90	27.66	143.22	29.34
16	180.78	61.48	26.90	143.87	32.91
17	191.07	64.26	26.84	164.23	36.74
18	201.37	67.34	28.10	173.26	42.38

Table 17 Heat loss testing of Ni-Al coated thickness 299 μm

Test	Average absorber temperature (°C)	Average glass temperature (°C)	Average ambient temperature (°C)	Absorber – Ambient temperature (°C)	Heat loss W/m
1	30.86	27.98	26.88	3.99	0.03
2	40.88	29.32	27.16	13.72	0.93
3	50.52	31.39	27.50	23.02	2.29
4	60.41	33.18	27.92	32.49	3.66
5	70.23	35.08	28.32	41.91	5.37
6	80.29	37.05	28.77	51.53	7.23
7	90.06	39.08	29.14	60.93	13.61
8	100.45	42.03	29.81	70.64	12.51
9	110.60	43.88	30.02	80.58	13.63
10	120.09	49.02	29.96	90.13	13.74
11	129.83	51.06	29.75	100.08	20.44
12	139.83	54.13	30.54	109.29	17.71
13	149.48	57.12	30.51	118.98	20.50
14	158.99	58.71	30.82	128.16	23.71
15	168.38	60.07	30.54	137.84	27.30
16	178.42	64.27	30.80	147.62	32.97
17	188.58	66.99	30.80	157.79	40.26
18	198.60	69.30	30.04	168.56	39.48

APPENDIX C SOLAR ABSORPTANCE CALCULATION

Table 18 Solar absorptance data calculation of Ni-Al solar absorber surface thickness 195 μm

wavelength λ	Solar radiation		Reflectance, R		Integrate		Solar absorptance	
	$W/m^2 \cdot nm^{-1}$	I_{sol} W/m^2	%	$1-R$	$\int I_{sol}(1-R(\lambda))d\lambda$	$\int I_{sol}(\lambda)d\lambda$	α	$\alpha \cdot I_{sol}$
300	4.56E-04	1.37E-01	9.569	0.904	0.123	0.000	0	0.00E+00
301	9.19E-04	2.77E-01	9.635	0.904	0.000	0.000	90.587	8.33E-04
302	1.46E-03	4.40E-01	9.686	0.903	0.001	0.001	90.333	1.32E-03
303	3.73E-03	1.13E+00	9.738	0.903	0.003	0.002	90.276	3.37E-03
304	5.10E-03	1.55E+00	9.799	0.902	0.004	0.004	90.226	4.60E-03
305	8.93E-03	2.72E+00	9.854	0.901	0.008	0.007	90.165	8.06E-03
306	1.02E-02	3.11E+00	9.912	0.901	0.009	0.009	90.115	9.15E-03
307	1.52E-02	4.68E+00	9.968	0.900	0.013	0.012	90.053	1.37E-02
308	2.08E-02	6.39E+00	10.026	0.900	0.018	0.017	89.998	1.87E-02
309	2.23E-02	6.89E+00	10.075	0.899	0.020	0.021	89.948	2.01E-02
310	2.78E-02	8.63E+00	10.125	0.899	0.025	0.025	89.896	2.50E-02
311	4.54E-02	1.41E+01	10.183	0.898	0.040	0.036	89.838	4.08E-02
312	5.09E-02	1.59E+01	10.232	0.898	0.045	0.048	89.790	4.57E-02

Table 18 (cont.)

wavelength λ	Solar radiation		Reflectance, R		Integrate		Solar absorptance	
	$W/m^2 \cdot nm^{-1}$	I_{sol} W/m^2	%	$1-R$	$\int I_{sol}(1-R(\lambda))d\lambda$	$\int I_{sol}(\lambda)d\lambda$	α	$\alpha \cdot I_{sol}$
.
.
.
2480	8.00E-03	1.98E+01	-21.155	-0.212	-0.001	0.060	-19.878	-1.59E-03
2485	5.58E-03	1.39E+01	-22.983	-0.230	-0.007	0.033	-21.906	-1.22E-03
2490	3.50E-03	8.70E+00	-24.745	-0.247	-0.005	0.022	-23.661	-8.27E-04
2495	2.86E-03	7.15E+00	-26.500	-0.265	-0.004	0.015	-25.535	-7.32E-04
2500	7.03E-03	1.76E+01	-27.773	-0.278	-0.006	0.024	-27.404	-1.93E-03

Table 19 Solar absorptance data calculation of Ni-Al solar absorber surface thickness 215 μm

wavelength λ	Solar radiation		Reflectance, R		Integrate		Solar absorptance	
	$\text{W/m}^2 \cdot \text{nm}^{-1}$	W/m^2	%	$1-R$	$\int I_{sol}(1-R(\lambda))d\lambda$	$\int I_{sol}(\lambda)d\lambda$	α	$\alpha \cdot I_{sol}$
300	4.56E-04	1.37E-01	10.185	0.898	0.122	0.000	0	0.00E+00
301	9.19E-04	2.77E-01	10.241	0.898	0.000	0.000	89.981	8.27E-04
302	1.46E-03	4.40E-01	10.296	0.897	0.001	0.001	89.724	1.31E-03
303	3.73E-03	1.13E+00	10.353	0.896	0.003	0.002	89.662	3.35E-03
304	5.10E-03	1.55E+00	10.404	0.896	0.004	0.004	89.616	4.57E-03
305	8.93E-03	2.72E+00	10.470	0.895	0.007	0.007	89.553	8.00E-03
306	1.02E-02	3.11E+00	10.531	0.895	0.009	0.009	89.496	9.08E-03
307	1.52E-02	4.68E+00	10.586	0.894	0.013	0.012	89.435	1.36E-02
308	2.08E-02	6.39E+00	10.649	0.894	0.018	0.017	89.377	1.85E-02
309	2.23E-02	6.89E+00	10.704	0.893	0.019	0.021	89.322	1.99E-02
310	2.78E-02	8.63E+00	10.766	0.892	0.024	0.025	89.261	2.48E-02
311	4.54E-02	1.41E+01	10.816	0.892	0.040	0.036	89.202	4.05E-02
312	5.09E-02	1.59E+01	10.873	0.891	0.045	0.048	89.153	4.54E-02

Table 19 (cont.)

wavelength λ	Solar radiation		Reflectance, R		Integrate		Solar absorptance	
	$W/m^2 \cdot nm^{-1}$	I_{sol} W/m^2	%	$1-R$	$\int I_{sol}(1-R(\lambda))d\lambda$	$\int I_{sol}(\lambda)d\lambda$	α	$\alpha \cdot I_{sol}$
.
.
.
2480	8.00E-03	1.98E+01	124.86	-24.867	-0.001	0.060	-23.589	-1.89E-03
2485	5.58E-03	1.39E+01	126.72	-26.721	-0.001	0.033	-25.629	-1.43E-03
2490	3.50E-03	8.70E+00	128.53	-28.534	-0.000	0.022	-27.419	-9.58E-04
2495	2.86E-03	7.15E+00	130.20	-30.200	-0.000	0.015	-29.284	-8.39E-04
2500	7.03E-03	1.76E+01	131.38	-31.387	-0.002	0.024	-31.043	-2.18E-03

Table 20 Solar absorptance data calculation of Ni-Al solar absorber surface thickness 299 μm

wavelength λ	Solar radiation		Reflectance, R		Integrate		Solar absorptance	
	$\text{W/m}^2 \cdot \text{nm}^{-1}$	I_{sol} W/m^2	%	$1-R$	$\int I_{\text{sol}}(1-R(\lambda))d\lambda$	$\int I_{\text{sol}}(\lambda)d\lambda$	α	$\alpha \cdot I_{\text{sol}}$
300	4.56E-04	1.37E-01	10.160	0.898	0.122	0.000	0	0.00E+00
301	9.19E-04	2.77E-01	10.215	0.898	0.000	0.000	90.005	8.27E-04
302	1.46E-03	4.40E-01	10.278	0.897	0.001	0.001	89.745	1.31E-03
303	3.73E-03	1.13E+00	10.350	0.896	0.003	0.002	89.670	3.35E-03
304	5.10E-03	1.55E+00	10.411	0.896	0.004	0.004	89.614	4.57E-03
305	8.93E-03	2.72E+00	10.475	0.895	0.007	0.007	89.548	8.00E-03
306	1.02E-02	3.11E+00	10.539	0.895	0.009	0.009	89.490	9.08E-03
307	1.52E-02	4.68E+00	10.600	0.894	0.013	0.012	89.424	1.36E-02
308	2.08E-02	6.39E+00	10.659	0.893	0.018	0.017	89.365	1.85E-02
309	2.23E-02	6.89E+00	10.723	0.893	0.019	0.021	89.307	1.99E-02
310	2.78E-02	8.63E+00	10.784	0.892	0.024	0.025	89.242	2.48E-02
311	4.54E-02	1.41E+01	10.850	0.891	0.040	0.036	89.174	4.05E-02
312	5.09E-02	1.59E+01	10.906	0.891	0.045	0.048	89.119	4.54E-02

Table 20 (cont.)

wavelength λ	Solar radiation		Reflectance, R		Integrate		Solar absorptance	
	$W/m^2 \cdot nm^{-1}$	I_{sol} W/m^2	%	$1-R$	$\int I_{sol}(1-R(\lambda))d\lambda$	$\int I_{sol}(\lambda)d\lambda$	α	$\alpha \cdot I_{sol}$
.
.
.
2480	8.00E-03	1.98E+01	121.64	-0.216	-0.001	0.060	-20.345	-1.63E-03
2485	5.58E-03	1.39E+01	123.50	-0.235	-0.001	0.033	-22.390	-1.25E-03
2490	3.50E-03	8.70E+00	125.25	-0.235	-0.000	0.022	-24.174	-8.45E-04
2495	2.86E-03	7.15E+00	126.90	-0.269	-0.000	0.015	-25.994	-7.45E-04
2500	7.03E-03	1.76E+01	127.97	-0.280	-0.001	0.024	-27.666	-1.95E-03

APPENDIX D DATA OF THERMAL PERFORMANCE

Table 21 Thermal performance data calculation of Ni-Al solar absorber surface thickness 195 μm

T_{in} ($^{\circ}\text{C}$)	T_{out} ($^{\circ}\text{C}$)	T_{am} ($^{\circ}\text{C}$)	G_B (W/m^2)	$(T_{in}-T_{am})/G_B$	η
39.8	40.3	31.9	178.95472	0.04415	0.23375
39.9	40.4	31.6	180.76309	0.04592	0.23141
40.1	40.6	32.6	182.83476	0.04102	0.22879
40.2	40.7	32.2	183.70472	0.04355	0.2277
40.1	40.6	32.4	183.20107	0.04203	0.22833
40.2	40.7	32.2	187.48176	0.04267	0.22312
40.3	40.8	32.6	189.86245	0.04056	0.22032
40.2	40.7	32.4	191.5794	0.04071	0.21834
40.1	40.6	32.4	183.20107	0.04203	0.22833
40.2	40.7	32.2	187.48176	0.04267	0.22312
47.1	47.5	34.5	195.3794	0.06449	0.17128
47.3	47.7	33.4	194.84142	0.07134	0.17175
47.3	47.7	33.4	200.03777	0.06949	0.16729
47.1	47.5	33.3	200.17511	0.06894	0.16717
47.2	47.6	32.7	199.21373	0.07279	0.16798
47.3	47.7	33.6	197.96609	0.0692	0.16904
47.3	47.7	33.4	200.03777	0.06949	0.16729
47.1	47.5	33.3	200.17511	0.06894	0.16717
47.3	47.7	33.4	200.03777	0.06949	0.16729
47.3	47.7	33.6	197.96609	0.0692	0.16904
53.7	54	32.6	208.59925	0.10115	0.12032
54	54.3	32.3	209.29742	0.10368	0.11992
54.3	54.6	31.5	206.21856	0.11056	0.12171
54.5	54.8	32.8	206.71073	0.10498	0.12142
55.9	56.1	32.3	208.64506	0.11311	0.08019

Table 21 (cont.)

T_{in} (°C)	T_{out} (°C)	T_{am} (°C)	G_B (W/m ²)	$(T_{in}-T_{am})/G_B$	η
57.5	57.7	33.6	208.16427	0.11481	0.08038
57.5	57.8	34.4	209.61792	0.1102	0.11973
54.5	54.8	32.8	206.71073	0.10498	0.12142
54	54.3	32.3	209.29742	0.1102	0.11973
54.5	54.8	32.7	205.91973	0.11055	0.12134

Table 22 Thermal performance data calculation of Ni-Al solar absorber surface thickness 215 μ m

T_{in} (°C)	T_{out} (°C)	T_{am} (°C)	G_B (W/m ²)	$(T_{in}-T_{am})/G_B$	η
36.3	37.3	29.3	227.897	0.03072	0.3671
36	37	28.5	229.93433	0.03262	0.36384
37	38	31.2	226.31749	0.02563	0.36966
36.9	37.9	30.6	227.3133	0.02772	0.36804
36.9	37.9	30.1	227.64517	0.02987	0.3675
36.9	37.9	29.2	227.39345	0.03386	0.36791
37.5	38.5	30.1	237.24818	0.03119	0.35263
37.3	38.4	30.2	238.30118	0.02979	0.38618
37.2	38.3	30.3	237.98079	0.02899	0.3867
37.2	38.2	29.2	238.69034	0.03352	0.3505
42.8	43.7	30.4	245.35182	0.05054	0.30688
42.5	43.5	30.5	247.67532	0.04845	0.33778
42.4	43.4	30	249.1633	0.04977	0.33576
42.1	43.1	29.1	250.39946	0.05192	0.33411
41.8	42.7	30	256.79764	0.04595	0.2932
42	42.9	29.8	259.7735	0.04696	0.28984
41.8	42.8	31.5	257.31266	0.04003	0.32513
41.8	42.9	31.1	256.88916	0.04165	0.35823

Table 22 (cont.)

T_{in} (°C)	T_{out} (°C)	T_{am} (°C)	G_B (W/m ²)	$(T_{in}-T_{am})/G_B$	η
41.9	43	31.3	256.86631	0.04127	0.35826
41.8	42.9	32.2	257.66749	0.03726	0.35715
46.7	47.6	31.3	261.47897	0.0589	0.28795
46.8	47.7	31.6	263.56202	0.05767	0.28568
46.5	47.5	33.2	261.13552	0.05093	0.32037
46.7	47.7	32.2	258.80064	0.05603	0.32326
46.6	47.6	31.8	261.89099	0.05651	0.31945
45.6	46.5	31.8	265.65665	0.05195	0.28343
45.9	46.9	32.5	260.09399	0.05152	0.32165
46	47	32.7	261.28433	0.0509	0.32019
46.1	47.1	33.1	262.06266	0.04961	0.31924
45.9	46.9	32.3	263.96266	0.05152	0.31694
53.8	54.7	31.2	271.97468	0.0831	0.27684
54	54.9	32.3	269.91448	0.0804	0.27896
54.2	55.1	32.2	268.02586	0.08208	0.28092
54.2	55	32.9	264.55783	0.08051	0.25298
54.2	55	31.2	266.18315	0.08641	0.25144
54.5	55.3	34.4	268.71266	0.0748	0.24907
54.4	55.3	33.8	268.93015	0.0766	0.27998
54.3	55.2	31	269.88015	0.08633	0.27899
54.3	55.1	31.7	272.94764	0.0828	0.2452
54	54.9	32.3	269.91448	0.0804	0.27896
58.3	59.1	32.7	268.06019	0.0955	0.24968
58.2	59	30.8	272.753	0.10046	0.24538
58.6	59.4	33.4	267.09882	0.09435	0.25057

Table 22 (cont.)

T_{in} (°C)	T_{out} (°C)	T_{am} (°C)	G_B (W/m ²)	$(T_{in}-T_{am})/G_B$	η
58.5	59.4	32.4	267.57951	0.09754	0.28139
58.7	59.5	32	267.2133	0.09992	0.25047
58.7	59.5	32.9	261.69635	0.09859	0.25575
58.5	59.2	32	259.55601	0.1021	0.22562
58.4	59.2	31.8	261.79936	0.1016	0.25565
59.4	60.1	31.8	267.35064	0.10324	0.21905
58.7	59.5	32.9	261.69635	0.09859	0.25575

Table 23 Thermal performance data calculation of Ni-Al solar absorber surface thickness 299 μ m

T_{in} (°C)	T_{out} (°C)	T_{am} (°C)	G_B (W/m ²)	$(T_{in}-T_{am})/G_B$	η
39.9	41.6	35.1	279.01384	0.0172	0.50973
39.1	40.8	34.9	277.93798	0.01511	0.5117
38.8	40.4	34	275.47715	0.01742	0.48591
39	40.5	34.3	274.87049	0.0171	0.45654
39.2	40.7	35.1	278.14399	0.01474	0.45117
39.6	41	34.6	278.36148	0.01796	0.42076
40	41.5	34.7	281.31448	0.01884	0.44608
40.4	41.9	35.4	280.54753	0.01782	0.4473
39	40.5	34.3	274.87049	0.0171	0.45654
40.9	42.3	35.1	281.66931	0.02059	0.41582
42.1	43.4	34.4	279.24281	0.02757	0.38947
42	43.3	31.8	281.01685	0.0363	0.38702
42.2	43.5	35.3	281.41749	0.02452	0.38646
42.5	43.8	34.8	278.71631	0.02763	0.39021
43.2	44.5	35.8	281.16567	0.02632	0.38681
43.5	44.8	35	280.58187	0.03029	0.38762

Table 23 (cont.)

T_{in} (°C)	T_{out} (°C)	T_{am} (°C)	G_B (W/m ²)	$(T_{in}-T_{am})/G_B$	η
43.3	44.5	34.8	277.68616	0.03061	0.36153
43.5	44.8	34.6	273.43981	0.03255	0.39774
43.8	45.1	34.7	275.7632	0.033	0.39439
43.7	45	35	278.7735	0.03121	0.39013
50.7	51.9	35.6	276.32414	0.05465	0.36331
51.2	52.4	35.9	280.34152	0.05458	0.35811
51.1	52.3	36.3	283.50064	0.0522	0.35412
51.3	52.5	35	277.9265	0.05865	0.36122
51.6	53	35.9	284.51931	0.05518	0.41166
51.8	53.1	35.7	286.15601	0.05626	0.38007
51.6	52.9	35.8	288.15901	0.05483	0.37742
51.7	53	35.8	286.48798	0.0555	0.37962
51.9	53.1	36	285.12586	0.05576	0.3521
51.9	53.1	35.3	282.50483	0.05876	0.35536
57.2	58.3	35.5	280.02103	0.07749	0.32864
56.9	58	34.6	278.67049	0.08002	0.33023
57.6	58.7	36	279.59753	0.07725	0.32914
57.6	58.7	35.4	277.74335	0.07993	0.33133
57.7	58.8	35.3	282.76803	0.07922	0.32545
57.9	59	33.6	280.76502	0.08655	0.32777
57.8	58.9	33.3	282.76803	0.08664	0.32545
57.9	59	35.9	278.55601	0.07898	0.33037
58	59.1	35.3	278.8765	0.0814	0.32999
57.9	59	34.7	280.62768	0.08267	0.32793

APPENDIX E

Key Engineering Materials Vols. 675-676 (2016) pp 477-481
© (2016) Trans Tech Publications, Switzerland
doi:10.4028/www.scientific.net/KEM.675-676.477

Submitted: 2015-06-02
Revised: 2015-08-03
Accepted: 2015-08-18

Characterization of Ni-Al Solar Absorber Prepared by Flame Spray Technique

Chanon Bumemphiphit^{1, a}, Tawat Suriwong^{1, b, *}, Somchai Jiajitsawat^{2, c}
and Nuchjira Dejang^{2, d}

¹ School of Renewable Energy Technology, Naresuan University, Phitsanulok, 65000, Thailand.

² Department of Physics, Faculty of Science, Naresuan University, Phitsanulok, 65000, Thailand.

^achanonbumemphiphit@gmail.com, ^b*tawats@nu.ac.th, ^csomchaij@nu.ac.th, ^dnuchjirad@nu.ac.th

Keywords: Flame spray technique, Intermetallic materials, Ni-Al composite, Nickel aluminides, Solar absorber

Abstract. In this research, a Ni-Al solar absorber was successfully prepared by the flame spray technique with Ni-5 wt.%Al particles as a starting material. The Ni-5 wt.%Al particles were melted and sprayed on to the outer surface of a stainless steel 316L tube in order to form a Ni-Al composite coating. The phase, morphology and reflectance (*R*) spectrum of the Ni-Al solar absorber were characterized by X-ray Diffraction (XRD), a Scanning electron microscope (SEM) equipped with an energy dispersive X-ray (EDX) analyzer and an Ultraviolet-visible-near infrared spectrophotometer at the wavelengths 300-2500 nm. The results revealed that the surface of the Ni-Al solar absorber was rough, and its cross section was overlapping layers. The Ni-Al solar absorber was composed of Nickel (Ni) and aluminum (Al) phases. NiO and Al₂O₃ phases were also found on the surface. The chemical composition of the Ni-Al solar absorber was Ni (72.94 wt.%), Al (11.76 wt.%) and O (15.29 wt.%). The solar absorptance (α) of this solar absorber was 0.77. This demonstrates that a Ni-Al composite coating can be applied as a solar absorber material for solar collectors at high operating temperatures.

1. Introduction

Ni-Al composite coating is one of the intermetallic compounds used for special applications requiring a high melting point (1911 K), low density (5890 Kg.m⁻³), excellent oxidation resistance up to 1573 K, high thermal conductivity and fabrication of a coating with a uniform composition [1, 2]. Ni-Al composite coatings have been extensively observed as having thermal and spectral selective properties. Nickel displays high solar absorptivity, good corrosion resistance, heat resistance and durability, while aluminium exhibits high reflectivity in the IR region, which indicates low thermal emission from the solar absorber surface to the ambient environment [3]. NiAl-Al₂O₃ cermet coating is one of the solar selective absorber materials with high optical performance (α/ϵ) of the coating on the Cu substrate (0.94/0.97) and on the stainless steel (SS) substrate (0.95/0.078) [4]. Adding black NiAl particles into the black paint coating improves the thermal efficiency of solar water heating systems (SWHSs) and increases the corrosion resistance of the paint [3]. Xu et al. observed that the corrosion resistance of the Ni-Al composite coating decreased with increasing Al content. They demonstrated by a galvanic corrosion test that a Ni-5wt.%Al coating, prepared by the plasma spray process, exhibited no surface corrosion [5], indicating that the formation of Al₂O₃ on the surface of the Ni-Al composite coating was the best anti-corrosion material [2, 6]. The flame spray technique is not a complicated process, allows a high production rate, is a rapid process and has low environmental impact and low cost. As well, this technique can be used as a coating application in an open environment and can also be used for recoating cracked surfaces. There is little prior research published regarding Ni-Al composite coatings on SS pipe prepared by the flame spray techniques. Especially, the solar absorptance (α) of this coating is unknown, or unreported.

In the present study, therefore, we used Ni-Al as a solar absorber on SS 316L pipe, prepared by the flame spray technique. The Ni-Al solar absorber was characterized by phase, morphology and chemical composition. The solar absorptance (α) was also investigated and measured.

2. Experimental procedures

A stainless steel (SS) 316L tube with outer diameter 33.33 mm, inner diameter 27.9 mm, and 1000 mm. in length was applied as the substrate material. Commercially available Ni-5wt.%Al particles (450NS, Oerlikon Metco, Switzerland) with a size distribution 45-90 μm of a spheroidal shape were used as a starting material. CastoDyn DS 8000 flame spray equipment (Castolin Eutectic, Switzerland) was used to fabricate the Ni-Al solar absorber, as shown in Fig.1(a). Fig. 1(b) illustrates the flame spray setup of the coating process. The SS 316L tube was installed on a rotating stand, and rotated at 50 rpm. The flame spray gun was held 150 mm from the substrate and sprayed on the outer surface of SS 316L tube along the vertical axis. The Ni-5wt.%Al particles are directly fed and melted in the flame spray gun using acetylene gas; oxygen; air (1:5.7:0.8 bar), then projected on to the substrate.

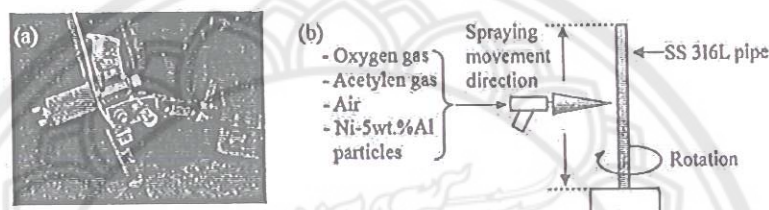


Fig. 1 (a) CastoDyn DS 8000 flame spray gun from Castolin Eutectic, Switzerland and (b) Schematic drawing of flame spray setup for coating process

The phase of the starting material and Ni-Al solar absorber was identified by X-ray diffraction (Rigaku miniflex II, Japan). The surface morphology, cross-sectional microstructure, and chemical composition of the Ni-Al solar absorber were characterized by using a JEOL JSM-5910LV scanning electron microscope (SEM) equipped with an energy dispersive X-ray (EDX) analyzer. Reflectance (R) of the coating was measured using a Shimadzu UV-3101PC spectrophotometer in the wavelength 300-2500 nm. The solar absorptance (α) was calculated from the reflectance spectrum in Equation 1, from [7]:

$$\alpha = \frac{\int_{0.3\mu\text{m}}^{2.5\mu\text{m}} I_s(\lambda)(1-R(\lambda))d\lambda}{\int_{0.3\mu\text{m}}^{2.5\mu\text{m}} I_s(\lambda)d\lambda} \quad (1)$$

where $R(\lambda)$ is the measured spectral reflectance of the coating at a specific wavelength between 300-2500 nm, and $I_s(\lambda)$ is the solar spectral irradiance at air mass AM 1.5 [8].

3. Result and Discussion

Fig. 2 shows the XRD pattern of the Ni-5wt.%Al particles (starting material) and the Ni-Al composite coating on SS 316L pipe. The spectra were indexed and compared with the JCPDS database Nos. 4-0850, 01-85-1327, 1-1239 and 47-1292 for Ni, Al, NiO and Al_2O_3 , respectively. The starting material combined the pure Ni and Al phases. Analysis of the Ni-Al solar absorber revealed the Ni, Al, NiO and Al_2O_3 phases. During the flame spray process, melted Ni and Al particles were oxidized with oxygen gas in the environment and transformed into NiO and Al_2O_3 phases. NiAl, AlNi_3 or Al_3Ni_5 were not detected in the Ni-Al solar absorber due to the low Al content in this composite coating, according to the Ni-Al binary phase diagram [9].

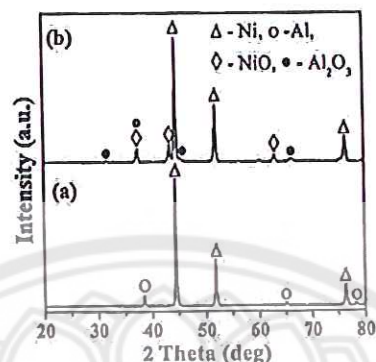


Fig. 2. XRD patterns of (a) Ni-5wt.%Al particles and (b) Ni-Al solar absorber.

Typical SEM and EDX mapping images on the surface of the NiAl solar absorber are shown in Fig. 3. The SEM image indicates that the sample has a rough surface which was built up by spraying the melted Ni and Al particles, injected from the flame spray gun, layer by layer. The EDX mapping analysis detected Ni, Al, and Sb which were distributed relatively homogeneously on the surface of the sample. As the EDX analysis shows, the chemical composition of the fundamental elements of this sample were Ni 72.94 wt.%, Al 11.76 wt.% and O 15.29 wt.%. According to the XRD pattern of the Ni-Al solar absorber, the melted Ni and Al particles on the SS 316L pipe substrate reacted with the oxygen in the environment during rotation of the pipe until it cooled to room temperature. In addition, the formation of Al₂O₃ and NiO on the surface of the Ni-Al solar absorber is able to offer an increasing anti-corrosion effect on the surface [2, 6, 10].

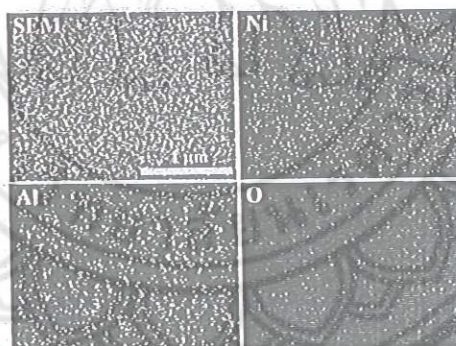


Fig. 3. SEM image and EDX mapping analysis on the top-surface of NiAl solar absorber.

Fig 4. shows the cross-section SEM image of the Ni-Al solar absorber. It can be observed that this coating has overlapped layers with the layer structure parallel to the surface of the SS 316L pipe. This layer structure was similar to the microstructure of the Ni-Al composite coating prepared by other techniques [5, 11, 12]. The sample exhibited relative roughness of the surface with an average thickness of ~230 μm. The coating had high adhesion contact with the substrate, indicating a good bonding between the melted Ni-Al particles and the substrate. In addition, the rough surface of the Ni-Al solar absorber provides a good bonding to the top coating [5]. It was found that the two different contrast regions in the Ni-Al solar absorber indicate the different phases identified in the EDX analysis results. The light gray phase corresponded to the Ni rich area, while the dark gray

phase corresponded to the Al rich area. Splats were predominantly in the Ni rich area. The Al phase was not uniformly distributed in the matrix of this sample due to the discontinuously piling up of the melting Al particle at the interface of the layer. In addition, the coating of the Ni-Al solar absorber included pores with different sizes. Basically, most of the melted particles of the starting material were coated on the substrate. The pores were made from un-melted and imperfectly melted particles of the starting material during the flame spraying process. Other reasons for these un-melted and imperfectly melted particles were splashed intensely onto the substrate. The large porous size was created from the agglomeration of the un-melted particles, while the small porous size was created from the imperfectly melted particles of the starting material.

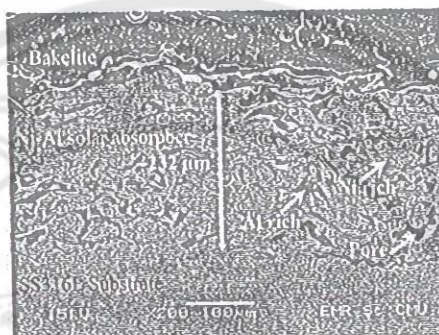


Fig. 4. Cross-section SEM image of Ni-Al solar absorber.

Fig. 5. presents the measured reflectance (R) and calculated solar absorptance (α) spectra of the NiAl solar absorber, compared with the sun spectrum at AM 1.5. It was found that R slightly increases with the increasing wavelength. In the UV-Visible spectrum region (300-800 nm), the R was relatively low, while in the near infrared region, the R was high and close to 1 at 2450 nm. The α of the Ni-Al solar absorber gradually decreased with the increasing wavelength. Over the whole wavelength of the solar spectrum, the calculated α was 0.77.

It is therefore clear that the Ni-Al solar absorber prepared by the flame spray technique is a good candidate as a solar absorber material in the field of high-temperature solar collectors.

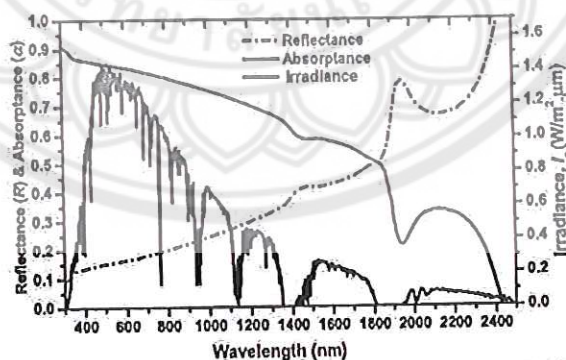


Fig. 5. Measured reflectance and calculated solar absorptance spectra of Ni-Al solar absorber, comparing to the sun spectrum at AM 1.5 [8].

Conclusions

In the present study, Ni-Al solar absorbers were coated on a substrate; a SS 316L pipe, and were successfully prepared by the flame spray technique using Ni-5 wt.%Al particles as a starting material. The surface of the Ni-Al solar absorber showed dark gray color tone and roughness. The Ni-Al solar absorber was composed of Ni, Al, NiO and Al₂O₃ phases. The microstructure of the sample had overlapping layers with the layer structure parallel to the surface of the substrate. Most splats were found predominantly in the Ni rich area. The α of the Ni-Al solar absorber was 0.77 over the whole solar spectrum range. The results show that the Ni-Al solar absorber is a good candidate as a solar absorber material for solar collectors operating at high operating temperatures.

Acknowledgements

We are grateful to University of Phayao, the National Research Council of Thailand (NRCT), and Naresuan University, Thailand for providing financial support, including the Graduate School of Naresuan University, Thailand for general funding. Many thanks to Mr. Roy Morien of the Naresuan University Language Centre for his editing assistance and advice on English expression in this document.

Reference

- [1] H.X. Dong, Y. Jiang, Y.H. He, M. Song, J. Zou, N.P. Xu, B.Y. Huang, C.T. Liu, P.K. Liaw, Formation of porous Ni-Al intermetallics through pressureless reaction synthesis, *J. Alloys Compd.*, 484 (2009) 907-913.
- [2] F. Cai, C. Jiang, Influences of Al particles on the microstructure and property of electrodeposited Ni-Al composite coatings, *Appl. Surf. Sci.*, 292 (2014) 620-625.
- [3] E. AlShamailah, Testing of a new solar coating for solar water heating applications, *Sol. Energy*, 84 (2010) 1637-1643.
- [4] Y. Xue, C. Wang, W. Wang, Y. Liu, Y. Wu, Y. Ning, Y. Sun, Spectral properties and thermal stability of solar selective absorbing AlNi-Al₂O₃ cermet coating, *Sol. Energy*, 96 (2013) 113-118.
- [5] C. Xu, L. Du, B. Yang, W. Zhang, The effect of Al content on the galvanic corrosion behaviour of coupled Ni/graphite and Ni-Al coatings, *Corros. Sci.*, 53 (2011) 2066-2074.
- [6] F. Cai, C. Jiang, X. Wu, X-ray diffraction characterization of electrodeposited Ni-Al composite coatings prepared at different current densities, *J. Alloys Compd.*, 604 (2014) 292-297.
- [7] G. Katumba, L. Olumekor, A. Forbes, G. Makiwa, B. Mwakikunga, J. Lu, E. Wäckelgård, Optical, thermal and structural characteristics of carbon nanoparticles embedded in ZnO and NiO as selective solar absorbers, *Sol. Energy Mater. Sol. Cells*, 92 (2008) 1285-1292.
- [8] C.A. Gueymard, The sun's total and spectral irradiance for solar energy applications and solar radiation models, *Sol. Energy*, 76 (2004) 423-453.
- [9] K. Morsi, Review: reaction synthesis processing of Ni-Al intermetallic materials, *Mater. Sci. Eng., A*, 299 (2001) 1-15.
- [10] A. Rahman, R. Jayaganthan, S. Prakash, V. Chawla, R. Chandra, High temperature oxidation behavior of nanostructured Ni-Al coatings on superalloy, *J. Alloys Compd.*, 472 (2009) 478-483.
- [11] S. Sampath, X.Y. Jiang, J. Matejček, L. Prchlik, A. Kulkarni, A. Vaidya, Role of thermal spray processing method on the microstructure, residual stress and properties of coatings: an integrated study for Ni-5 wt.%Al bond coats, *Mater. Sci. Eng., A*, 364 (2004) 216-231.
- [12] Y. Wang, Z. Wang, Y. Yang, W. Chen, The effects of ceria on the mechanical properties and thermal shock resistance of thermal sprayed NiAl intermetallic coatings, *Intermetallics*, 16 (2008) 682-688.